8.26 Coordination Chemistry of Iron-Dinitrogen Complexes With Relevance to Biological N_2 Fixation

William R. Buratto and Leslie J. Murray, Department of Chemistry, Center for Catalysis and Florida Center for Heterocyclic Compounds, University of Florida, Gainesville, FL, United States

8.26.1 Introduction

Dinitrogen (N_2) is the most abundant gas in the Earth's atmosphere, comprising ~78%,[1] and is an essential component for sustaining life on Earth due to its role in the production of ammonia (NH_3).[2] The constantly growing human population is supported by well-established agriculture systems where synthetic fertilizers, of which NH_3 is a major component, are necessary to maintain and increase crop yields. Microorganism and industrial ammonia production account for roughly equal portions of the available NH_3 (140 and 136 megatons/year, respectively).[3] In addition to the primary application of ammonia as a fertilizer, it is also a major source for industrial nitrogen-containing chemicals, such as hydrazine (N_2H_4), hydrogen cyanide (HCN), acrylonitrile, and urea, which are critical reagents in the syntheses of polymers, explosives, pesticides, and pharmaceuticals (Fig. 1). The central importance of nitrogen fixation to the biosphere and society has understandably driven the search for discrete model compounds, which employ similar ligand fields as, and can reproduce the reactivity or aspects thereof, the biological systems. As an entry point into iron-dinitrogen chemistry, we will first consider the thermodynamics of N_2 fixation to ammonia, followed by a brief summary of anthropogenic and biological nitrogen fixation—highlighting the common theme of iron-based catalysis and reactivity—and subsequently treat molecular iron-dinitrogen systems.

8.26.1.1 Thermodynamics of NH_3 Production Through N_2 Fixation

In the simplest thermodynamic sequence, the fixation of N_2 as NH_3 can be defined by the homolytic bond dissociation energies (BDEs)—which are 941, 513, and 274 kJ/mol for N_2, diazene (N_2H_2), and hydrazine (N_2H_4), respectively[4]—and the reduction potentials ($E^0_{1/2}$) of N_2, H_2, and NH_3, the latter of which are given in the equations below:

$$N_2 + e^- \rightleftharpoons N_2^- \qquad E^\circ = -4.16 \text{ V vs RHE}$$

$$N_2 + H^+ + e^- \rightleftharpoons N_2H \qquad E^\circ = -3.20 \text{ V vs RHE}$$

$$N_2 + 2H^+ + 2e^- \rightleftharpoons N_2H_2 \qquad E^\circ = -1.10 \text{ V vs RHE}$$

$$N_2 + 4H^+ + 4e^- \rightleftharpoons N_2H_4 \qquad E^\circ = -0.33 \text{ V vs RHE}$$

$$N_2 + 6H^+ + 6e^- \rightleftharpoons 2NH_3 \qquad E^\circ = -0.148 \text{ V vs RHE}$$

Despite the negative reduction potentials, the conversion of N_2 and H_2 to NH_3 is thermodynamically favored ($\Delta G_f^o = -16.48$ kJ/mol),[5] but does not occur under ambient conditions.[6] Comparison of dinitrogen to acetylene, which is

Comprehensive Coordination Chemistry III, 2021, 659–706

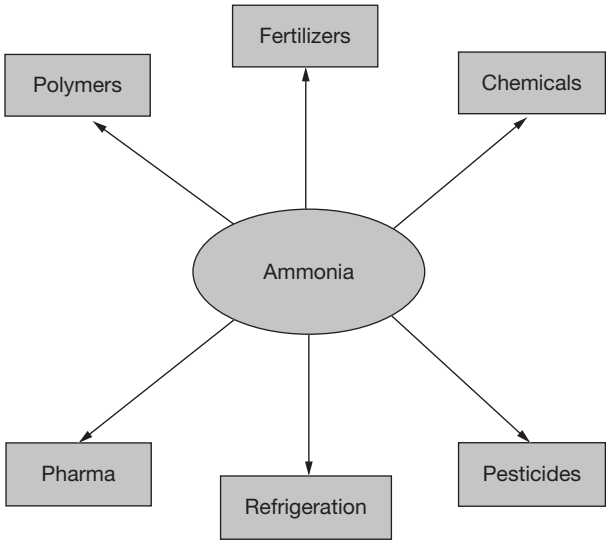

Fig. 1 A basic representation of the applications of ammonia.

more reactive at room temperature yet has a similar BDE (viz. 962 kJ/mol), reveals that the energy required to cleave the first π-bond of these two molecules are disparate; conversion of N≡N to N═N requires 410 kJ/mol whereas breaking the first π-bond in HC≡CH requires only 222 kJ/mol, which is nearly half of that for N_2.[5] This difference reflects the unfavorable ΔG_f^o of diazene and hydrazine as compared to those for ethylene and ethane. Thus, potential states along the N_2 to ammonia conversion pathway are uphill with respect to N_2. In addition to the energetic costs to access the potential intermediates, the reaction is kinetically limited because of the large HOMO-LUMO gap of 10.82 eV, large ionization potential and negative electron affinity, and low proton affinity of N_2 as compared to isoelectronic diatomics (e.g., CO). The primary need and challenge for catalysts in dinitrogen fixation, therefore, is to facilitate this initial functionalization of N_2 and the development of such catalysts remains the subject of considerable research effort.[7] Within this context, one must consider the mode of interaction of N_2 with the catalytic centers, usually metal ions, which will be the focus of the next section.

$$N_2(g) + 3H_2(g) \rightarrow 2NH_3(g) \quad (1)$$

8.26.1.2 Dinitrogen Coordination to Transition Metal Centers

In the context of metal-based activation of small molecules, the predominant pathway begins with coordination of substrate to a metal ion with π-donation by the metal to the accessible anti-bonding orbitals of the substrate. The manner in which dinitrogen coordinates varies depending on the metal centers involved, and the surrounding ancillary ligands coordinated to those centers. The common modes for metal-dinitrogen interactions to one or two metal ions are depicted in Fig. 2.

The most prevalent coordination modes for a dinitrogen molecule are terminal end-on and bridging end-on (A and B in Fig. 2) with one or both lone pairs of the N_2 molecule interacting in a σ fashion with the metal center(s). Indeed, myriad Fe–N_2 complexes have been isolated and characterized and, in all cases, the N_2 has been found to coordinate in a terminal or μ-1,2 fashion. The μ-η^1:η^2 and μ-η^2:η^2 coordination modes (C and D, Fig. 2) are observed primarily for dinitrogen adducts of early transition metal centers and of lanthanides and actinides and, consequently, will not be discussed in detail here. Dinitrogen is a poor σ-donor and the metal-dinitrogen interaction requires further stabilization by back-donation of electron density from the metal center(s) to the empty π* orbitals on N_2. The metal-ligand π-backbonding and the σ-bonding interactions for dinitrogen bear similarity to those observed in metal carbonyl complexes, albeit weaker. Consequently, N_2 is best described as both a weak σ-donor and

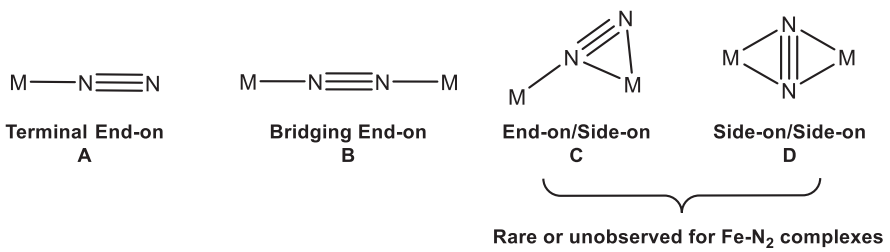

Fig. 2 Binding modes of N_2. Degree of N_2 activation in each mode is not depicted.

a weak π-acceptor,[8] and has traditionally been thought to require an electron-rich or reduced metal center to favor π-backbonding. As such, non-π acidic or strongly σ-donating ancillary ligands and low-valent metal centers are common motifs throughout iron-dinitrogen chemistry. As is the trend for the activation of many small molecules, the bond lengths for the bound small molecule (dinitrogen, for our purposes) for complexes characterized by X-ray crystallography and/or by the stretching frequency of the small molecule fragment (e.g., N–N vibration) observed in either IR or Raman spectroscopy are the common reporters for the extent of activation. For reference, the N—N bond distances and ν_{NN} values for free dinitrogen, diazene, and hydrazine are 1.09, 1.25, and 1.47 Å and 2359, 1583/1529, and 885 cm^{-1}, respectively.[9] The lack of a dipole in dinitrogen contributes to the challenges in its activation, which is reflected in iron-dinitrogen adducts; whereas the μ-1,2 mode leads to greater N—N bond activation, reduction and further functionalization of the coordinated N_2 is usually observed for the terminal-bound N_2 species. The Haber-Bosch process and N_2-reduction at the iron-molybdenum cofactor of molybdenum-dependent nitrogenases have been the major inspirations for synthesizing and exploring the reactivity of Fe–N_2 complexes; as such, we will briefly consider these two systems prior to discussing the discrete molecular chemistry.

8.26.1.3 Inspirations for Fe–N_2 Complexes for Nitrogen Fixation

8.26.1.3.1 Haber-Bosch process

Industrially, ammonia is produced by the quintessential N_2 reduction process discovered by Fritz Haber and Carl Bosch in the early 20th century. Deemed to be one of the most important technological innovations of the 20th century,[10] the Haber-Bosch process (HBP) is a heterogeneously catalyzed conversion of N_2 to NH_3 that produces roughly 140 million tons of NH_3 per annum, with most of this ammonia used as fertilizer. The HBP utilizes the Mittasch catalyst, which consists of iron nanoparticles covered by a potassium sub-monolayer as an electronic promoter.[11] Based on ammonia production yield, the Mittasch catalyst is the most efficient synthetic catalyst hitherto for reduction of N_2 with H_2 with ~70% of the theoretical NH_3 output,[12] albeit using harsh conditions. Despite the reaction of H_2 with N_2 to afford NH_3 being exothermic (−46 kJ/mol), the HBP operates at high temperatures (300–550 °C) and pressures (100–300 atm) to overcome the significant activation barrier (Eq. 2). These energy-demanding conditions required for and the scale of the HBP consume a large portion of the world's commercial energy supply (~1.1%)[13] and the process is also reliant on fossil fuels, which signals a need for novel approaches to fix dinitrogen to ammonia. To that end, heterogeneous catalysts consisting of heavier group 8 metals Ru and Os have been of interest and many additional variations to catalyst chemical composition investigated (e.g., using a Ba instead of a K sub-monolayer). Other attempted strategies have been to use mixtures of transition metals in the catalyst, as well as using titanium oxides with light or electrochemical potential.

$$N_2(g) + 3H_2(g) \xrightarrow[300-550^{\circ}C,\ 100-300\ atm]{\text{Haber-Bosch Catalyst}} 2NH_3(g) \qquad (2)$$

Studies on the mechanism of the HBP were performed using a variety of single-crystal iron surfaces. The proposed pathway by which N_2 to NH_3 conversion occurs arising from these investigations is as follows. Rate-controlling dissociative chemisorption of N_2 and H_2 on the iron surface to generate N and H adatoms is succeeded by recombination of these N and H adatoms with sequential formation of surface bound NH, NH_2, and NH_3 and ultimate desorption of the formed NH_3. The sites for N_2 binding are postulated to be Fe sites at steps at which second- and third-layer Fe atoms are exposed.[14] With respect to N_2 coordination as it relates to activation, two accessible chemisorption phases have been reported: a γ-phase with an adsorption enthalpy of ~24 kJ/mol and an α-phase with an adsorption enthalpy of ~31 kJ/mol.[15] The γ-phase N_2 molecules have been characterized as a terminally bound to the active Fe surface, whereas the α-phase comprises N_2 molecules bound parallel to the surface through an interaction between the N—N π-bond and the metal surface. In Fig. 3, we have depicted the N_2 coordination to proceed in the *cis* mode to simplify the illustration for N_2 splitting on the catalyst surface, although this geometry cannot be assumed as the catalyst surface is not flat on an atomic scale. Dinitrogen initially binds in the γ-phase, and subsequently isomerizes to the α-phase ($\Delta G^{\ddagger} \approx 20$ kJ/mol) from which the N≡N bond can be cleaved.[13] The identification of the α-phase on the Fe surface as the catalytically relevant conformer points to the potential importance of utilizing multiple Fe centers with a side-on coordination mode for the conversion of N_2 to NH_3. Notably, many of the simplest side-on interactions such as an η^2-dinitrogen bound to one Fe center or a *cis*-μ-1,2 mode have not been reported in synthetic systems, providing synthetic targets to explore coordination-mode dependent reactivity of N_2.

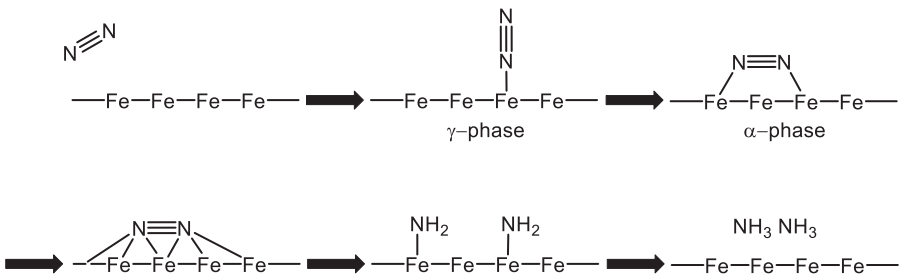

Fig. 3 Simplified HBP mechanism at the surface of the Mittasch Catalyst. *Cis* orientation of the α-phase cannot be assumed as the catalyst surface is not flat on an atomic scale.

8.26.1.3.2 Biological N_2 reduction-nitrogenase enzyme

The Haber-Bosch process accounts for ~29% of the total nitrogen fixation occurring on Earth.[3] The nitrogenase enzymes produce approximately the same amount of NH_3 as the HBP; however, these biological catalysts operate under ambient conditions. Although these enzymes are less energy-efficient based on ATP consumption and H_2 production as compared to the energy recycling employed in HBP plants, the ability to execute this chemistry under such mild conditions is a key source of inspiration for novel N_2-reduction catalysts. The cofactors responsible for N_2 binding and activation in the nitrogenase enzymes all contain a cage-like cluster consisting of seven iron atoms, six μ_3-sulfides, three μ-sulfides, an interstitial μ_6-carbide, and an eighth metal center, which is Mo, V, or Fe depending on the specific isozyme. The cluster is ligated by one cysteine thiolate, coordinated to the apical Fe center, and one histidine, which, together with a homocitrate, completes the coordination sphere of the variable metal center (Fig. 4).[16] The iron-molybdenum cofactor (FeMoco) in the Mo-dependent nitrogenase enzymes with a composition of $[MoFe_7(\mu_3\text{-}S)_6(\mu_2\text{-}S)_3(\mu_6\text{-}C)]^{1-}$.[17] is the most effective for N_2 fixation and the most studied in this context. FeMoco converts N_2 to NH_3[18] using 8 electrons from NADH and 8 protons, with energy provided by the hydrolysis of 16 equiv. MgATP (Eq. 3).

$$N_2 + 8H^+ + 8e^- + 16MgATP \xrightarrow{\text{Nitrogenase}} 2NH_3 + H_2 + 16PO_4^{3-} + 16MgADP \quad (3)$$

In the resting state of the enzyme, six of the iron atoms lie centrally in the cluster—known collectively as the belt Fe sites—with each coordinated by two μ_3-sulfides, one μ-sulfide, and the μ_6-carbide in a distorted trigonal pyramidal arrangement. Data from recent ENDOR experiments has led to the proposal that an Fe_4S_4 face comprising four of these belt iron atoms (viz. Fe2, Fe3, Fe6, and Fe7) is the site for N_2 coordination and subsequent activation, hinting at a possible multimetallic pathway for N_2 fixation.[19] Computational studies suggest that Fe2 and Fe6 are the most likely sites for N_2 binding/activation as both of these metal ions have at least one available coordination site to accommodate N_2.[20] The coordination flexibility at these Fe sites is likely crucial to the turnover in this catalytic system as evidenced by recent crystallographic evidence for substitution of μ-sulfides during turnover.[21a,b] A detailed understanding of the electronic or structural effects afforded by the interstitial carbide donor remains to be determined. Hypotheses include that the expected covalent Fe—C bonds impart sufficient rigidity to the cluster, preventing possible deleterious distortions during catalytic turnover, that the C^{4-} is a site for protonation during proton and electron loading for the cofactor,[21c] and that the carbide is the site for N_2 binding and activation.[22]

In recent years, substantial progress has been made towards understanding the mechanism of N_2 activation by FeMoco. As a result of extensive kinetics studies conducted on the Mo-dependent nitrogenase, Lowe and Thorneley constructed the eponymous kinetic model for N_2 fixation by nitrogenase (Fig. 5).[23] In a simplified version of the Lowe-Thorneley (LT) model, E_0 represents the resting state and most oxidized form of the cluster. Each subsequent E_n state represents the protein upon accumulation of n electrons. Since FeMoco is the site for electron accumulation, E_n can be thought of as a representation of the number of electrons on FeMoco or one of its substrate-bound intermediates. Additionally, each electron-accumulating step occurs with the delivery of a proton to the cofactor in proton-coupled electron transfers. The important discoveries made in these studies are as follows. First, 8 equiv. of electrons and protons are required to reduce one molecule of N_2 to two molecules of NH_3. These equivalents are two more than the minimum required; the additional electron equivalents generate one mole of H_2 for every mole of N_2 reduced.[24] The LT scheme proposes that the release of H_2 occurs when FeMoco is in either the E_3 or E_4 states (i.e., accumulated 3 or 4 equiv. of $[e^-, H^+]$, respectively) and upon binding of a molecule of N_2. The order of H_2 reductive elimination and N_2 coordination remains unclear; ENDOR data suggest that H_2 reductive elimination may precede N_2 binding whereas N_2 binding can occur with retention of hydrides in model compounds.[25]

The assertion of ambiguity for the order of the H_2 reductive elimination and N_2 coordination derives from the following. First, Guth and Burris' data suggests that $E_4(4H2N)$ is inactive towards NH_3 production based on their kinetic simulations; their model then concludes that H_2 must be lost (or reductively eliminated) prior to productive N_2 binding.[24b] Second, the well-known HD experiments require that N_2 binding correlates with H_2 reductive elimination. The Occam's razer argument is that $E_4(4H2N)$ is an important transient; however, those experiments do not exclude rapid oxidative addition of H_2 by a transiently formed $E_4(2H)^*$—the state from reductive elimination of H_2 from $E_4(4H)$—prior to exchange of H_2 and D_2 and that N_2 can effectively trap $E_4(2H)^*$.[24b] Third, Hoffman and coworkers' data demonstrate conversion of the $E_4(4H)$ state to the $E_2(2H)$ state by a hydride protonation mechanism,[26e] indicating the intrinsic instability of $E_4(4H)$. Four, low temperature photolysis of $E_4(4H)$ affords a state distinct from $E_2(2H)$ and is proposed to be $E_4(2H)^*$. This state oxidatively adds H_2 upon warming above 12 K and implies that H_2 reductive elimination is possible in the absence of N_2.[26f] Fifth, progression of $E_4(4H)$ to the $E_4(2H2N)$ species is inhibited by H_2, with $E_4(4H)$ decaying to $E_2(2H)$ by hydride protonation as noted in the third point above.[26g] Sixth, $E_4(2H2N)$ and $E_4(4H)$ are in equilibrium

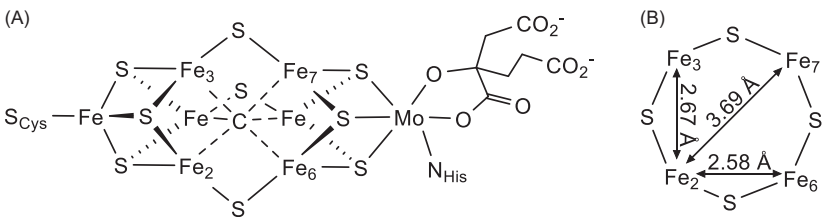

Fig. 4 (A) Top-view of the FeMoco cage-like cluster. (B) Structural parameters of the $[Fe_4S_4]$ face.

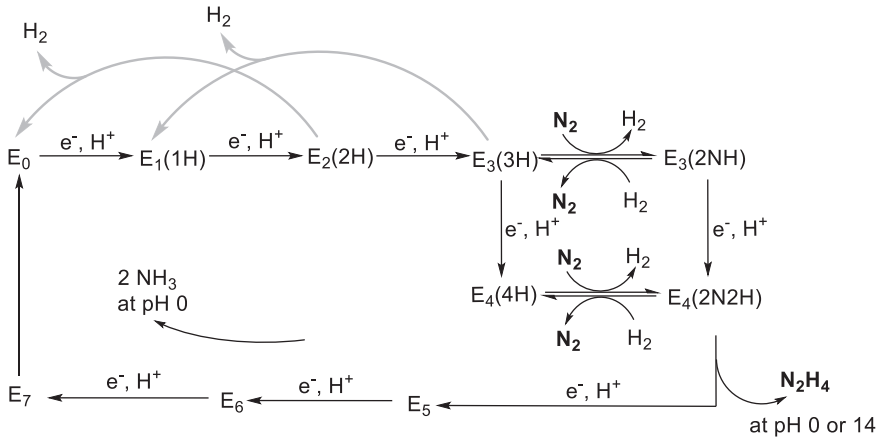

Fig. 5 A simplified schematic depicting the titular Lowe-Thorneley kinetic model of the conversion of N_2 to NH_3 by nitrogenase enzymes. Adapted from Thorneley, R.N.F.; Lowe, D.J. *Molybdenum Enzymes*. Wiley-Interscience Publications, New York, 1985; Vol. 7, pp. 221–284.

governed by [H_2] and [N_2] under cryoannealing conditions.[26h] Readers are also directed to the review by Burgess and Lowe,[18b] which summarized the kinetic consequences of the HD experiments and where no conclusions were stated regarding the order of N_2 binding and H_2 reductive elimination. Rather, those authors concluded only that H_2 release and N_2 coordination must be connected. Given these results and that the rates must be such that E_4(4H2N) remains elusive (i.e., the equilibrium constants favor E_4(4H) and E_4(2H2N) over E_4(4H2N)), one cannot exclude transient formation of an E_4(2H) + H_2 state for which N_2 binding is competitive with oxidative addition of H_2 to reform E_4(4H). The lack of evidence for E_4(2H)* binding N_2 or that E_4(2H)* is catalytically relevant may suggest that a transient E_4(4H2N) species is the on-pathway intermediate and imply N_2 binding prior to H_2 reductive elimination. However, the absence of such data may simply be a consequence of relative rate constants and not reflect the reaction pathway. Thus, definitive statements on the order of H_2 reductive elimination and N_2 binding do not faithfully represent the body of work hitherto in the literature, and the order of N_2 binding and H_2 reductive elimination remains unresolved.

Further investigation of the mechanism of nitrogen fixation by FeMoco using ENDOR spectroscopy studies on wild-type and site-directed variants of the enzyme suggest that the E_4 state contains two protonated sulfide bridges and two [Fe–H–Fe] units. The proposal that reactivity derives from the E_4 state only contrasts the original LT scheme in which E_3 is also a N_2 reactive state. Electrons are in essence stored in Fe—H bonds with no observable change in the formal Fe oxidation states, consistent with prior Mößbauer measurements.[26,27] Reductive elimination of the two bridging hydride units releases H_2 from the E_4 state to afford one or two low-valent iron centers, which can coordinate N_2. With dinitrogen coordinated to the reduced Fe center(s) on FeMoco, charge transfer from the cluster to the bound substrate is accompanied by proton transfer from the nearby SH units to afford an E_4(2N2H) state (**Fig. 6**). The formation of the E_4(2N2H) state illustrates the importance of a push-pull type of reactivity to perform the initial reduction of N_2. Electrons are pushed from electron-rich metal centers to N_2, and the SH protons pull the electron density to complete the reduction of the N_2 substrate. This mechanistic insight addresses two major questions in the understanding of nitrogenase-catalyzed N_2 reduction; that is, the extra pair of electrons to reduce N_2 to NH_3 is required to prime the cluster for N_2 binding, and the PCET pathway allows for catalysis under ambient conditions. Indeed, the formation of N—H bonds enables cleavage of a N_2 π-bond as expected from the thermodynamics of N_2 reduction (vide supra) and highlights potential molecular approaches to effect N_2 fixation. Despite the significant progress made towards understanding the mechanism of N_2 reduction by nitrogenase enzymes, a number of mechanistic questions remain unanswered. For example, the number of Fe centers participating in binding and the coordination mode of N_2 (e.g., μ-1,1 or *cis*-μ-1,2), the structure and accumulation of e^-/H^+ in the early E_n states, and the mechanism for conversion of the diazenide- and hydrazide-level intermediates to liberate NH_3 molecule are undetermined. Importantly, there is limited precedent in synthetic chemistry for these lingering mechanistic questions, such as hydride insertion into an N_2 derived ligand in a metal complex. Developing such synthetic chemistry, therefore, will play a key role in supporting our understanding of FeMoco catalysis.

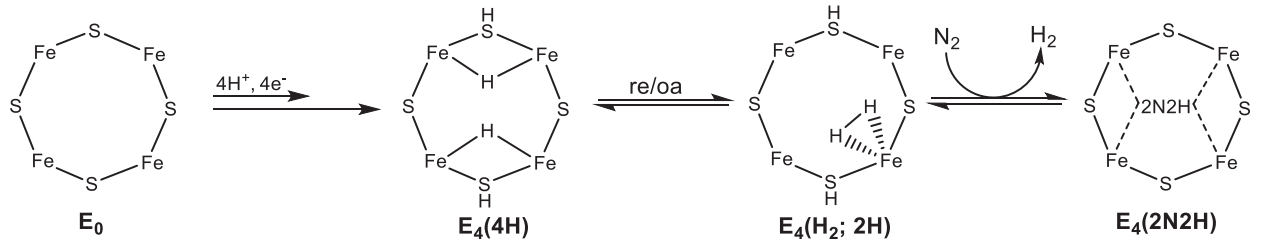

Fig. 6 Proposed *re* mechanism for N_2 binding at the E_4 state.

8.26.2 Early Fe–N_2 Complexes (1968–2000)

The first Fe–N_2 complex (**2–1**) was isolated by Sacco and Aresta in 1968[28] when a *cis*-dihydrido-tris(ethyl-diphenyl)phosphine Fe(II) complex was exposed to a N_2 atmosphere (Fig. 7). Infrared (IR) spectroscopy supported coordination of N_2 with an absorption at 2055 cm^{-1}, which shifted to lower energy in the $^{15}N_2$ isotopologue as expected. The analogous complex bearing *n*-butyldiphenylphosphine ligands instead of Ph_2EtP was isolated in 1971.[29] Attempts to protonate the dinitrogen ligand to generate ammonia were unsuccessful; addition of HCl to a solution of **2–1** resulted in quantitative production of H_2, N_2, $PEtPh_2$, and $FeCl_2(PEtPh_2)_2$. Despite the lack of ammonia production from **2–1**, the complex was reactive towards other small molecules, such as insertion of carbon dioxide and ethylene into the Fe—H bond.[30]

In 1970, Schrauzer and Schlesinger published results of the reduction of several substrates of nitrogenase, such as acetylene, methylacetylene, alkyl isocyanides, and sodium azide, by a molybdenum complex, providing support for a critical role for Mo in the activation of dinitrogen in FeMoco.[31] However, Newton and coworkers demonstrated that iron was similarly competent for reduction of unsaturated substrates.[32] Using dichlorotetrapyridinoiron(II) as the catalyst (Fig. 8), they were able to reduce several unsaturated substrates with sodium borohydride, including sodium azide to ammonia, and cyanide to a mixture of methane, ammonia, and ethane. This collection of early discoveries was the genesis of iron-dinitrogen complex chemistry.

Over the subsequent two decades, a number of Fe–N_2 complexes were isolated and spectroscopically characterized. The majority of these complexes relied on the use of organophosphine ancillary ligands and are epitomized by work from the groups of Berke,[33] Sacconi,[34] Shilov,[35] and Muetterties[36] (Fig. 9). Of these early reports, Leigh's in 1991 on the production of ammonia from protonation of a Fe–N_2 complex was one of the most important (Fig. 10). Exposure of $[Fe(H)(\eta^2\text{-}H_2)(dmpe)_2]^+$ (dmpe = bis(dimethylphosphino)ethane) to an atmosphere of N_2 in ethanol produced $[Fe(H)N_2(dmpe)_2]^+$ (**2–2**) in good yield.[37] Deprotonation of **2–2** by KO^{t}Bu resulted in the formation of the neutral Fe(0) complex (**2–3**), which was purported to react with excess strong acid to liberate ammonia in up to 12% yield per complex by the indophenol test. The proposed mechanism for this transformation is depicted in Fig. 10.[38] However, Komiya and Field later cast doubt on dinitrogen activation as the source of the positive indophenol test.

Hirano et al. synthesized an analogous complex to that of Leigh with Me in **2–3** substituted for Et in **2–4** as the substituents on the phosphine ligands to afford $Fe(N_2)(depe)_2$ (depe = bis(diethylphosphino)-ethane) (**2–4**). Addition of HCl to **2–4** did not generate NH_3 (Fig. 11).[39] In 2015, Field conducted a series of experiments that demonstrated that ammonia is not liberated from **2–3** upon addition of acid. Using **2–3** and **2–4**, addition of HCl yielded no ammonium as detected by ^{1}H-NMR.[40] Addition

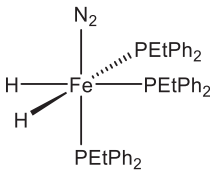

(2-1)

Fig. 7 The first isolated Fe–N_2 complex. Adapted from Sacco, A.; Aresta, M. *Chem. Commun.* **1968**, *4*, 1223–1224.

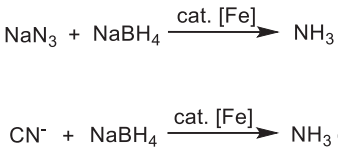

Fig. 8 Dichlorotetrapyridinoiron(II) ([Fe]) successfully catalyzed the reduction of sodium azide and cyanide in the presence of sodium borohydride. Adapted from Newton, W. E.; Corbin, J. L.; Schneider, P. W.; Bulen, W. A. *J. Am. Chem. Soc.* **1971**, *93*, 268–269.

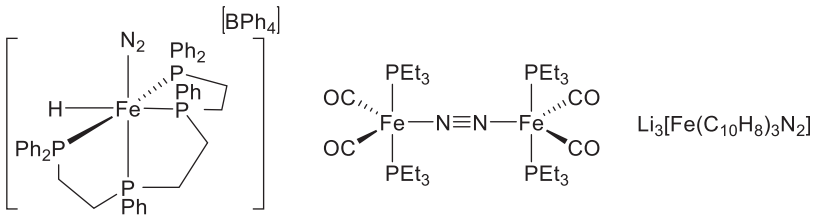

Fig. 9 Examples of early Fe–N_2 complexes. Adapted from Birk, R.; Berke, H.; Huttner, G.; Zsolnai, L. *Chem. Ber.* **1988**, *121*, 471–476; Stoppioni, P.; Mani, F.; Sacconi, L. *Inorg. Chim. Acta* **1974**, *11*, 227–230; Ghilardi, C. A.; Midollini, S.; Sacconi, L.; Stoppioni, P. *J. Organomet. Chem.* **1981**, *205*, 193–202; Bazhenova, T. A.; Ivleva, I. N.; Kachapina, L. M.; Shilova, A. K.; Shilov, A. E.; Tchoubar, B. *J. Organomet. Chem.* **1985**, *296*, 95–101; Gerlach, D. H.; Peet, W. G.; Muetterties, E. L. *J. Am. Chem. Soc.* **1972**, *94*, 4545–4549.

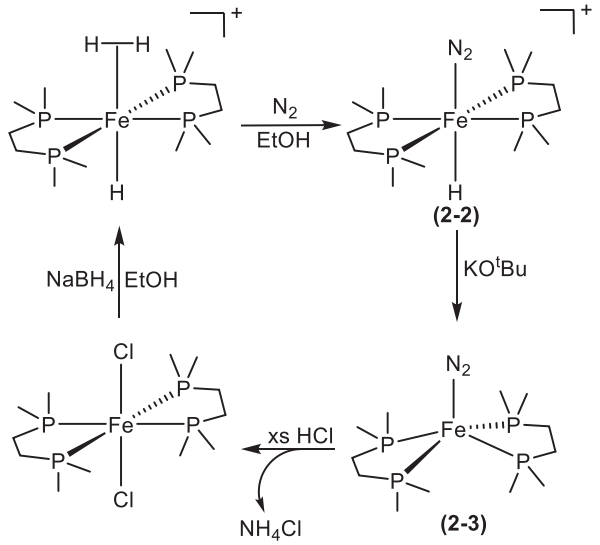

Fig. 10 Initial proposed scheme by Leigh for the conversion of N_2 to NH_3 by a Fe–N_2 complex. Adapted from Hills, A.; Hughes, D. L.; Jimenez-Tenorio, M.; Leigh, G. J. *J. Organomet. Chem.* **1990**, *391*, C41–C44; Leigh, G. J.; Jimenez-Tenorio, M. *J. Am. Chem. Soc.* **1991**, *113*, 5862–5863.

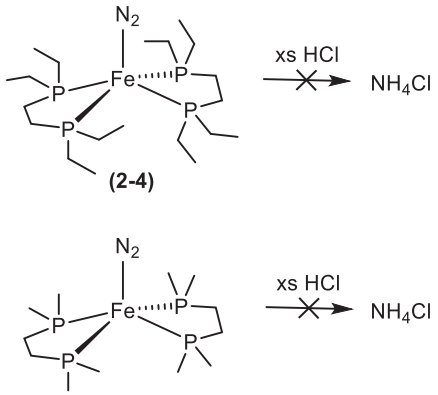

Fig. 11 Komiya performed the top reaction, raising doubts about Leigh's results. Field substantiated the doubts 20 years later. Adapted from Hirano, M.; Akita, M.; Morikita, T.; Kubo, H.; Fukuoka, A.; Komiya, S. *J. Chem. Soc., Dalton Trans.* **1997**, *26*, 3453–3458; Field, L. D.; Hazari, N.; Li, H. L. *Inorg. Chem.* **2015**, *54*, 4768–4776.

of exogenous NH_4Cl to the reaction mixtures did not convolute the ^1H NMR spectra, with a single resonance observed in the ^{14}N spectrum and, consequently, no evidence for a signal corresponding to acid generated NH_4^+ arising from dinitrogen fixation by these complexes. Indeed, Field's work highlights the caveats associated with the indophenol assay; that is, the test is not specific for NH_3, but rather may provide positive results with iron or residual DMPE.

Although the system reported by Leigh and coworkers does not fix dinitrogen, that report sparked an increased interest in transition metal-dinitrogen complexes, and particularly iron-dinitrogen adducts. In 1995, George et al. successfully generated NH_3 and N_2H_4 from the protonation of an Fe–N_2 complex that had been previously isolated by Sacconi.[41] From Sacconi's tris(diphenylphosphinoethyl)amine-supported iron-dinitrogen complex (**2–5**), George et al. synthesized the Fe(0) congener (**2–6**) by deprotonation of the hydride ligand with *n*-butyllithium (Fig. 12). X-ray crystallography data show the N_2 ligand is bound in a terminal end-on fashion and ν_{NN} has decreased in energy to 1967 cm^{-1}. This Fe(0) complex was shown to produce ammonia (3% yield) and hydrazine (11% yield) by addition of HBr in a dichloromethane solution of **2–6**.

Closely related to the dinitrogen-adducts presented above, Sellmann and coworkers targeted complexes of the N_2H_x adducts (x = 2, 3, or 4) employing a variety of iron complexes with sulfur-rich coordination spheres (Fig. 13). Notably, treating an iron-carbonyl complex supported by a NS_4 ligand with hydrazine yielded the corresponding iron-hydrazine adduct (**2–7**).[42] Oxidation of **2–7** in DMF at −60 °C led to a novel diiron species containing a *trans*-μ-1,2-diazene (**2–8**). Complex **2–8** was the first iron-based system to coordinate diazene. Moreover, **2–8** employed a biologically relevant donor set, incorporated hydrogen-bonding interactions between the thiolates and the bridging N–H centers, and effects the microscopic reverse of the reduction of diazene to hydrazine by FeMoco. In this light, this report was the first complex to model both the functionality and structure of nitrogenase.[43]

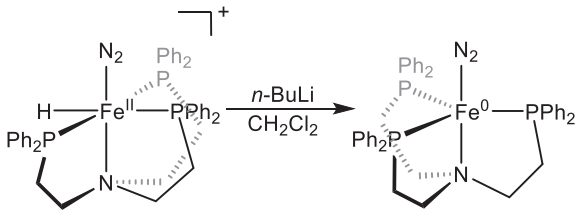

(2-5) (2-6)

Fig. 12 An early example of an Fe(0)–N_2 complex by George and coworkers. Adapted from George, T. A.; Rose, D. J.; Chang, Y.; Chen, Q.; Zubieta, J. *Inorg. Chem.* **1995**, *34*, 1295–1298.

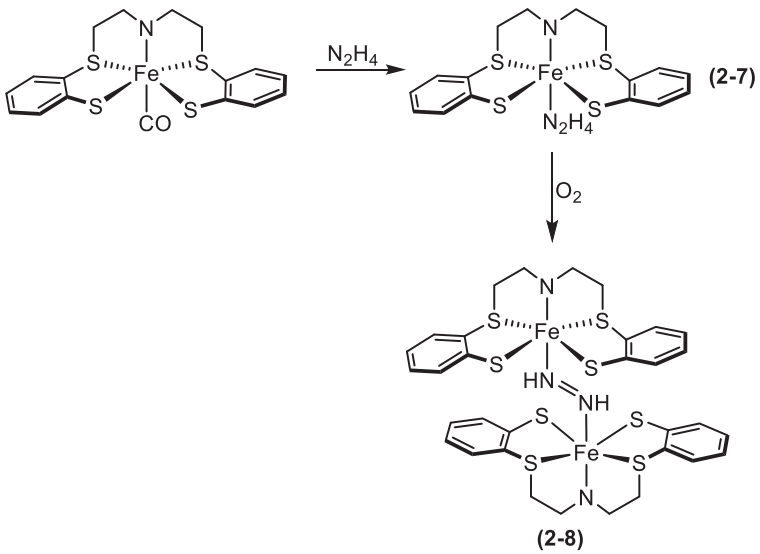

(2-7) (2-8)

Fig. 13 The first iron-diazene complex. Adapted from Sellmann, D.; Kunstmann, H.; Knoch, F.; Moll, M. *Inorg. Chem.* **1988**, *27*, 4183–4190; Sellmann, D.; Soglowek, W.; Knoch, F.; Moll, M. *Angew. Chem. Int. Ed.* **1989**, *28*, 1271–1272.

8.26.3 Contemporary Fe–N_2 Complexes (2000-Present)

After the turn of the century, the number of reports describing Fe-centered N_2-fixation model complexes notably increased as compared to the preceding 30+ years. From 1968 to 1999, only 11 Fe–N_2 compounds had been structurally characterized by X-ray crystallography with 60 manuscripts describing the downstream reaction chemistry of these compounds published in the same timeframe.

Contrastingly, the number of publications has more than doubled from 2000 to the present with approximately 140 reports with 154 distinct complexes structurally characterized; here, we only consider Fe—N≡N complexes and their immediate reaction intermediates and products. A handful of research groups have been at the forefront of the increased effort and focus on the synthesis of mono- and multi-nuclear iron-dinitrogen complexes, and their reports constitute the majority of the work described below. The complexes that highlight novel coordination modes and structural features will be discussed in detail with a briefer treatment of related species. The sections below are broadly organized by the supporting ligand architecture, beginning with the trigonal pseudo-C_{3v} ligand systems, then the meridionally-coordinated pincer-type ligands, followed by the complexes of bidentate donors. The last section will examine current efforts to incorporate more biologically relevant donors in these complexes, such as S- and C-based donors. Our primary objective is to consider complexes with relevance to dinitrogen fixation, and not to provide an exhaustive overview of all iron-dinitrogen species. For example, the majority of η^6-arene or η^5-cyclopentadienyl iron complexes are not discussed as the dinitrogen in these complexes is not functionalized and the compounds are used as precursors or catalysts for unrelated chemical transformations (e.g., C—C coupling).

8.26.3.1 Fe–N_2 Complexes Supported by Ligands Imposing Trigonal Symmetry

In this section, we begin by describing the stoichiometric chemistry of iron-dinitrogen species supported by tri(phosphinomethyl) borate ligands, which impose a pseudotetrahedral coordination environment upon binding of an exogenous axial donor, in Section 8.26.3.1.1 and follow with the tetradentate EP_3 (E = N, Si, B, Al, P) ligands in Section 8.26.3.1.2. The latter ligand family sought to

impose trigonal bipyramidal geometries at the iron center upon N_2 coordination, although six-coordinate metal centers were observed in a number of cases. In Section 8.26.3.1.1, we briefly consider the related tris(imidazolyl) borate and the tris[(*N*-heterocyclic) carbene] complexes. We conclude Section 8.26.3.1.2 with a discussion with the catalytic reduction of dinitrogen to ammonia by the complexes discussed therein.

8.26.3.1.1 Pseudotetrahedral tri(phosphinomethyl)borate complexes

In 2003, Betley and Peters constructed a trigonally coordinated iron complex, $[PhBP_3^{iPr}]FeCl$, ($[PhBP_3^{iPr}]^- = [PhB(CH_2P^iPr_2)_3]^-$) **(3–1)**. Two-electron reduction of **3–1** with Mg^0 results in the anionic four-coordinate Fe–N_2 complex **(3–2)** in which dinitrogen is coordinated in an end-on terminal fashion. This iron-dinitrogen adduct displays activation of the coordinated N_2 ligand based on IR spectroscopy with $\nu_{NN} = 1830\ cm^{-1}$ (cf. $\nu_{NN}(N_{2(g)}) = 2331\ cm^{-1}$). The mono-iron dinitrogen -ate complex can be readily converted to a neutral diiron species as oxidation of **3–2** with ferrocenium yields the μ-1,2-dinitrogen complex, ($[PhBP_3^{iPr}]Fe)_2(\mu\text{-}1,2\text{-}N_2)$ **(3–3)**. This dinuclear complex displays a modest increase in N–N bond length to 1.138 Å (cf. $N_2(g) = 1.098$ Å). Consistently then, one-electron reduction of **3–1** also affords the μ-1,2-dinitrogen diiron adduct **3–3**. As might be expected, the dinitrogen ligand is more activated in the μ-1,2 bridging mode of **3–3** as compared to the terminally-ligated N_2 in **3–2**. Further reduction of **3–3** by prolonged exposure to Na/Hg forms a mixed-valent Fe^0/Fe^I complex **(3–4)** (Fig. 14), in which further elongation of the N–N bond to 1.171 Å is observed in the solid-state structure. Direct conversion of a coordinated N_2 to the diazenide or hydrazide congeners by addition of an electrophile (R^+) was hitherto unknown for any first-row transition metal complex. Coordination of dinitrogen in **3–2** presented the first step towards dinitrogen functionalization in this system and access to complexes with relevance to the diazene-level intermediate in FeMoco.[44] Reaction of methyl *p*-toluenesulfonate (or MeOTs) with anionic **3–2** affords the product Fe(II)-diazenide complex **3–5**. IR spectroscopy provided strong evidence for successful alkylation of the N_2 ligand with a significant bathochromic shift of the N–N stretching vibration from 1830 cm^{-1} in **3–2** to 1597 cm^{-1} in **3–5**. The latter energy is consistent with double bond character and thus suggestive of an η^1-diazenido moiety.[45]

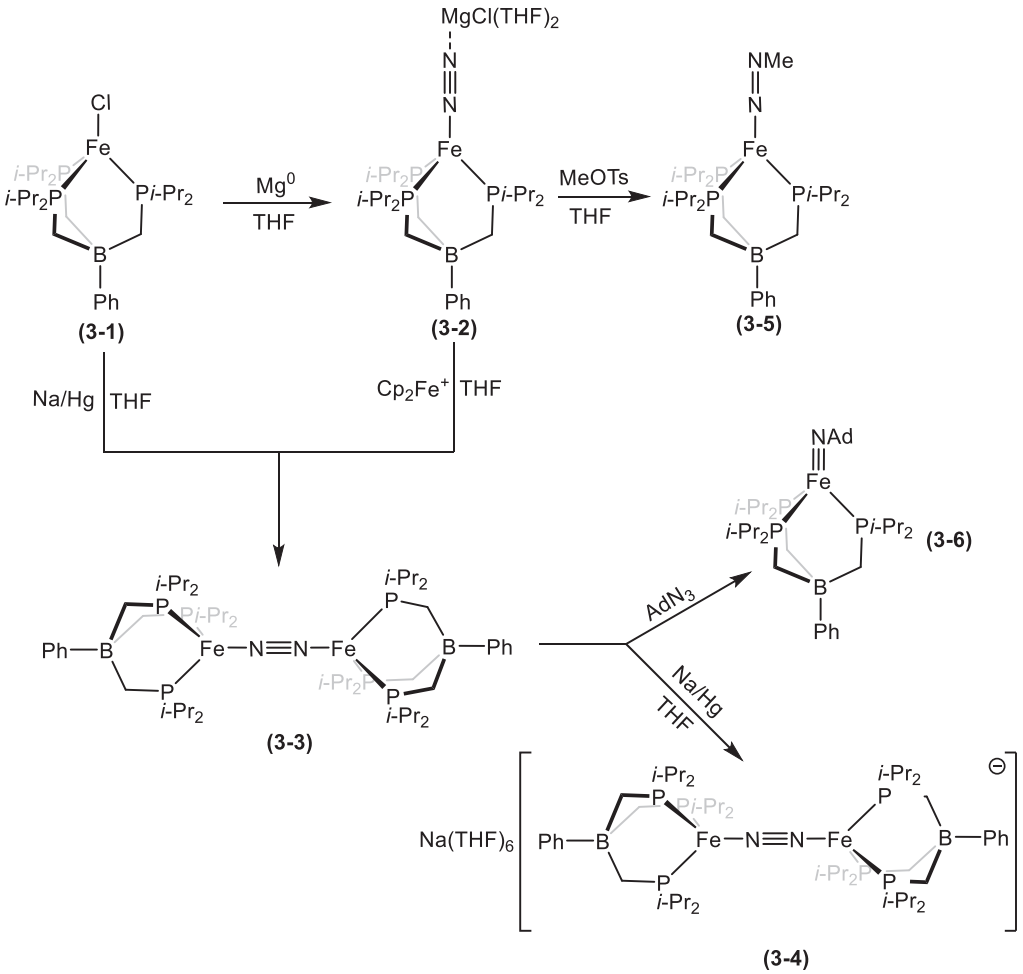

Fig. 14 Reactivity schematic for $[PhBP_3^{iPr}]Fe$ complexes. Adapted from Betley, T. A.; Peters, J. C. *J. Am. Chem. Soc.* **2003**, *125*, 10782–10783.

Along with the dinitrogen to alkyl diazene reactivity of **3–2**, Betley et al. demonstrated that the μ-1,2-dinitrogen diiron species **3–3** was a useful Fe(I) synthon; reaction of **3–3** with adamantyl azide (AdN_3) produces the (adamantylimido)iron(III) product, **3–6**. Taken together, the data and transformations accessible starting from **3–1** provided important advances in the general arena of iron dinitrogen chemistry. First, the $[PhBP_3^{iPr}]^-$ ligand can support an iron center competent for binding N_2, diazenide, and imide moieties. Second, the metal center in the $[PhBP_3^{iPr}]Fe$ fragment can readily access four formal metal oxidation states (viz. 0, I, II, III), with evidence for reactivity in two distinct redox couples $Fe^{0/II}$ and $Fe^{I/III}$. The latter couple is evidenced in the conversion of **3–3** to **3–6**, whereas the former in the conversion of **3–2** to **3–5**. Contemporary work executed on the Co congener of **3–1** revealed comparable chemistry with dinitrogen and imide complexes readily accessible.

In 2003, Schrock and coworkers successfully accomplished catalytic conversion of dinitrogen to ammonia by a molybdenum complex operating between the Mo^{III} and Mo^{VI} states in a Chatt-type cycle. Here, the η^1-dinitrogen ligand undergoes successive reduction and protonation at the distal N atom, leading to N_2 cleavage to liberate NH_3 and a $Mo^{VI}{\equiv}N$ complex.[46] Given the access to iron imide, diazenide, and dinitrogen complexes of $[PhBP_3^{iPr}]^-$, a similar cycle traversing the Fe^{I} and Fe^{IV} oxidation states seemed feasible. Starting from the $[PhBP_3^{iPr}]FeCl$ complex **3–1**, the first terminal Fe^{IV} nitride[47] **(3–7)** was isolated and spectroscopically characterized (**Fig. 15**). The nitride complex was generated by warming a $[PhBP_3^{iPr}]Fe(dbabh)$ (dbabh = 2,3: 5,6-dibenzo-7-aza bicyclo[2.2.1]hepta-2,5-diene) complex in THF to room temperature, which results in loss of anthracene from the $dbabh^-$ ligand. In the absence of an X-ray single crystal structure solution (vide infra), the ^{31}P and ^{15}N NMR spectra provided the key data in support of a terminal nitride structure of **3–7**, with the ^{15}N NMR resonance at 952 ppm being a diagnostic reporter for the terminal nitride. Attempts to crystallize **3–7** proved to be unsuccessful as the stability of **3–7** is sensitive to the solution concentration with this compound dimerizing to the dinuclear complex **3–3**. In the absence of an X-ray crystal structure, X-ray absorption spectroscopy (XAS) provided support for the purported structure of **3–7**.[48] Deconvolution of the EXAFS region of the absorbance spectrum of **3–7** evidenced a C/N scatterer located 1.52(2) Å from the iron center, consistent with a short $Fe^{IV}{\equiv}N$ bond predicted from the DFT calculations and the Fe–N vibration at 1034 cm^{-1} observed in the IR spectrum.[49]

The coupling of two metal nitride complexes to generate the dinitrogen species was previously reported for Os and Ru by Taube, Wong, and Brown,[50] but this report by Peters and coworkers was the first example of this six-electron redox process in iron chemistry. Both Fe centers are reduced formally from the Fe^{IV} to Fe^{I} states with oxidation of the nitride ligands; the *N*-ligand converts from the π-basic nitride in two molecules of **3–7** to the π-acidic N_2 in **3–3**. Efforts to thermally revert **3–3** to **3–7** were unsuccessful; however, addition of a $Mn^{V}{\equiv}N$ complex to **3–3** effects the desired transformation by acting as the oxidant, facilitating scission of the bridging N_2 moiety.

Using a cyclohexyl-substituted derivative of the $[PhBP^{iPr}{}_3]^-$ scaffold, Saouma et al. synthesized an Fe(II) acetate complex capable of coordinating N_2 and its reduced derivatives (**Fig. 16**).[51] Cooling the acetate-iron complex under dinitrogen affords a diiron complex bearing a μ-1,2-N_2 moiety **(3–9)** for which a N—N bond length of 1.120 Å and a stretching band at 2083 cm^{-1} indicate minimal N_2 activation. This complex is thermally sensitive, however, and reverts to the starting N_2-free complex upon warming to room temperature. The bound dinitrogen in **3–9** can be readily substituted with N_2H_4 at −78 °C to yield the related μ-1,2-hydrazine-bridged compounds, **3–11**. This hydrazine adduct is also thermally unstable; warming to −10 °C results in disproportionation of **3–11** to the diiron diazene complex **(3 − 10)** and monomeric Fe–NH_3 species **(3 − 12)**. Access to the diazene complex by formal oxidation is reminiscent of the earlier work by Sellmann and coworkers (vide supra). Isolation of this family of complexes signifies this platform as a potential model system for further investigation into the alternating N_2 reduction pathway.

Chomitz and Arnold synthesized another example of a 4-coordinate dinitrogen-bridged diiron complex utilizing their anionic N_2P_2 ligand, ^{t}BuNSiMe$_2$N(CH$_2$CH$_2$P^{i}Pr$_2$)$_2$. Treatment of $([N_2P_2]Fe)_2Cl$ with 1 equiv. KC_8 affords the dinuclear iron(I) dinitrogen complex $\{([N_2P_2]Fe)_2(\mu_2\text{-}\eta^1{:}\eta^1\text{-}N_2)\}$ (**Fig. 17**), in which the two iron centers adopt a tetrahedral environment bridged by an N_2 ligand.[52] The N—N bond length of 1.166(3) Å is slightly longer than the related 4-coordinate example from Peters and coworkers, complex **3–3** (1.138 Å). The N–N stretching band in the resonance Raman was observed at 1760 cm^{-1}, significantly shifted to lower energy with respect to free N_2, indicating substantial π-back donation from the iron centers to the dinitrogen ligand in $([N_2P_2]Fe)_2(\mu_2\text{-}\eta^1{:}\eta^1\text{-}N_2)$.

The tris(pyrazolyl)borate (Tp) or tris(imidazolyl)borate ligands impose similar tripodal coordination environments to the tris(phosphinomethyl)borate ligands and can access related pseudotetrahedral iron-dinitrogen species, albeit with the latter affording

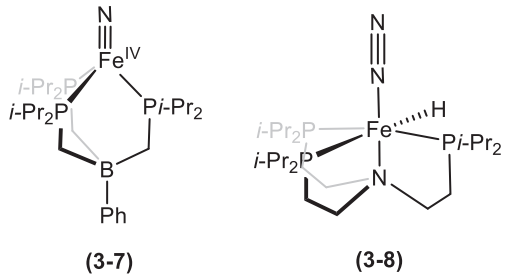

(3-7) **(3-8)**

Fig. 15 $[PhBP_3^{iPr}]Fe{\equiv}N$(7) was the first isolated terminal Fe^{IV} nitride. Adapted from Betley, T. A.; Peters, J. C. *J. Am. Chem. Soc.* **2004**, *126*, 6252–6254; MacBeth, C. E.; Harkins, S. B.; Peters, J. C. *Can. J. Chem.* **2005**, *83*, 332–340.

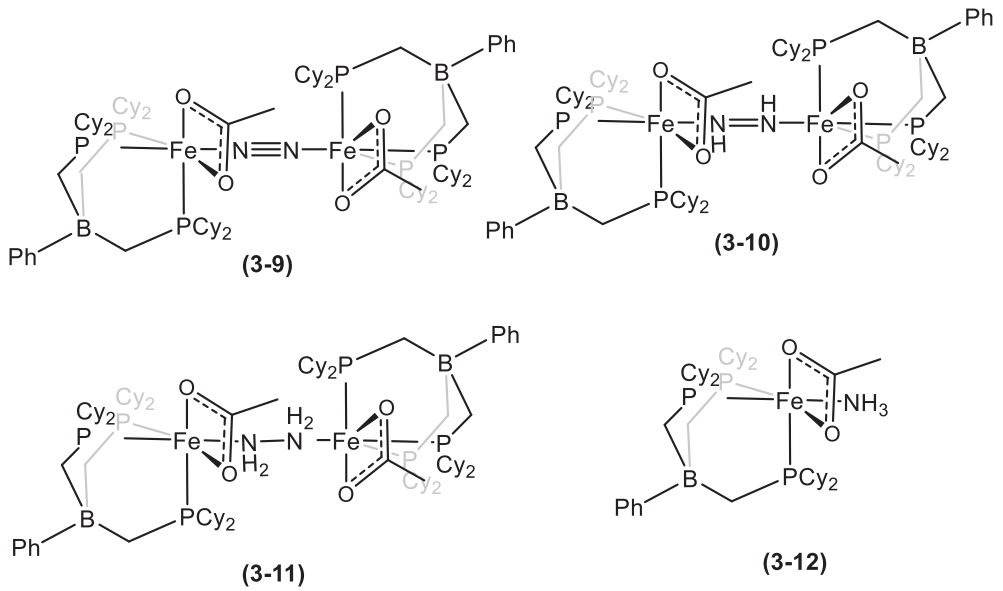

Fig. 16 A suite of N_2 reduction complexes stabilized by a pseudotetrahedral BP_3 ligand. Adapted from Saouma, C. T.; Moore, C. E.; Rheingold, A. L.; Peters, J. C. *Inorg. Chem.* **2011**, *50*, 11285–11287.

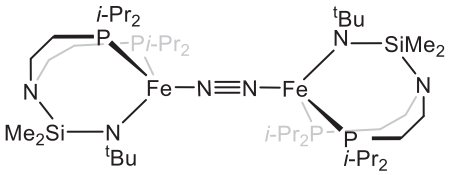

Fig. 17 A pseudotetrahedral diiron-N_2 complex. Adapted from Chomitz, W.A.; Arnold, J. *Dalton Trans.* **2009**, 1714–1720.

a stronger ligand field compared to the former. Despite the widespread and longstanding use of Tp ligands in synthetic inorganic chemistry, the report by McSkimming and Harman in 2015 was the first example of a Tp-ligated iron-dinitrogen complex.[53] Varying the substituents on the Tp ligand allowed for control of the nuclearity of the species. The phenyl substituents allowed access to the μ-1,2-dinitrogen diiron complex (**3 − 13**) whereas the more encumbering adamantyl-substituted ligand affords the mononuclear η^1-dinitrogen species (**3–14**). Notably, EPR measurements of **3–14** demonstrate that the ground state is $S = 3/2$, which was the first example of a terminally-ligated high-spin iron(I)-dinitrogen species. Comparison of the vibrational spectroscopic data for **3–14** (IR) and **3–13** (Raman) evidence substantial activation of the N_2 ligand, with that for the μ-1,2-dinitrogen observed at 1779 cm^{-1} being lower in energy than for the terminal N_2 at 1959 cm^{-1}. As one might anticipate, the N—N bond distances observed by X-ray crystallography are consistent with the vibrational data with values of ∼1.119 and ∼1.180 Å for **3–14** and **3–13**, respectively. Cummins et al. reported the related diiron-(μ-1,2-N_2) complex utilizing the Tp scaffold bearing *tert*-butyl substituents (**3–15**).[54] This complex, however, exhibits dynamic interconversion between the μ-1,2-dinitrogen-diiron and the terminal monoiron dinitrogen species, based on IR spectra collected in solution and on solid samples and EPR spectra recorded under vacuum or an N_2 atmosphere. As with the compounds reported by Harman and coworkers, the iron(I) centers are high-spin and the N_2 ligand is similarly activated if one compares the crystallographic N—N bond distance in **3–15** to that in **3–13**, and the solid-state IR absorption at 1967 cm^{-1} for **3–15** (proposed to arise from the monoiron species) to that for **3–14**. Based on the spectroscopic data, the N_2 ligand in the Tp complexes is nominally more activated than those for the related tris(phosphinomethyl)borate compounds **3–3** and **3–4** (Fig. 18).

Smith and coworkers used a tris(imidazolyl)borate ligand scaffold to synthesize an Fe(IV)-nitride complex **3–16**,[55] which bears a strong resemblance to the nitride species **3–7**; however, **3–16** can be crystallographically-characterized and is not susceptible to dimerization to the dinitrogen complex. In a later report, Hickey et al. prepared an Fe(II)–N_2 complex starting from the mesitylene-substituted tris(imidazolyl)borate iron hydridophenylphosphide complex; insertion of the PHPh ligand into the *ortho*-methyl C—H bond of a mesityl substituent on one of the carbene arms of the ligand under a N_2 atmosphere affords compound **3–18**.[56] The isolated S = 0 complex displays a minimally activated N_2 moiety (1.105 Å, $\nu_{NN} = 2105$ cm^{-1}) and can be thermally decomposed with expulsion of H_2 and concomitant Fe—C bond formation to a second mesityl arm (**3–18**) (Fig. 19).

Related to the tripodal system reported by Smith and coworkers, a tris-*N*-heterocyclic carbene high-spin Fe–N_2 complex was reported by Deng and coworkers in which congeners with iron in the 2+, 1+, and 0 oxidation states are isolable.[57] Addition of 6 equiv. ICy (ICy = 1,3-biscyclohexylimidazolylidene) and 2 equiv. $NaBH_4$ to a THF solution of Fe(tmeda)Cl_2 (tmeda = *N,N,N′,N′*-tetramethylethylenediamine) followed by reduction with KC_8 yielded the Fe(I)–N_2 complex bearing three

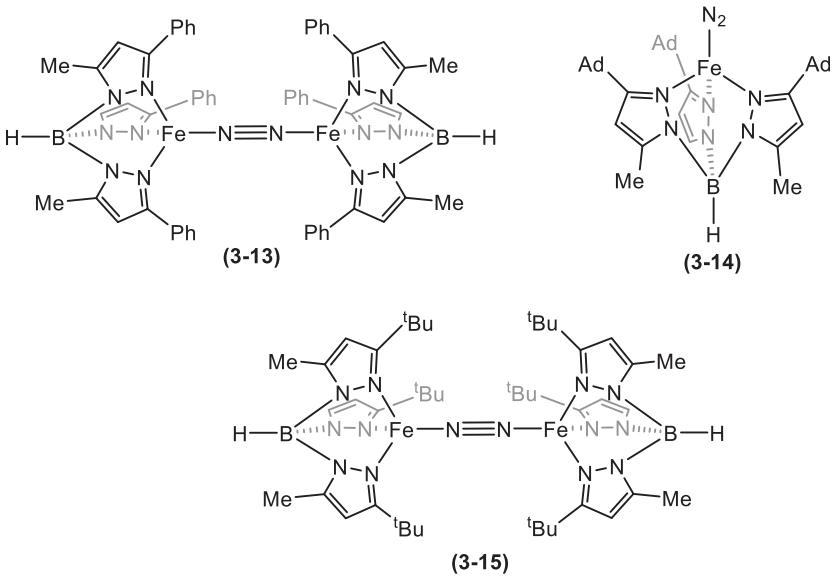

Fig. 18 *Top*: Harman's (Tp)Fe–N_2 complexes. *Bottom*: Theopold's (Tp)Fe–N_2 dinuclear complex. Adapted from McSkimming, A.; Harman, W. H. *J. Am. Chem. Soc.* **2015**, *137*, 8940–8943; Cummins, D. C.; Yap, G. P. A.; Theopold, K. H. *Eur. J. Inorg. Chem.* **2016**, 2349–2356.

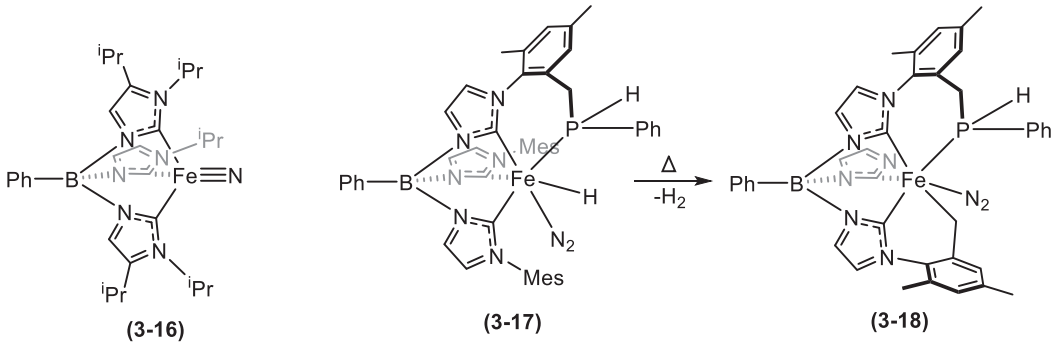

Fig. 19 Unique [PR] insertion into a C–H bond is observed in this Fe–N_2 system. Adapted from Scepaniak, J. J.; Fulton, M. D.; Bontchev, R. P.; Duesler, E. N.; Kirk, M. L.; Smith, J. M. *J. Am. Chem. Soc.* **2008**, *130*, 10515–10517; Martinez, J. L.; Lin, H.-J.; Lee, W.-T.; Pink, M.; Chen, C.-H.; Gao, X.; Dickie, D. A.; Smith, J. M. *J. Am. Chem. Soc.* **2017**, *139*, 14037–14040; Hickey, A. K.; Muñoz III, S. B.; Lutz, S. A.; Pink, M.; Chen, C.-H.; Smith, J. M. *Chem. Commun.* **2017**, *53*, 412–415.

ICy ligands **3–19** (Fig. 20). The Fe center exhibits a distorted tetrahedral coordination geometry with N_2 coordinated in an end-on mode (1.112 Å). The N–N stretching band occurs at 1967 cm^{-1}, lower than that reported by Hickey et al. as expected for the differences in iron formal oxidation states.

In contrast to the low-spin complex **3–17**, however, Mößbauer spectra, magnetic moment, and Fe–C_{NHC} bond lengths are indicative of a high-spin Fe(I) center in **3–19**. Further reduction by KC_8 in THF resulted in the isolation of the Fe(0) congener **3–19′** in which the N–N bond of 1.138 Å is slightly elongated and the energy of the N–N stretching band (viz. 1853 and 1841 cm^{-1}) is

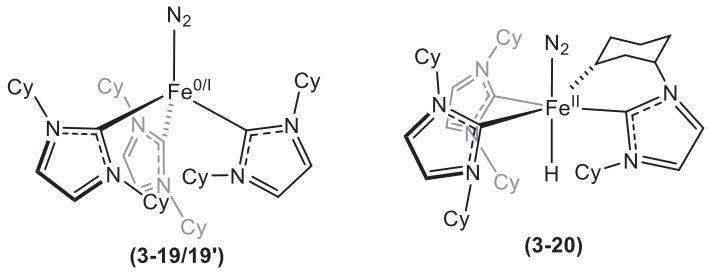

Fig. 20 A tri-NHC ligated Fe–N_2 family of complexes. Adapted from Ouyang, Z.; Cheng, J.; Li, L.; Bao, X.; Deng, L. *Chem. Eur. J.* **2016**, *22*, 14162–14165.

decreased relative to **3–19**. The Fe(II) analog, which results from oxidative addition across a C–H bond of a cyclohexyl substituent, exists in equilibrium with the Fe(0) complex in solution and observed in the solution-phase IR spectrum of the Fe(0) complex (**3 − 20**). The solid-state structure of the Fe(II) complex revealed the formation of a metal-hydride bond. The N–N stretching frequencies observed in this family of complexes are among the lowest observed for the broader family of pseudo-tetrahedral iron-dinitrogen species, hinting at the potential importance of the strong σ-donor properties of the interstitial carbide of FeMoco in facilitating N_2 activation. However, the electronic effects imparted by a μ_6-carbide are expected to differ significantly from that of an *N*-heterocyclic carbene donor.

8.26.3.1.2 Incorporating a trans*-axial donor: EP_3-ligated Fe centers (E = B, C, Si, N, Al, P)*

Contemporaneous with these initial reports of N_2 coordination and activation by low-valent iron centers using the tripodal tris-sphosphine ligands was the observation of electron density consistent with a light atom at the interstitial site μ_6 site of FeMoco in high-resolution X-ray crystallographic data.[16a] Such a light atom would result in a trigonal pyramidal coordination environment for each of the belt Fe centers. Indeed, later work from the groups of Rees, DeBeer, and Ribbe provided the strongest evidence for a central C donor at this site.[16c,17b,c] Incorporation of a donor atom at the anionic B atom and extending the P-to-heteroatom linker by one methylene unit would allow access to phosphine analogs of tris(2-aminoethyl)amine (tren); the tren platform allowed ready access to the trigonal pyramidal complexes in the molybdenum system reported by Schrock and coworkers. Thus, the $[PhBP_3^{iPr}]^-$ system evolved to a series of pseudo or potentially trigonal pyramidal architectures, wherein the axial donor was systematically varied from N to Group 13 and 14 donor atoms. Using the work of Sacconi and coworkers (vide supra) as a starting point, an Fe^{II}–N_2 complex was synthesized, supported by the tetradentate NP^{iPr}_3 ($NP^{iPr}_3 = N(CH_2CH_2P(^iPr)_2)_3$) ligand scaffold, which was the first member of this family of complexes. Reacting the cationic $(NP^{iPr}_3)FeCl$ complex with $Li[BEt_3H]$ in THF produces the diamagnetic cationic species $[(NP^{iPr}_3)Fe(H)(N_2)]^+$ (**3–8**).[58a] Complex **3–8** (**Fig. 15**) was characterized by X-ray crystallography and IR spectroscopy; IR spectra evidence a weakly activated N_2 ligand ($\nu_{NN} = 2087\ cm^{-1}$) which agrees with the crystallographically-measured N–N bond length of 1.114 Å. Attempts to generate the Fe^I–N_2 adduct of this ligand were unsuccessful, preventing a direct comparison of the effects of the axial donor atom (N vs. a proximal borate) on N_2 activation.

Seemingly in lockstep with the confirmation of FeMoco as a carbide-centered cluster and after the reported challenges accessing an Fe^I–N_2 moiety with the NP_3 ligand, Peters and coworkers reported the low-valent iron complexes of the silicide analog of the NP_3 ligand.[58b] Exposing a benzene solution of a tris(phosphino)silane, $HSiP^{Ph}_3$ ($P^{Ph}_3 = 2\text{-}Ph_2PC_6H_4$) to mesityliron(II) at 65 °C yields $[(SiP^{Ph}_3)FeMes]$ (**3–21**) (Mes = 2,4,6-trimethylphenyl). This intermediate is converted to the Fe^I–N_2 target in two steps (**Fig. 21**): protonolysis with HCl affords the iron(II) chloride compound, which can then be reduced with Na/Hg in THF to yield $(SiP^{Ph}_3)Fe(N_2)$ (**3–22**). This terminal Fe^I–N_2 complex has a short N–N bond of 1.106(3) Å, consistent with the observed weakly shifted N–N stretching frequency ($\nu_{NN} = 2041\ cm^{-1}$). Reduction of **3–22** with Na/Hg in the presence of 12-crown-4 results in the anionic Fe^0–N_2 congener (**3–23**), which exhibits the expected greater activation of the bound N_2 ($\nu_{NN} = 1965\ cm^{-1}$) arising from increased backbonding from the more electron-rich iron(0) center. Substitution of the phenyl groups for isopropyl groups on the phosphine

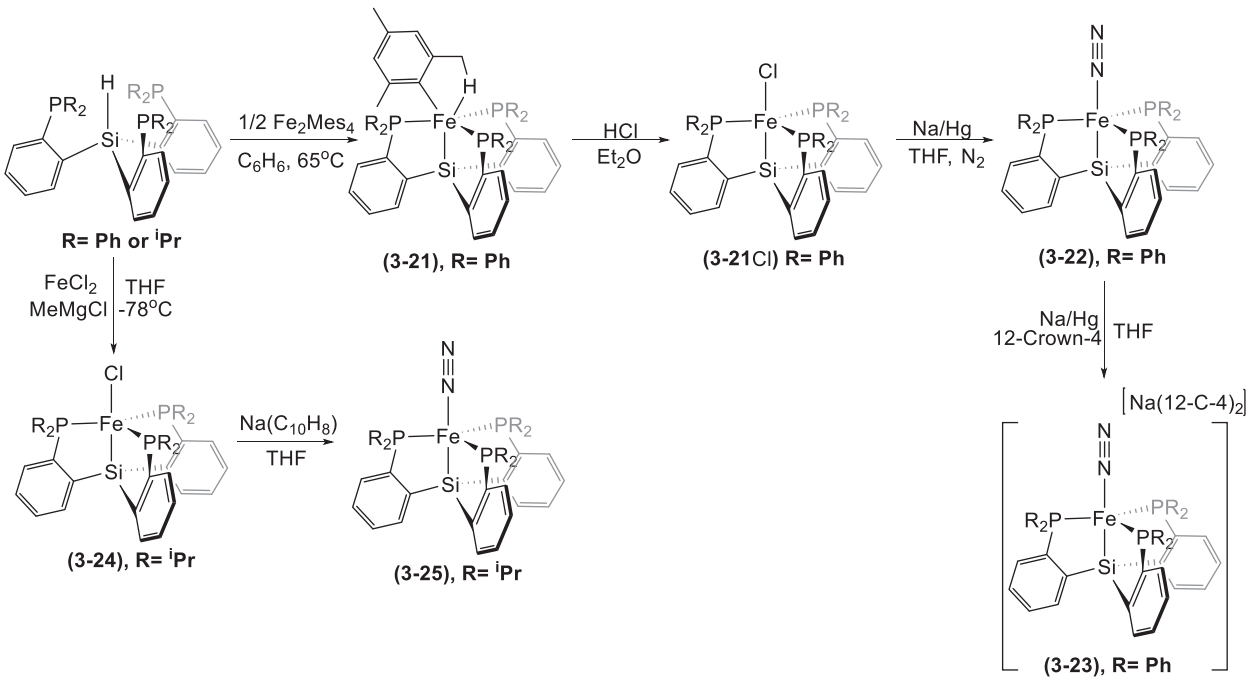

Fig. 21 Synthetic scheme of Peters' Fe^I–N_2 SiP_3 complexes. Adapted from Mankad, N. P.; Whited, M. T.; Peters, J. C. *Angew. Chem., Int. Ed.* **2007**, *46*, 5768–5771.

arms (viz. $HSiP^{iPr}_3$) required a minor variation in the synthetic route to the analogous Fe^I–N_2 species (Fig. 21). The Fe^I–N_2 complex **3–25** was accessed by reducing **3–24** with $Na(C_{10}H_8)$; IR spectra of **3–25** displayed a N–N stretching vibration at 2008 cm^{-1}, which implies a more activated N_2 ligand than the closely related **3–22** and consistent with the iPr vs. Ph substituent on the P donor atom.

Subsequent reactivity studies of the iron complexes of these two related $[SiP^R_3]^-$ ligands elucidated the likely consequences of the minor differences in donor strengths and sterics resulting from the phosphine substituents. Methyl-coordinated analogs (**3–26**) to **3–21Cl** and **3–24** were treated with the strong acid $[H(OEt_2)_2][BAr^F_4]$ to produce the cationic THF-adducts **3–27** in both cases. Only for the $(SiP^{iPr}_3)Fe(THF)$ complex, however, is the coordinated solvent molecule sufficiently labile to be readily replaced by dinitrogen, yielding a cationic Fe^{II}–N_2 complex (**3–28**). Complex **3–28** can be synthesized independently by protonating either complex **3–22** or **3–25** with H_2 formation as a reaction byproduct (Fig. 22). Further highlighting the differences in the effect of phosphine substituents on the reactivity of the iron-dinitrogen species, **3–28** (**R = iPr**) could be reduced with sodium naphthalenide, $Na[C_{10}H_8]$, to afford the iron(0) complex, $[Na(THF)_3][SiP^{iPr}_3Fe(N_2)]$ (**3 − 30**). Encapsulation of the Na^+ counterion by 2 equiv. of 12-crown-4 yielded $[Na(12\text{-crown-}4)_2][SiP^{iPr}_3Fe(N_2)]$, **3–31**. The crystal structures acquired for complexes **3–25**, **3–28**, **3–30**, and **3–31** were the first set of terminally bound N_2 complexes of any transition metal in three separate oxidation states ($Fe^{0,I,II}$).[59] As expected, lowering the valence state on the iron center consequently increased activation of the terminally-coordinated N_2 ligand with values of 2143 cm^{-1} (**3–28**), 2003 cm^{-1} (**3–25**), 1891 cm^{-1} (**3–30**), and 1920 cm^{-1} (**3 − 31**). Notably, the energy of the N–N vibration is lower for **3–30** as compared to **3–31** likely arising from the push-pull effect of the Lewis acidic sodium cation associated with the distal N atom. In addition to the spectroscopic differences, structural changes are observed for the complexes, such as the shortening of the Fe−N and Fe−Si bonds as the metal formal oxidation state decreases.

The phenyl and isopropyl congeners of the $(SiP^R_3)Fe$ compounds could also be readily derivatized to several Fe–N_2H_x complexes. The hydrazine adducts, $[SiP^R_3Fe^{II}(N_2H_4)][BAr^F_4]$ (R = Ph, iPr), were prepared by exposing the cationic THF (**3–27**) or N_2 (**3–28**) adducts to hydrazine or, alternatively, by slow addition of hydrazinium triflate ($N_2H_5CF_3SO_3$) producing the

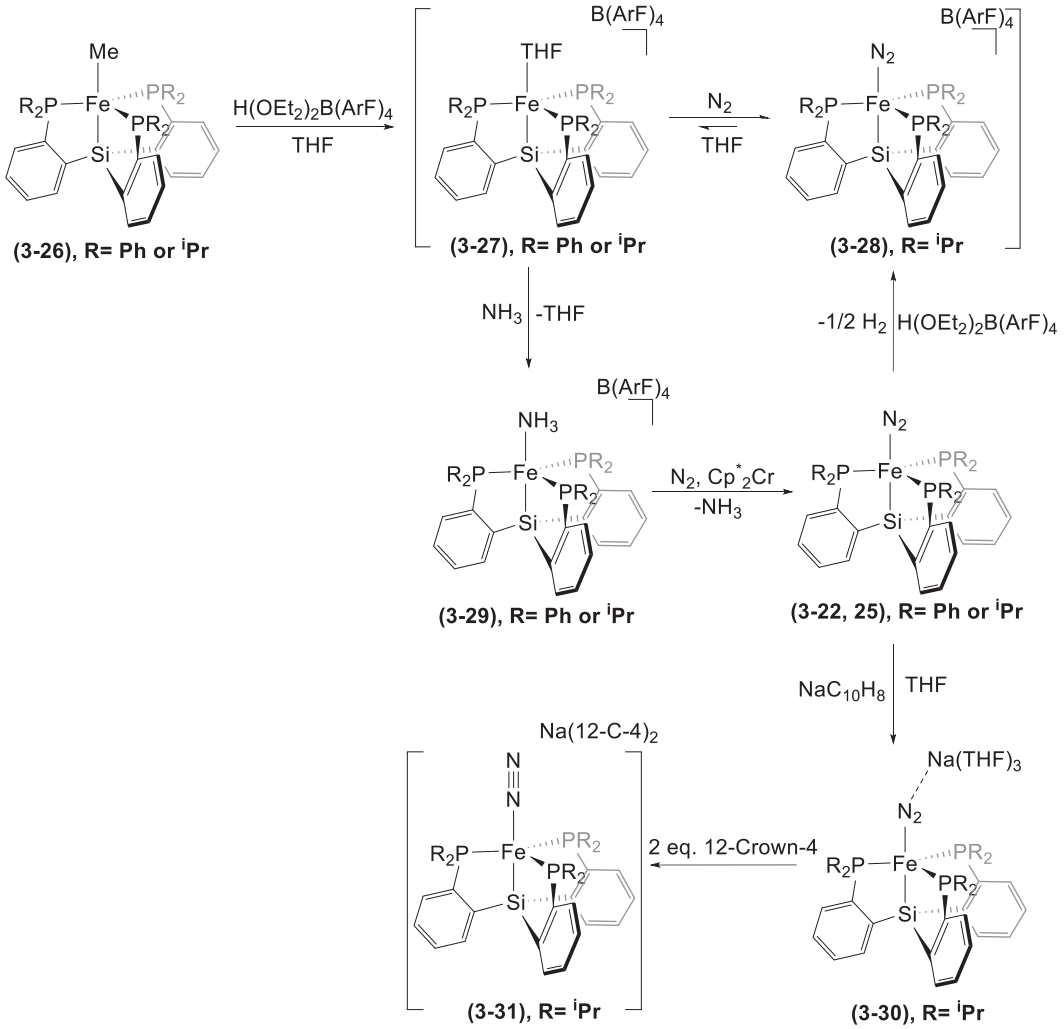

Fig. 22 The $[SiP_3]$ ligand scaffold houses myriad Fe–N_2 complexes of varying degrees of N_2 activation. Adapted from Lee, Y.; Mankad, N.P.; Peters, J.C. *Nat. Chem.* **2010**, *2*, 558–565.

analogous hydrazine compounds; few complexes containing an η^1-hydrazine have been reported.[60] In the vein of Sellmann's report of oxidative conversion of hydrazine to diazene at iron centers, attempts to oxidize the hydrazine adducts to the iron-diazene (HN=NH) species were unsuccessful, which was attributed to the lability of the hydrazine as it is readily replaced by a triflate anion upon oxidation. The lability of N_2H_4 also led to challenges synthesizing the iron-hydrazide ($N_2H_3^-$) complex by deprotonation of the coordinated hydrazine. Interestingly, however, reaction of $[(SiP^{Ph}_3)Fe(\eta^1\text{-}N_2H_4)][OTf]$ with a stoichiometric equivalent of N^1,N^1,N^8,N^8-tetramethylnaphthalene-1,8-diamine leads to an intramolecular rearrangement in which one phosphine arm is oxidized to a formally P^V by insertion of NH, from the coordinated N_2H_4, to yield the paramagnetic Fe–NH_3 complex (**3–34**) (Fig. 23). Completing the proposed cycle of potential intermediates along an N_2 reduction pathway, two Fe–NH_3 complexes (**3–29**) were accessed from the THF complex **3–27** (R = Ph) or N_2 complex **3–28** by addition of a THF solution of NH_3 (Fig. 22). Interestingly, only **3–29** was isolable whereas the corresponding Fe^I–NH_3 was not, suggesting that NH_3 can only coordinate to the $(SiP^R_3)Fe$ platform when iron is in the +2 oxidation state. Indeed, this hypothesis is validated by the quantitative release of NH_3 upon reduction of **3–29** and reversion to the Fe^I–N_2 complexes **3–22** or **3–25** (Fig. 22). These data provide evidence for the feasibility of a Fe^I–N_2 catalyst for NH_3 production as the recovery of **3–22** (or **3–25**) would be a key requirement for catalytic turnover. Further support for a possible Fe^I–N_2 catalyst was accomplished by isolation of the N_2 complexes upon reduction of the corresponding iron-hydrazine adducts (**3–32** and **3–33**). The terminal hydrazide complex remained elusive for the SiP^R_3 system; however, inclusion of a Lewis acid (viz. $B(C_6F_5)_3$ or BCF) allowed for isolation of the μ-hydrazide species. Addition of the BCF-N_2H_3 adduct to a solution of **3–26** yielded the neutral zwitterionic complex (**3–35**), which was characterized by X-ray crystallography, ^1H and ^{19}F NMR spectroscopy. The BCF stabilizes the otherwise labile $N_2H_3^-$ ligand through unusual hydrogen bonds between one of the *ortho*-fluorine atoms on the BCF ring and hydrogen atoms on both N_α and N_β of the coordinated hydrazide ligand (Fig. 24).

As observed in the trigonal tris(phosphinomethyl)borate system, direct functionalization of the dinitrogen complex provided a route to the corresponding diazenide complex (Fig. 25). Reduction of complex **3–25** with Na/Hg in the presence of trimethylsilyl (TMS) chloride affords the desired diazenide product (**3–36**). Complex **3–36** displays an N–N stretching frequency of 1748 cm^{-1}, significantly higher in energy than that observed in the pseudo-tetrahedral complex **3–5** (viz. 1597 cm^{-1}). Diazenide compound **3–36** can also be generated from the iron(0)-dinitrogen -ate complex **3–30** by reaction with Me_3SiCl or Me_3SiOTf in a frozen THF solution, implying that the reaction proceeds through complex reduction prior to reaction with the silyl cation source (Fig. 25). Interestingly, **3–36** is diamagnetic in contrast to the analogous phenyl-diazenide complex having a $S = 1$ ground state; this difference in ground state spin multiplicity is due to increased backbonding (cf. phenyl-diazenide complex, a d^6 iron complex) from the d^8 iron center into the empty π^* orbital on the coordinated N_2SiMe_3 moiety.

Although the $[SiP^R_3]^-$ ligand scaffold was able to support a diverse portfolio of complexes containing Fe—N single bonds, complexes containing Fe—N multiple bonds in a trigonal bipyramidal geometry were not accessible. The inability to synthesize such compounds is attributed to low-lying Fe–N π^* orbitals, which are readily populated upon reduction and destabilize the desired iron-nitrogen multiple bond.[61] If one also considers the chemistry of **3–5** in which the axial donor *trans* to the N_2 is absent, varying the identity of the donor atom at the silicide site can modulate the electron density at the Fe center to favor stronger Fe—N π-interactions and allow for isolation of Fe—N multiple-bonded species.

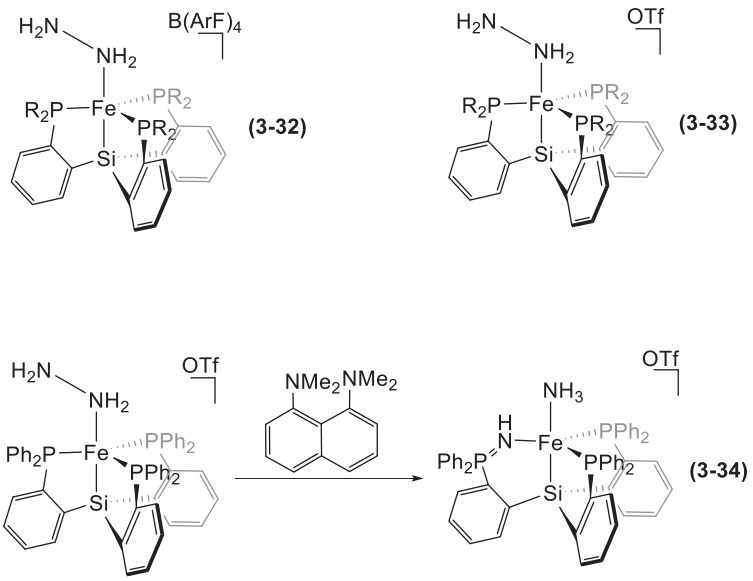

Fig. 23 Isolated iron-hydrazine complexes in the SiP^R_3 ligand scaffold. Adapted from Lee, Y.; Mankad, N.P.; Peters, J.C. *Nat. Chem.* **2010**, *2*, 558–565.

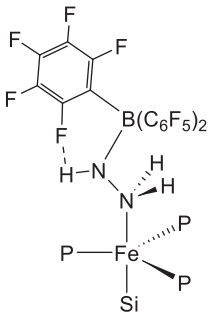

(3-35)

Fig. 24 A simplified core structure of **3–35** showing only one of the BCF–N_2H_3 hydrogen bonding interactions. Remaining H-bond interactions omitted for clarity. Adapted from Lee, Y.; Mankad, N.P.; Peters, J.C. *Nat. Chem.* **2010**, *2*, 558–565.

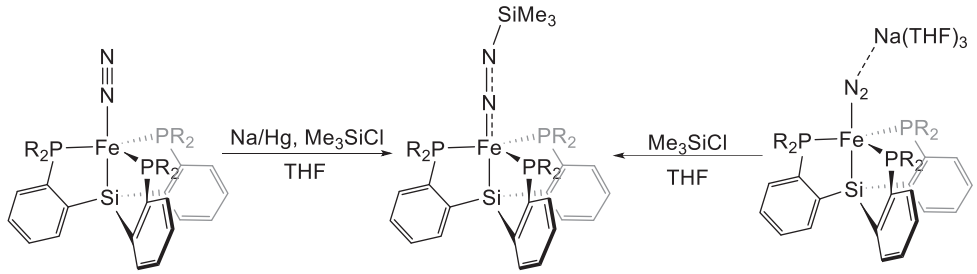

(3-25), R= ^{i}Pr (3-36), R= ^{i}Pr (3-30), R= ^{i}Pr

Fig. 25 Preparation of the TMS-functionalized diazenido complex was performed under two different sets of conditions. Adapted from Lee, Y.; Mankad, N.P.; Peters, J.C. *Nat. Chem.* **2010**, *2*, 558–565.

Using the same basic architecture as the $[SiP^{R}_{3}]^{-}$ scaffold, a tris(phosphino)borane[62] (BP^{iPr}_{3} or TPB) was synthesized in which the more donating Si^{-} apical site was replaced by the Lewis acidic B atom. An iron(0)-dinitrogen complex (**3–37**) was isolated in this BP^{iPr}_{3} ligand (Fig. 26) by reduction of an iron(I) bromide precursor with sodium naphthalenide under N_2.[63] Only a partial structure solution was possible for **3–37**, precluding an accurate measure of the N–N distance; however, the strong isotope-sensitive IR absorption at 2011 cm^{-1} evidences partial activation of N_2 ligand. Alternatively, two-electron reduction of the iron(I)

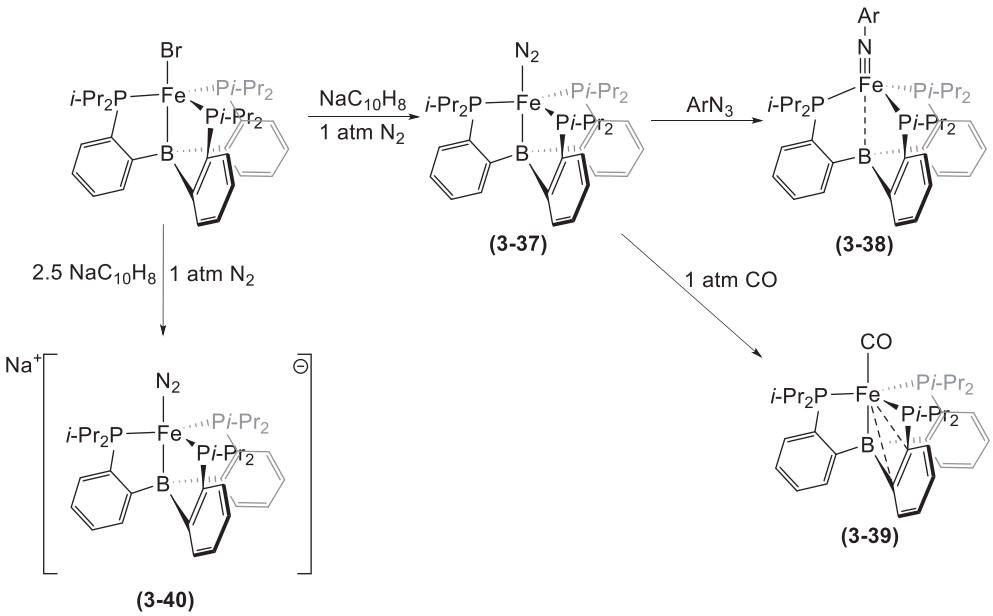

(3-37) (3-38) (3-40) (3-39)

Fig. 26 The TPB ligand scaffold provides support for several trigonal bipyramidal Fe–N_2 complexes as well as a pseudotetrahedral Fe(II)-imido complex. Adapted from Moret, M.-E.; Peters, J. C. *Angew. Chem. Int. Ed.* **2011**, *50*, 2063–2067.

bromide complex resulted in the formation of the iron-dinitrogen -ate complex, **3–40**. Two bands in the unsaturated region at 1918 and 1877 cm^{-1} are observed in IR spectra of **3–40**, which are assigned as the N–N stretches for the free anionic $[Fe{-}N{\equiv}N]^-$ complex and the Na^+-capped $[Fe{-}N{\equiv}N]^-$ ion pair (cf. **3–30** and **3–31**). Indeed, the Na–N_2 interaction is supported by IR spectra of **3–40** in the solid state (1879 cm^{-1}) and in the less coordinating solvent Et_2O (1862 cm^{-1}). The N_2 vibration in the absence of the bound Lewis acid was confirmed by IR spectroscopy after addition of 12-crown-4 ether to a THF solution of **3–40** (1918 cm^{-1}). Additionally, crystal structures were successfully obtained for both forms of **3–40**. The structures of both forms showed slightly distorted trigonal bipyramidal geometries at the iron centers, arising from Jahn-Teller distortions from the three-electron occupation of the degenerate d_{xy} and $d_{x^2} - y^2$ orbitals.

The isolation of **3–40** provided evidence that the TPB-Fe complexes could support one-electron redox processes for the iron-dinitrogen complexes, but did not provide any differentiation from the $[SiP^R_3]Fe$ complexes. To that end, reaction of the neutral Fe^0–N_2 complex (**3–37**) with an aryl-azide (Ar = *p*-methoxyphenyl) affords the diamagnetic aryl-imide complex (**3–38**). The structure of **3–38** displayed an Fe—N bond distance of 1.668 Å—only slightly longer than that for the pseudotetrahedral imide complex **3–6** (1.651 Å)—suggesting the assignment of a d^6 imido-iron complex as valid. The geometry at the iron center in **3–38**, however, is pseudotetrahedral and significantly distorted from the starting trigonal bipyramidal geometry. Consideration of the orbital splitting diagrams for complexes of the BP^R_3 ligand illustrates the effect of electron count and axial ligand on the geometry of the TPB–Fe complexes (**Fig. 27**). In the most reduced species **3–40**, the Z-type interaction from the iron center to the B atom is strongest, which contracts the Fe—B bond length and pulls the iron into the pocket of the ligand and in plane of the three phosphorous sites. The pseudo trigonal bipyramidal arrangement also maximizes the in-plane bonding interactions between the P donors and the Fe center, increasing the energy of the frontier orbitals of d_{xy} and $d_{x^2} - y^2$ parentage and decreasing the energy of the M–N_2 π-bonding orbitals. Oxidation of the complex compresses the energy separations between the frontier orbitals with weakening of the Fe—P and Fe—B bonding interactions as well as the Fe—N_2 π-bonds. Substitution of the π-acidic N_2 to bromide with further oxidation extends this trend, giving rise to occupation of all frontier molecular orbital of d parentage and the observed high spin state for this complex. For the imide complex, however, the strongly σ- and π-donating imide dominates the ligand field, raising the energies of the Fe–N π* orbitals derived from d_{xz} and d_{yz} iron atomic orbitals. Similarly, the relative energies of molecular orbitals derived from the σ-type atomic orbitals along the B–Fe–N axis are strongly influenced by the change from the weakly σ-donating N_2 to the imide, with the effect being a destabilization of the orbital of significant Fe—B σ-bonding character. Here, the Fe—B bond provides electronic flexibility as the complex cycles through oxidation states and from N_2 to the imide.

The functionalization of the N_2-ligand on complex **3–40** was further explored to illustrate the ability of the TPB scaffold to support species with metal-nitrogen multiple bond character. Complex **3–40** was treated with Me_3SiCl to yield the TMS-capped diazenide complex (**3–41**). The in situ reduction of the iron bromide precursor in the presence of Me_3SiCl, however, affords only a minor yield of **3–41**, with the major species being **3–42**, which is the one-electron reduction product of **3–41**. A significantly elongated N—N bond of 1.260(3) Å and an η^3-interaction with one of the phenylene linkers are observed in the solid-state structure of **3–42** (**Fig. 28**). Addition of an excess of 12-crown-4 reverts the compound to the Fe–N_2 species **3–40** with release of hexamethyldisilane and encapsulation of the Na cation by two crown ether molecules. This redox pathway is not available in the $[SiP^R_3]^-$ system, highlighting the significance of the flexibility of the TPB ligand system relative to its participation in Fe–N_x redox chemistry. The TPB–FeN_2 complexes could also be functionalized by reacting the disilylating agent 1,2-bis(chlorodimethylsilyl)ethane, in lieu of Me_3SiCl, and Na/Hg amalgam with the Fe(I)–Br complex, yielding the disilyl-hydrazide complex **3–43**. ^{31}P and ^{11}B NMR were used to elucidate the structure of **3–43** with resonances at chemical shifts comparable to the imido complex **3–38** observed in the NMR spectra. DFT calculations suggested iron-nitrogen triple bond character in the optimized geometry and the calculated frontier orbitals are strikingly similar to those calculated for **3–38**.

The holistic changes observed for the N—N bond lengths, N—N stretching frequencies, and Fe—N bond lengths, as one progresses from **3–40** to **3–43** are consistent with increased population of the N—N π^* orbital and formation of Fe—N multiple bonds. As such, these compounds provide the outline for a potential iron-based Chatt cycle for N_2 activation with the silyl substituents viewed as proton surrogates.[64]

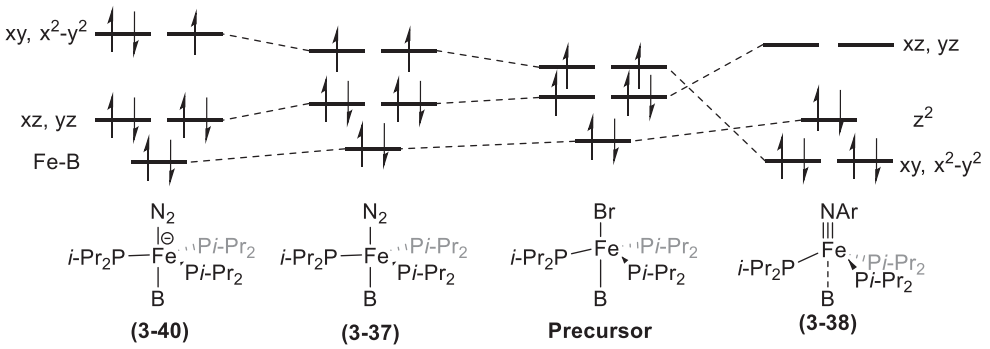

Fig. 27 Orbital splitting diagram of the relevant BP^{iPr}_3Fe complexes. Energy axis not scaled. Adapted from Moret, M.-E.; Peters, J. C. *Angew. Chem. Int. Ed.* **2011**, *50*, 2063–2067.

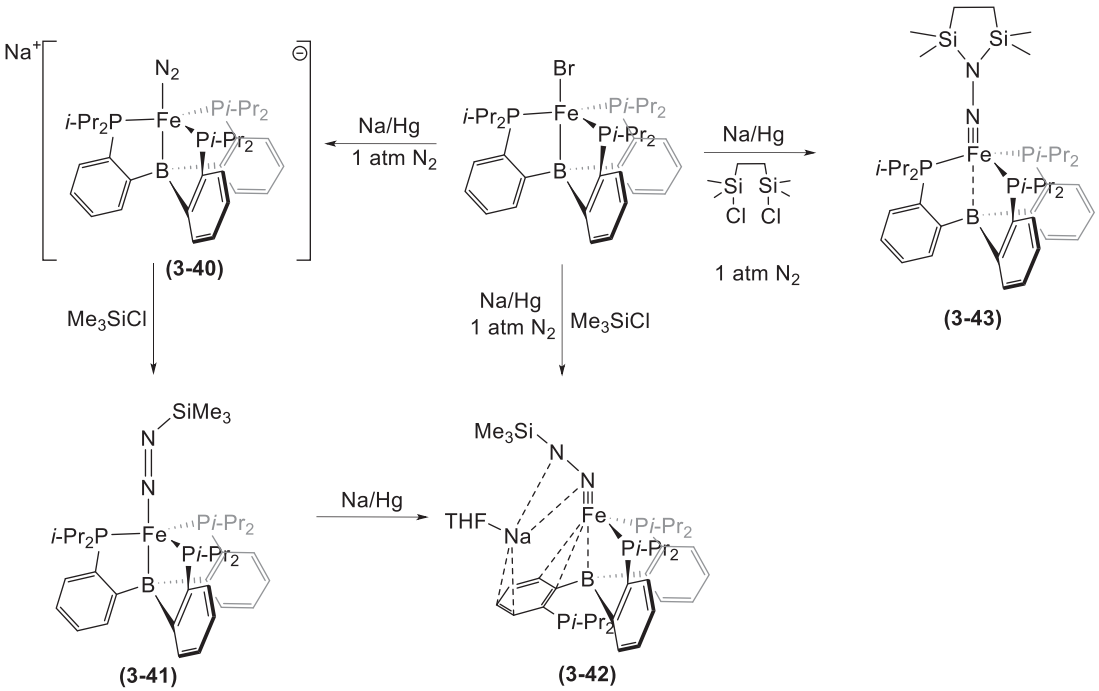

Fig. 28 The series of functionalized (TPB)Fe–N_2 products shows similarities to the Chatt cycle. Adapted from Moret, M.-E.; Peters, J. C. *J. Am. Chem. Soc.* **2011**, *133*, 18118–18121.

Secondary coordination sphere effects were investigated by Creutz and Peters using an analog of the $[SiP^R_3]^-$ ligand platform (Fig. 29).[65] Installation of one or three pendant azaphosphine ring(s) into the $[SiP^R_3]^-$ framework yielded a ligand primed for intramolecular hydrogen bonding interactions with the axially-bound substrate. An Fe(II) chloride precursor was reduced using Na/Hg to produce the corresponding Fe(I)–N_2 complexes (**3–44** and **3–44′**). The N_2 units of **3–44** and **3–44′** were virtually equivalent with stretching frequencies of 2005 and 2007 cm^{-1}, respectively, and independent of the number of pendant hydrogen-bonding groups. Addition of hydrazine or ammonia following oxidation of **3–44** (or **3–44′**) led to the formation of the corresponding Fe–N_xH_y adducts. Relatively strong hydrogen bonds occur between the pendant amine(s) and the coordinated N_xH_y and the azaphosphine rings undergo a conformational change to the less-favored boat conformation.

DFT calculations estimate the stabilization energy gained from each hydrogen bond to be moderately strong with computed energies of ~4.1 kcal/mol per bond. Reduction of **3–44** and **3–44′** with Na/Hg produce similar results, but with different solid-state structures. The product from reduction of **3–44** exhibits intermolecular coordination of a sodium cation to afford an infinite chain (Fig. 30), whereas the structure of reduced **3–44′** is a monomeric structure with intramolecular coordination of a sodium cation between the pendant amine and the N_β of the bound N_2. Catalysis investigations demonstrated that these reduced complexes, despite the presence of potential secondary sphere assistance, showed no catalytic activity as no NH_3 was detected in the reaction products. This lack of catalytic reactivity is proposed from computational methods to arise from a change in the preferred site of protonation. The bound N_2 is preferred over the metal center in the $[SiP^{iPr}_3]^-$ complex, whereas the pendant amines facilitate proton transfer from the N_2 to the Fe center by the pendant amines, forming a catalytically inert Fe–H species.

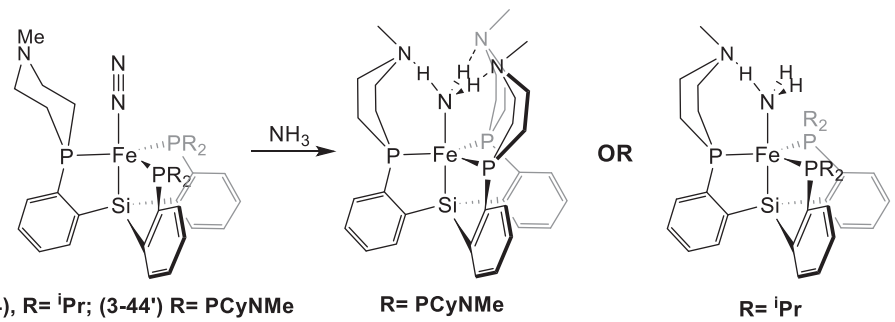

Fig. 29 Utilizing secondary-coordination sphere effects for N_2 activation by complexes in a $[SiP_3]$ scaffold. Adapted from Creutz, S. E.; Peters, J. C. *Chem. Sci.* **2017**, *8*, 2321–2328.

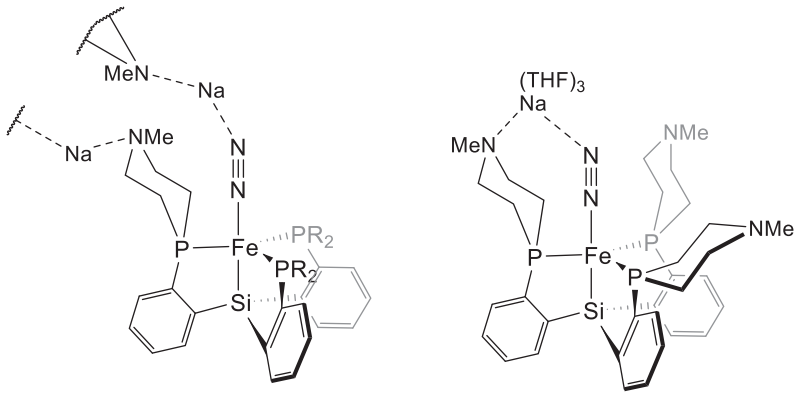

Fig. 30 Secondary-sphere effects dictate the solid-state structures of **3–44/44′**. Adapted from Creutz, S. E.; Peters, J. C. *Chem. Sci.* **2017**, *8*, 2321–2328.

Lu and coworkers sought to probe the effects of a metalloligand on the reactivity of a transition metal reaction center; those results bear relevance to the BP^{iPr}_3 and $[SiP^R_3]^-$ complexes. In the context of iron-dinitrogen chemistry, Rudd et al. reported a heterobimetallic iron-alane complex, which was competent for dinitrogen coordination and functionalization.[66] Reaction of the alumatrane-phosphine complex with an equivalent of $FeBr_2$ and 2 equiv. KC_8 afforded the zero-valent iron-alane-N_2 complex, **3–45**. Solid-state IR spectra of the complex display a single band at 2010 cm^{-1}, which is consistent with an end-on terminally coordinated N_2 molecule. The energy of this vibration is comparable to that observed for Moret and Peters' Fe^0–N_2 complex (**3–37**), highlighting the similar effects conferred by the two Group 13 axial Z-type ligands. Although monomeric in solution, **3–45** crystallizes as the μ-1,2-dinitrogen diiron complex **3–45′** in which the N—N bond length is elongated to 1.146 Å (cf. N_2(g) = 1.098 Å) with an estimated vibrational frequency of ~1800 cm^{-1} from the Badger's rule treatment reported by Holland.[9] The greater activation of the N—N bond in **3–45′** can be readily attributed to the bridging nature of the N_2 ligand. Given the comparable degree of activation of the N_2 fragment in **3–45** and **3–37**, one might anticipate that similar downstream reduction chemistry would be accessible. Indeed, employing 3 equiv. KC_8 in the preparation of the iron-alane complex affords the anionic Fe–Al complex, **3–46**, in which the η^1-N_2 ligand is more activated (ν_{NN} = 1925 cm^{-1}) as compared to the neutral complex **3–45** (**Figs. 31 and 32**).[67]

From the solid-state structure, the N—N bond length of 1.135 Å in this monoiron species is expectedly longer than in the precursor complex and this change agrees with the observed energy for the N–N vibration. Conversion of this dinitrogen complex to a hydrazide species displaying Fe—N multiple bond character is readily accomplished by reacting **3–46** with bis(chlorodimethylsilyl)ethane in the presence of an electron source. Crystallographic results demonstrate that **3–46** contains a disilylated-hydrazide ligand with remarkable similarity to the DFT optimized structure of **3–43** and reinforces the comparable electronic effects mediated by the Group 13 apical donor (Al vs. B) on the reactivity of the Fe^I–N_2 species towards the silylating agent.

Complementing the work discussed thus far on complexes in which the *trans* axial ligand donor atom is varied, the Field group utilized a tripodal tetradentate phosphine ligand, PP^{iPr}_3 (where $PP^{iPr}_3 = P(CH_2CH_2P^iPr_2)_3$), to prepare five-coordinate trigonal bipyramidal Fe–N_2 complexes. Reduction of the Fe(II) chloride complex with KC_8 under a N_2 atmosphere (**Fig. 33**) produces the corresponding Fe^0–N_2 complex, **3–47**.[68] From the solid state structure, the Fe center in **3–47** retains the approximate trigonal bipyramidal geometry from the chloride precursor with the N_2 ligand being minimally activated given the observed N—N bond length of 1.13 Å.

Attempts to protonate the coordinated N_2 moiety with 2,6-lutidinium sources failed to generate NH_x products, but rather led to protonation of the Fe center to afford the $[Fe(N_2)H(PP^{iPr}_3)]^+$ complex (**3–47H**). In a following report, a dimeric congener of **3–47H** was isolated and structurally characterized (**3–47′H$_2$**).[69] For this compound, a N—N bond length of 1.129(4) Å was reported, which is comparable to that for **3–47**. Addition of KO^{t}Bu or $KN(SiMe_3)_2$ to a THF solution of **3–47′H$_2$** yielded initially the monohydrido-diiron complex (**3–47′H**), which evolves to the hydride-free diiron species (**3–47′**). The monohydride compound was isolated and structurally characterized, whereas **3–47′** could only be detected in solution as a mixture with **3–47**. Complex **3–47′H** has a N—N bond length of 1.127(2) Å in the solid state; this value is comparable to that obtained for **3–47** and **3–47′**. Addition of strong acid (HCl and HBF_4) yielded no N_xH_y species and caused the dimetallic complexes to decompose. Recently, conditions for formation of ammonia and hydrazine from complex **3–47**, and analogous derivatives, were reported.[70] Using trifluoromethylsulfonic (or triflic) acid as the proton source, NH_3 was produced in yields up to 23% using the Fe–N_2 complex in a PP^{Ph}_3 ligand scaffold ($PP^{Ph}_3 = P(CH_2CH_2PPh_2)_3$). Hydrazine was also produced in the protonation reaction, with a maximum yield of 16% for **3–47**. The production of NH_3 and N_2H_4 from these Fe^0 complexes, without addition of an external reductant, provides strong support that iron(0) centers are sufficiently reducing to facilitate N_2 cleavage. The details of the mechanistic pathway, including the redistribution of reducing equivalents or the participation of multimetallic species, remains to be determined.

Returning to the TPB Fe complexes, the discussed work had demonstrated the feasibility of this system to support intermediates in a Chatt cycle for N_2 reduction. As an evolution of this chemistry, Anderson et al. reported the first iron-based mononuclear catalyst for NH_3 production from N_2 in 2013. Reaction of a derivative of **3–40** in which the Na^+ cation is encapsulated with [12-crown-4] (**3–40′**) with 6 equiv. $[H(OEt_2)_2][BAr^F_4]$ and a proton sponge in THF at −78 °C generated a mixture of iron species:

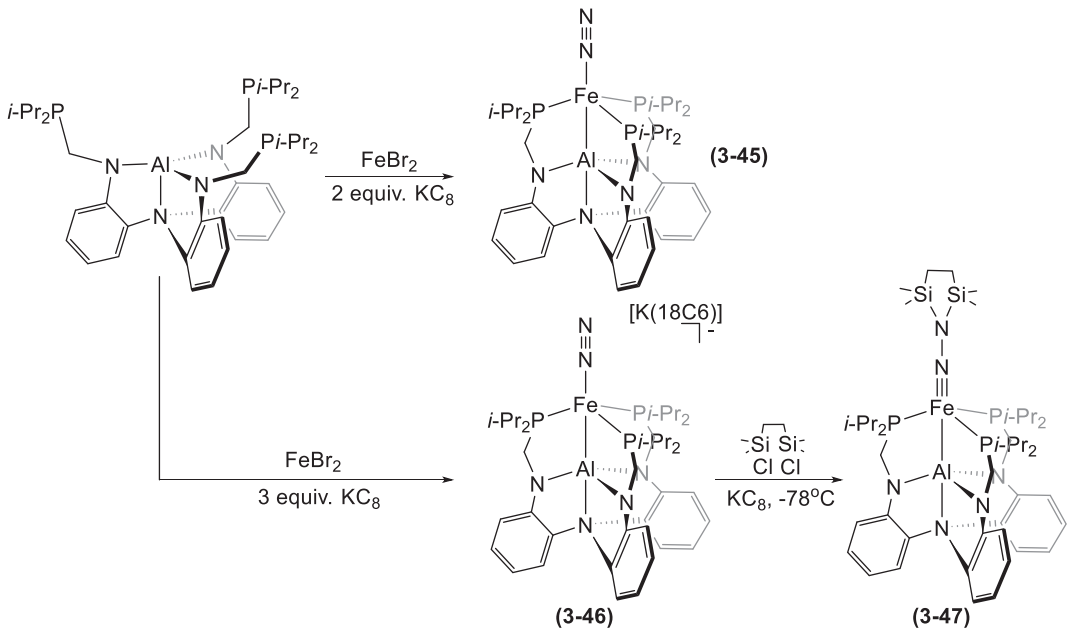

Fig. 31 The alumatrane-phosphine complex supports a family of Fe–N_2 complexes. Adapted from Rudd, P. A.; Liu, S.; Gagliardi, L.; Young, V. G., Jr.; Lu, C. C. *J. Am. Chem. Soc.* **2011**, *133*, 20724–20727; Rudd, P. A.; Planas, N.; Bill, E.; Gagliardi, L; Lu, C. C. Eur. *J. Inorg. Chem.* **2013**, 3898–3906.

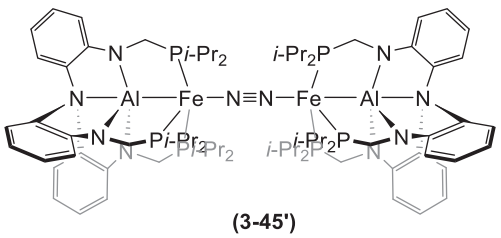

Fig. 32 The Fe^0-alane complex crystallizes as a dimetallic species with a μ-1,2-N_2 unit. Adapted from Rudd, P. A.; Liu, S.; Gagliardi, L.; Young, V. G., Jr.; Lu, C. C. *J. Am. Chem. Soc.* **2011**, *133*, 20724–20727.

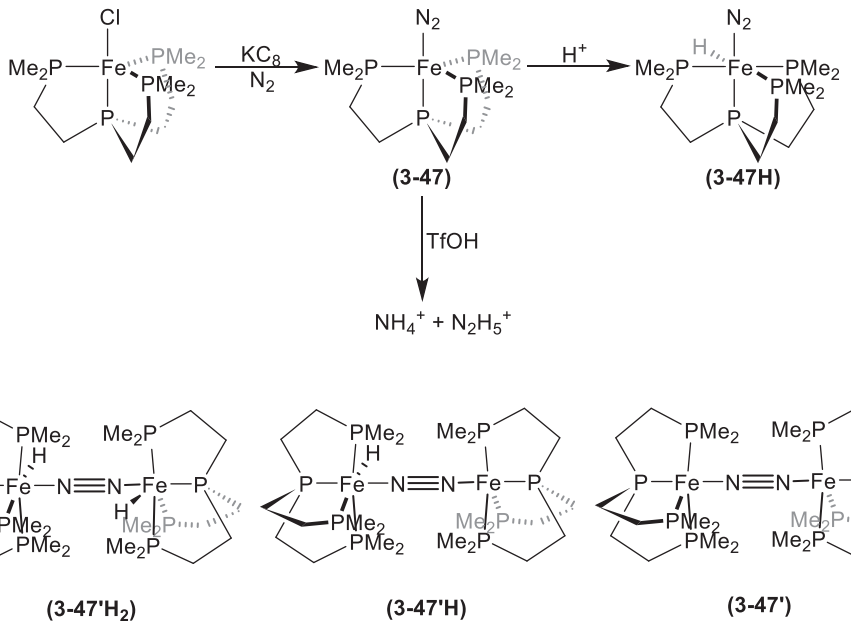

Fig. 33 A bulky tripodal phosphine Fe(0)–N_2 complex can produce NH_3 and N_2H_4 by acidification with strong acids with weakly coordinating anions. The dimeric species (*bottom*) decompose upon exposure to acid. Adapted from Field, L. D.; Guest, R. W.; Vuong, K. Q.; Dalgarno, S. J.; Jensen, P. *Inorg. Chem.* **2009**, *48*, 2246–2253; Field, L. D.; Guest, R. W.; Turner, P. *Inorg. Chem.* **2010**, *49*, 9086–9093; Field, L. D.; Li, H. L.; Dalgarno, S. J.; McIntosh, R. D. *Eur. J. Inorg. Chem.* **2019**, 2006–2011.

the [(TPB)Fe-NH_3][$BAr^F{}_4$] complex (30–35% of Fe), the substrate-free [(TPB)Fe][$BAr^F{}_4$] (40–45% of Fe), and two minor, unidentified paramagnetic species.[71] In later studies,[72] one of these unknown species was determined to be the hydrazide complex [(TPB)Fe≡N–NH_2]$^-$ by EPR, ENDOR, EXAFS, and computational analyses, and thus provided evidence for a stepwise protonation pathway of **3–40′** towards N_2 bond scission. Through a survey of reaction conditions (i.e., varying H^+ and e^- sources and solvent), maximal catalytic turnover was achieved using KC_8 (58 equiv.) and $\left[H(OEt_2)_2\right]\left[BAr^F{}_4\right]$ (48 equiv.) in diethyl ether at −78 °C, which afforded 8.5 equiv. of NH_3 per Fe. Significantly lower turnovers (0.7 NH_3/Fe) were observed for the analogous [$SiP^{iPr}{}_3$]$^-$ supported complex under the optimized catalytic conditions for **3–40′**. Further optimization of these initial conditions was later reported and included parameters such as variation of the temperature at different stages of the reaction. The maximum yields for both [$SiP^{iPr}{}_3$]Fe and TPB–Fe complexes were found for 1500 equiv. [$H(OEt_2)_2$][$BAr^F{}_4$] and 1800 equiv. KC_8, producing maximum yields of 4.4 and 64 equiv. of NH_3 per Fe, respectively. Through these and latter studies, it was demonstrated that the catalyst could be recycled over repeated batch additions of protons and electrons with minimal loss in fixed N_2 per cycle.[73]

A key species—the hydrido-borohydrido complex (TPB)-(μ-H)Fe$H(N_2)$ (**3–48**)ħ—in the catalytic pathway was discovered by Mößbauer spectroscopy. This compound predominates in the frozen reaction mixture after the initial 5 min. of the reaction; complex **3–48** reverts to the starting catalytic TPB–Fe(N_2) complex (**3–40′**) as the reaction progresses further. Reactivity studies evidenced that **3–48** is catalytically competent for N_2 fixation and that **3–40′** is formed during catalytic turnover (**Fig. 34**). Complex **3–48** is the proposed resting state of the catalyst, with the **3–48**-to-**3–40′** conversion accessed by H_2 reductive elimination. This reductive elimination can be facilitated by photolysis; irradiation of a reaction under conditions for catalytic turnover by a mercury lamp increase the maximum average yield of NH_3 to 94 equiv. of NH_3 per Fe.[74]

The results from the work by Peters and coworkers demonstrated that catalytic N_2 reduction by mononuclear iron complexes is accessible, but also recognized the importance of coordinative flexibility of the ligand bound *trans* to dinitrogen on the reactive iron center in N_2 fixation. Specifically, the interaction (e.g., Fe–B in the case of **3–40**) must accommodate the necessary changes to the iron oxidation state and the metal-nitrogen bonding interactions (i.e., single to triple bond in a Chatt cycle) required for N_2 reduction. Notably, the TPB system employs a boron-center and not the carbon-based donor observed in the nitrogenase cofactors; the extent to which the lessons learned in the TPB–Fe system translate to the Fe–C interactions in FeMoco remained unclear. To explore this question, iron complexes supported by tetradentate triphosphine ligands (viz. **3–49** and **3–50**) were synthesized and their catalytic properties evaluated (**Fig. 35**).[75] The results from the two alkyl systems evidenced that the Fe—C bond is indeed flexible during the N_2 reduction pathway.

First, the Fe–C interaction as a function of formal iron oxidation state was evaluated using the CO congener of **3–49** as a surrogate for the N_2 complex because of the greater stability of these carbonyl complexes relative to the dinitrogen adduct **3–49**. As the oxidation state decreased (from +2 to 0) the Fe—C bond distance increases from 2.138 Å (Fe^{II}) to 2.236 Å (Fe^{I}) to 2.303 Å (Fe^0). These results were corroborated by theoretical calculations that showed the Fe—C_{ligand} σ-bond to have significant ionic character, as compared to the strongly covalent Fe—Si interaction in the [$SiP^R{}_3$]$^-$ system. Despite exhibiting the similar effects on the Fe–X (X = B, C) bond length as a function of electron loading for the CO complexes, **3–49** was not competent for the catalytic fixation of N_2 to ammonia. As a more direct comparison to the TPB compounds, the H_2C–$SiMe_2$ in **3–49** was replaced by the *ortho*-substituted phenyl rings in **3–50**. The correlation between the Fe—C bond length and iron oxidation state across related **3–50** complexes is similar to that for the **3–49** derived carbonyl compounds, and the Fe—C bond was also similarly found to be strongly

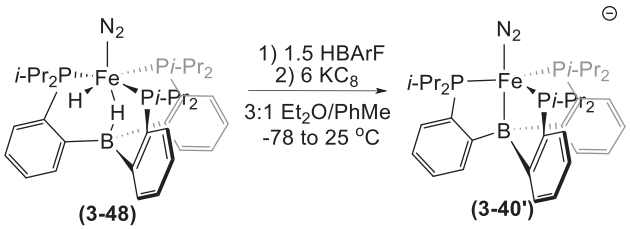

Fig. 34 Conversion of the purported resting state of the catalytic TPB–Fe(N_2) complex to the catalytically-active complex **3–40′**. Adapted from Del Castillo, T. J.; Thompson, N. B.; Peters, J. C. *J. Am. Chem. Soc.* **2016**, *138*, 5341–5350.

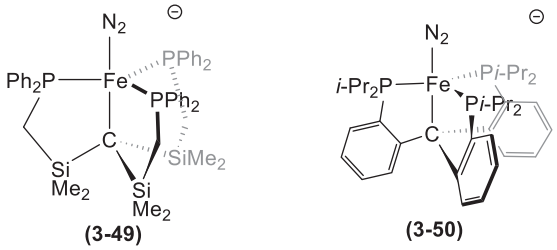

Fig. 35 Carbide-anchored Fe–N_2 complexes by Peters and co-workers, mimic the Fe–C moiety of nitrogenase enzymes. Adapted from Rittle, J.; Peters, J. C. *Proc. Natl. Acad. Sci. U.S.A.* **2013**, *110*, 15898–15903; Creutz, S. E.; Peters, J. C. *J. Am. Chem. Soc.* **2014**, *136*, 1105–1115.

polarized. Catalytic dinitrogen fixation by **3–50** was measured under the same conditions as the TPB complexes; addition of 38 equiv. $[H(OEt_2)_2][BAr^F{}_4]$ and 40 equiv. KC_8 to an ethereal solution of **3–50** at −78 °C generated 4.6 equiv. NH_3/complex. Further optimization of catalysis by **3–50** as performed for the TPB-Fe compounds led to a maximum yield of 47 equiv. NH_3 per Fe center.

Catalytic reduction of N_2 using KC_8—a very strong reductant with $E^0_{1/2} < -3.0$ V vs. the ferrocene/ferrocenium couple—is disparate from the use of milder reductants by the enzyme systems and the HBP. Therefore, various reductants, namely Na/Hg, decamethylcobaltocene, and an applied potential, and proton sources (inc. 2,6-dimethylanilinium, $Ph_2NH_2^+$, $PhNH_3^+$) were tested and all determined to effect catalytic N_2 fixation using **3–37**. These results present strong evidence that the Fe complex is, indeed, the catalytic species responsible for NH_3 production, but more surprising, is that decamethylcobaltocene ($Cp^*{}_2Co$) is a viable reductant and more effective (based on e^- productively consumed) than KC_8. Based on the reduction potentials determined from cyclic voltammetry, $[Cp^*{}_2Co]^{0/+}$ is less reducing than the $[BP^{iPr}{}_3FeN_2]^{0/1-}$ couple (viz. −1.96 V vs. −2.1 V, respectively, referenced to the Fc/Fc^+ couple). A detailed study revealed that $Cp^*{}_2Co$ can be protonated to generate $Cp^*Co(\eta^4\text{-}C_5Me_5H)^+$, which is a proton-coupled electron transfer (PCET) reagent. DFT calculations support favorable PCET from $Cp^*Co(\eta^4\text{-}C_5Me_5H)^+$ to **3–37** to afford the diazenide complex, $[BP^{iPr}{}_3]FeN_2H$, with all subsequent PCET events to ultimately generate the hydrazide complexes being more favorable. In this reaction system, the PCET pathway reduces accumulation of the dihydride resting state **3–48** and consequently retains more catalytically-active complex in solution. In addition, controlled potential electrolysis experiments employing catalytic amounts of $Cp^*{}_2Co^+$ and $BP^{iPr}{}_3FeN_2$ improves the yield of NH_3 as compared to experiments in the absence of the metallocene cocatalyst.[76]

8.26.3.2 Fe–N_2 Complexes Supported by Tridentate Meridional or C_{2v} Ligands

With respect to N_2 functionalization by pincer complexes, Nishibayashi and coworkers demonstrated that molybdenum complexes of a family of PNP pincer ligands wherein the phosphine substituents vary are precatalysts for reduction of N_2 into NH_3 (**Fig. 36**).[77] Contemporaneous with that result is the report by Yuki et al. that several 18-electron mononuclear iron complexes such as pentacarbonyliron(0), bis(trimethylsilyl)iron tetracarbonyl, 1,1′,2,2′,4,4′-hexakis(trimethylsilyl) ferrocene, and ferrocene are all competent for catalytic N_2 fixation to tris(trimethylsilyl)amine under ambient conditions.[78] It must be noted, however, that these 18-electron species are likely precatalysts for N_2 fixation insofar as all are coordinatively saturated. Extending the pincer systems to iron complexes then, reduction of an iron-based pincer complex (**3–51**) with potassium graphite affords the mononuclear Fe—N_2 compound, **3–52** (**Fig. 37**).[79]

Crystallographic data demonstrate that **3–52** adopts a distorted square planar geometry with a N—N bond distance of 1.134(2) Å, which correlates well with the observed IR absorption at 1964 cm^{-1}. EPR and magnetic susceptibility data point to the complex containing a low-spin iron(I) center.

When **3–52** was exposed to the catalytic N_2 reduction conditions utilized for the Mo PNP pincer catalysts (viz. cobaltocene and 2,6-lutidinium trifluoromethanesulfonate as the electron and proton sources, respectively, and room temperature), ammonia was not observed in the reaction mixture. Instead, employing the initial conditions by Peters and coworkers (viz. KC_8 reduction with

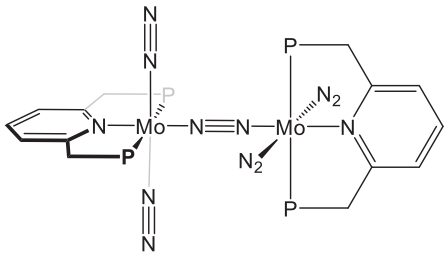

Fig. 36 Nishibayashi's Mo-pincer catalyst. (P = bis(*tert*-butyl)phosphine). Adapted from Arashiba, K.; Miyake, Y.; Nishibayashi, Y. *Nat. Chem.* **2011**, *3*, 120–125.

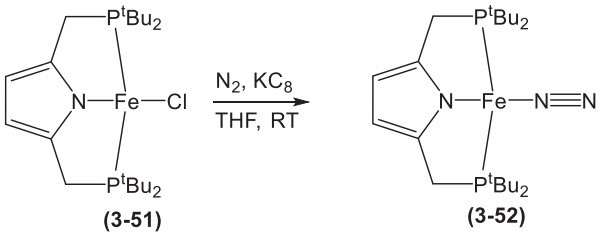

Fig. 37 A pincer-based Fe–N_2 complex. Adapted from Kuriyama, S.; Arashiba, K.; Nakajima, K.; Matsuo, Y.; Tanaka, H.; Ishii, K.; Yoshizawa, K.; Nishibayashi, Y. *Nat. Commun.* **2016**, *7*, 12181.

$[H(OEt_2)_2][BAr^F{}_4]$ as the proton source, and −78 °C in diethyl ether) lead to dinitrogen reduction with ammonia (up to 14.3 equiv.) and hydrazine (up to 2.4 equiv.) as the observable products after 1 h. The reaction solvent for this system has a profound impact on the product distribution. Changing the solvent from diethyl ether to THF led to only 2.9 equiv. NH_3 in the product mixture but retained hydrazine formation with 2.4 equiv. N_2H_4 observed. Methyl- and hydrido-iron analogs of **3–52** (Fig. 38) were also found to be catalytically active under these conditions. When **3–52Me** and **3–52H** were protonated with $\left[H(OEt_2)_2\right]\left[BAr^F{}_4\right]$ and then reduced by KC_8 in diethyl ether; hydrogen gas, methane, and complex **3–52** were recovered in the product mixture, indicating that the hydride and methyl complexes were likely converted to the N_2 complex under catalytic conditions.

From their initial work on the Mo-pincer complexes, the proposed dinitrogen reduction mechanism proceeds by a distal pathway in which the Mo–N_2 complex is first reduced and protonated to a $MoNNH_2$ species, which undergoes reduction and protonation to liberate an equivalent of NH_3 and the corresponding nitride complex. Further protonation and reduction of the nitride generates the second equivalent of ammonia and regenerates a catalytically active Mo complex. In contrast, isolation of hydrazine from the iron pyrrolide system suggested that the N_2 fixation by this catalyst may proceed by a different pathway. Thus, an alternating pathway—where the N_α and N_β are protonated in an alternating fashion—was proposed insofar as $FeNH_xNH_2$ species (x = 1 or 2) can be readily envisioned to prematurely exit the catalytic cycle to afford hydrazine. Ammonia would result from additional protonation and reduction of the hydrazine complex, also producing an Fe–NH_2 intermediate that would convert to the Fe–NH_3 complex upon protonation and reduction. The experimental data do not exclude formation of NH_3 from a distal-only pathway operating in parallel. Notably, recent work by Peters and coworkers argues that the distal and alternating protonation pathways may not be mutually exclusive in mononuclear iron-dinitrogen chemistry, but that the distal pathway can cross to an alternating-like mechanism (Fig. 39).[80]

Subsequent derivatization of the initial iron bisphosphino-pyrrolide complexes has focused primarily on changes to the pyrrole ring; specifically, substituting the protons on the ring for Me or Ph groups or substituting the pyrrole donor for a carbazole ring system.[81] Analogous to the progenitor system, reduction of the iron(II) chloride complexes with KC_8 under a N_2 atmosphere led to the iron-dinitrogen complexes, **3–53Me** and **3–53Ph** (Fig. 40). IR spectra of these two compounds contain N–N stretching bands at 1959 and 1969 cm^{-1}, respectively, which are comparable to that for **3–52**. The nominally more activated N_2 donor in **3–53Me** as compared to that observed in **3–52** is attributed to the increased back-donation into the N_2 ligand, which arises from the more-donating methyl substituents vs. the phenyl congener. The catalytic activity of **3–53Me** and **3–53Ph** was examined using the reaction conditions reported for **3–52**; both **3–53Me** and **3–53Ph** yielded smaller quantities of NH_3 and N_2H_4 (5.0 and 0.8 equiv. for **3–53Me** and 3.7 and 0.1 equiv. for **3–53Ph**). When larger amounts of reductant and proton source (200 and 184 equiv., respectively) were used, **3–53Me** showed considerably improved yields of NH_3 and N_2H_4 (22.7 and 1.7 equiv.), whereas **3–53Ph** showed very little improvement (4.7 and 1.2 equiv.).

For the analogous carbazole-supported complexes, reaction of the deprotonated bis(phosphinomethyl)carbazoles with $FeCl_2$ produced the Fe^{II}–Cl carbazole complex (**3–54**). Reduction of the ^{t}Bu derivative of **3–54** with KC_8 under a dinitrogen atmosphere

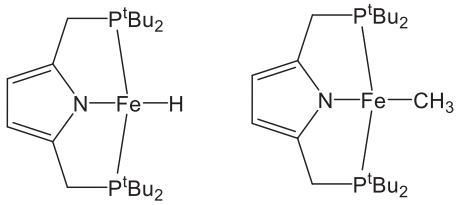

Fig. 38 Methyl and hydride analog complexes provided insight into potential intermediates. Adapted from: Kuriyama, S.; Arashiba, K.; Nakajima, K.; Matsuo, Y.; Tanaka, H.; Ishii, K.; Yoshizawa, K.; Nishibayashi, Y. *Nat. Commun.* **2016**, *7*, 12181.

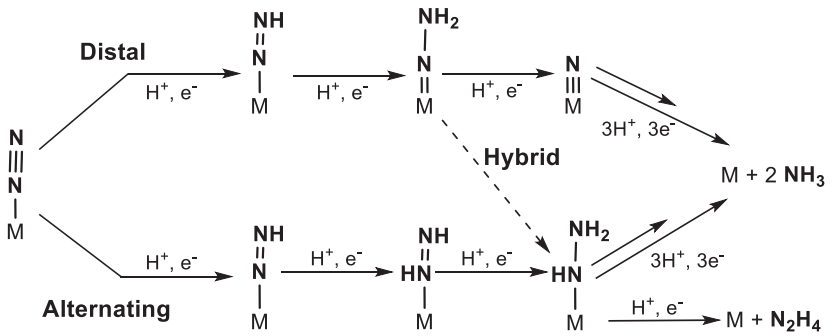

Fig. 39 Generic schematic of conversion of N_2 to NH_3 by distal, alternating, or hybrid pathways. M can be considered as either a single metal center or multiple metal centers. Adapted from Rittle, J.; Peters, J.C. *J. Am. Chem. Soc.* **2016**, *138*, 4243–4248.

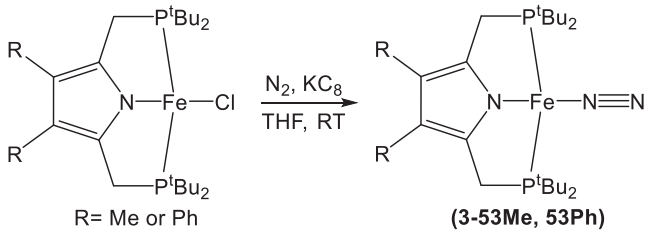

Fig. 40 Reduction of derivatized analogs of **3–51** yield Fe–N_2 complexes exhibiting similar spectroscopic data as the non-derivatized congener. Adapted from Sekiguchi, Y.; Kuriyama, S.; Eizawa, A.; Arashiba, K.; Nakajima, K.; Nishibayashi, Y. *Chem. Commun.* **2017**, *53*, 12040–12043.

afforded the N_2-bridged diiron complex, **3–55** (Fig. 41).[82] In contrast to the planar pyrrole-based PNP-pincer complexes, X-ray crystallography data reveal that the carbazole-pincer complex adopts a distorted tetrahedral geometry about the Fe center and solution magnetometry measurements are consistent with **3–54** being a high spin complex. The change in spin state and geometry is attributed to the size and rigidity of the chelate ring of the complex; the greater rigidity of pyrrole-based complexes favor the square-planar geometry whereas the more flexible six-membered chelate rings of the carbazole complex allow access to the less-strained tetrahedral arrangement. Catalytic N_2 fixation to NH_3 under the conditions employed for **3–52** and **3–53**, however, yielded minimal amounts of ammonia (0.5 equiv.). The consequences of the structural and electronic changes effected by the carbazole ligand on N_2 fixation remain to be determined.

Similar to the evolution of ligand design for the trigonal complexes and new insights into the composition of FeMoco (i.e., the interstitial carbide), pincer ligands employing Group 14 donors were targeted and their catalytic performance evaluated. The first PSiP-pincer Fe–N_2 complexes were prepared in 2017 by Nishibayashi and coworkers with the reaction of Fe(PMe_3)$_4$ with a diaryl silane under a N_2 atmosphere affording the corresponding iron-dinitrogen complex, **3–56** (Fig. 42).[83] IR spectroscopy of the complex revealed two diagnostic bands at 2041 and 1850 cm^{-1} corresponding to the N–N and Fe–H stretching modes, respectively. The N–N stretching frequency for **3–56** is comparable—albeit, slightly lower—to that of the trigonal [SiP^{iPr}_3]Fe(N_2) compound, consistent with the comparable donor sets. Complexes **3–56**, in which the silyl substituent is either Me or Ph, are catalytically active for N_2 reduction to NH_2, but to a much lesser extent than the PNP-pincer analogs. The PSiP complexes yielded up to 1.2 equiv. of ammonia without observable production of hydrazine. Transitioning away from proton sources towards softer silyl cation ones, **3–56** compounds were investigated for their ability to perform catalytic silylation of N_2 to N($SiMe_3$)$_3$. Reduction by Na metal and addition of Me_3SiCl as the silylating agent in the presence of the Me-substituted catalyst, 15 equiv. N($SiMe_3$)$_3$ were obtained whereas the phenyl-derivative showed nearly twice the activity at 26 equiv. N($SiMe_3$)$_3$/complex.

Much of the catalytic studies for iron-dinitrogen complexes has focused on the reduction of N_2 to NH_3 due to the relevance to biological and anthropogenic dinitrogen fixation. However, Fe–N_2 complexes have been utilized as precatalysts for a variety of transformations, including C–X (X = heteroatom or C) bond formation and hydrogenation reactions. Details of those organometallic reactions are beyond the scope of the dinitrogen chemistry discussed here; however, the parent N_2 adducts will be described where appropriate.

Chirik and coworkers have exploited iron-dinitrogen complexes of bis(imino)pyridine donors as precatalysts in a wide range of olefin reactions. In 2004, Bart et al. prepared an iron-bis(N_2) complex (**3–57**) by reducing the iron(II) dihalide complexes with sodium amalgam under N_2.[84] Dark green crystals of **3–57** were isolated and the solid-state structure was determined by X-ray crystallography. A distorted square pyramidal geometry about the Fe center was observed with two coordinated N_2 ligands—one bound at the apical site and the other completing the basal plane (Fig. 43). Complex **3–57** marked the first isolation of an iron-bis(N_2)

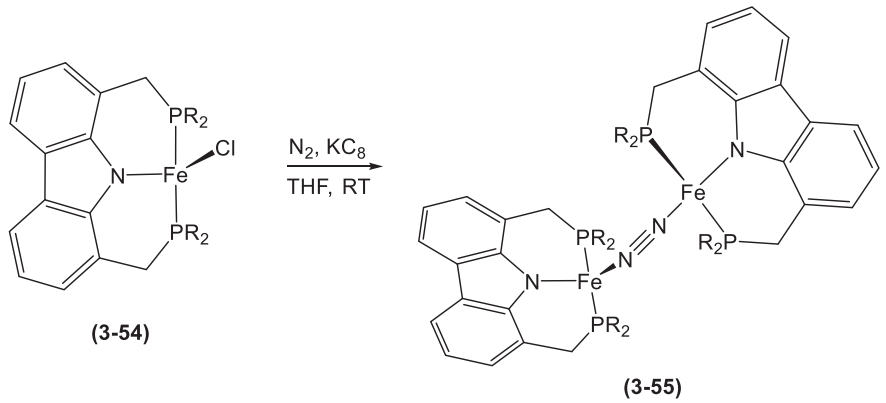

Fig. 41 Nishibayashi and coworkers utilized a bis(phosphino)carbazole ligand platform to yield **3–55**. Adapted from Higuchi, J.; Kuriyama, S.; Eizawa, A.; Arashiba, K.; Nakajima, K.; Nishibayashi, Y. *Dalton Trans.* **2018**, *47*, 1117–1121.

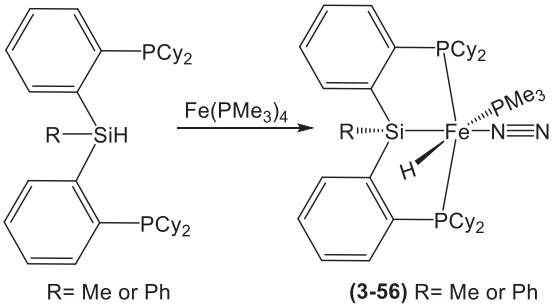

Fig. 42 Synthesis of an Fe–N_2 complex that was shown to be catalytically active for silylation of N_2. Adapted from Imayoshi, R.; Nakajima, K; Takaya, J.; Iwasawa, N.; Nishibayashi, Y. *Eur. J. Inorg. Chem.* **2017**, *32*, 3769–3778.

complex and was one of a limited number of Fe–N_2 complexes to have been crystallographically characterized at the time.[85] The two N–N stretches at 2053 and 2124 cm^{-1} observed in the IR spectrum of **3–57** are at higher energy than other Fe(0)–N_2 complexes,[86] which can be attributed to the π-accepting nature of the bis(imino)pyridine ligand backbone compared to the less accepting ligands from complexes reported by George and Leigh.,[39,86b] In addition, SQUID magnetometry revealed a $S = 1$ ground state for this complex; as such, **3–57** was suggested as the first example of a high spin Fe(0) complex. Later work has raised the question as to ligand non-innocence in the electronic structure description of this complex, that is, a ligand diradical anion with an iron(II) species as compared to a neutral formulation being the two extrema.[87] IR spectroscopy evidences that the complex is dynamic in solution, existing as an equilibrium mixture between **3–57** and its mono-dinitrogen congener (Fig. 44). Investigations into the electronic structures[88d] of the mono- and bis(N_2) complexes revealed that the four-coordinate species is best described as an intermediate-spin iron(II) derivative antiferromagnetically coupled to a bis(imino)pyridine diradical dianion. The five-coordinate complex, on the other hand, is highly covalent and assigned as an admixture of states comprising Fe(0) and low-spin Fe(II) complex. The drastic difference observed in this equilibrium mixture illustrates that coordination/dissociation of a N_2 unit can

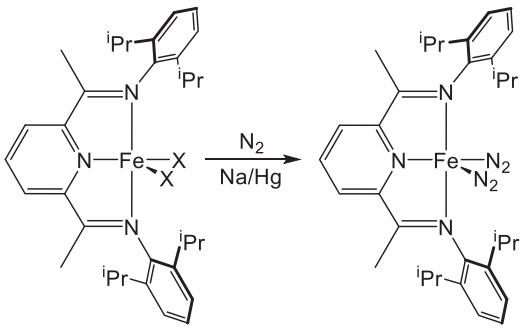

Fig. 43 Use of a bis(imino)pyridine ligand yielded an *Fe*-bis(N_2) complex. Adapted from Bart, S. C.; Lobkovsky, E.; Chirik, P. J. *J. Am. Chem. Soc.* **2004**, *126*, 13794–13807.

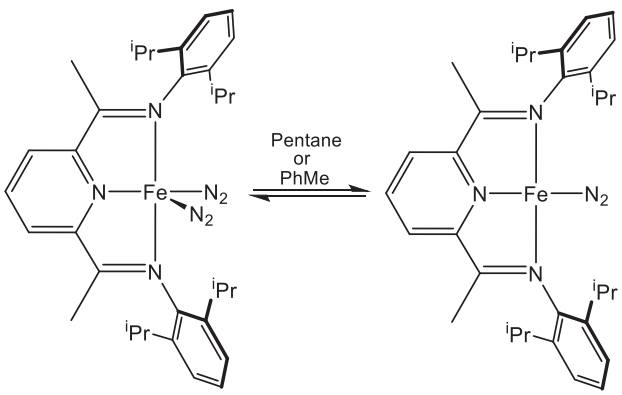

Fig. 44 The bis- and mono-N_2 complexes were observed as an equilibrium mixture in solution. Adapted from Bart, S. C.; Lobkovsky, E.; Chirik, P. J. *J. Am. Chem. Soc.* **2004**, *126*, 13794–13807.

have a significant impact on the ligand field and the spin state of the corresponding complex, especially in the context of multimetallic assemblies.

Decreasing the size of the aryl groups on the imine nitrogen atoms results in the production in several new Fe–N_2 complexes.[88] Of particular interest was the isolation of the diiron-(μ-N_2) complex (**3–58**).[89] Reduction of the iron(II)-dihalide precursor by sodium naphthalenide results in formation of the dimeric complex, which was readily characterized by a suite of spectroscopic techniques (**Fig. 45**).

With relevance to stabilizing species germane to the distal or alternating pathways for N_2 activation, the bis(imino)pyridine Fe–N_2 complexes can access imido-iron compounds, which generates the corresponding aniline in the presence of H_2 (**Fig. 46**).[90] Reaction of the bis(dinitrogen) complex **3–57** with aryl azides affords the iron aryl-imide intermediate with H_2 addition liberating 1 equiv. of the aniline and affording the neutral Kubas complex. Aryl isocyanates were produced when the imido-intermediate was exposed to 1 atm of CO.

Using the same ligand scaffold as Chirik and coworkers, Budzelaar demonstrated that the bis(imino)pyridine ligand could access complexes with greater activation of the N_2 ligand.[91] Reduction of the Fe(II)–Cl_2 complex with 3 equiv. NaH yielded an unstable Fe–N_2 complex (**3–59**). Structural data indicate deprotonation of one of the backbone methyl groups, signaling a monoanionic ligand coordinated to a formally Fe(0) center. The N_2 ligand is coordinated in an end-on mode to the iron center and η^2 with a sodium cation, and the N–N distance of 1.090(3) Å indicates minimal activation. The IR spectrum contradicts the minimal activation suggested by the solid-state structure, displaying a N–N stretching frequency of 1912 cm^{-1}, considerably lower than that for **3–57** (cf. 2053 cm^{-1}). Reduction with 4 or 6 equiv. NaH changes the product speciation from **3–59** and generates the Fe–N_2 complexes **3–60** and **3–61**. Capping of the N_2 moiety by $Na(Et_2O)_3$ in **3–60** (major product) significantly lengthens the N–N bond (1.154(6) Å), but the stretching frequency increases slightly (cf. **3–59**) to 1965 cm^{-1}. The minor product (**3–61**) exhibits similar structural parameters to **3–59**—except for the lack of a deprotonated imine-methyl—as the μ-η^1:η^2-N_2 bridges the iron center and one sodium cation. The additional Na^+ in **3–61** is associated with the pyridyl ring, suggesting increased reduction of the Fe center to a formal 2+ oxidation state, although ligand-based reduction cannot be rigorously excluded. Regardless of the localization of the additional reducing equivalents, IR data on **3–61** evidence greater N–N activation based on the dinitrogen stretching frequency observed at 1899 cm^{-1}. Attempts to functionalize the coordinated N_2 moieties in this family of complexes have not been reported, leaving the utility of bis(imino)pyridine complexes as N_2 reduction catalysts unclear (**Fig. 47**).

In 2011, Sun and coworkers reported the *ortho*-metalation of dibenzylphenylphosphine by Fe(II) through C–H bond activation of the benzyl substituents. Addition of *cis*-$(Me_3P)_4FeMe_2$ to dibenzylphenylphosphine under a dinitrogen atmosphere led to the isolation of the Fe(II)–N_2 complex **3–62**.[92] X-ray crystallography identified the minimally activated N_2 ligand bound end-on to

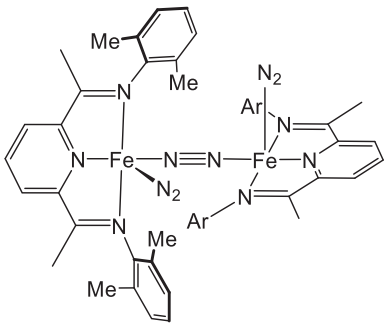

(3-58)

Fig. 45 Decreasing the steric bulk around the metal center yielded **3–58**. Adapted from Tondreau, A. M.; Atienza, C. C. H.; Weller, K. J.; Nye, S. A.; Lewis, K. M.; Delis, J. G. P.; Chirik, P. J. *Science* **2012**, *335*, 567–570.

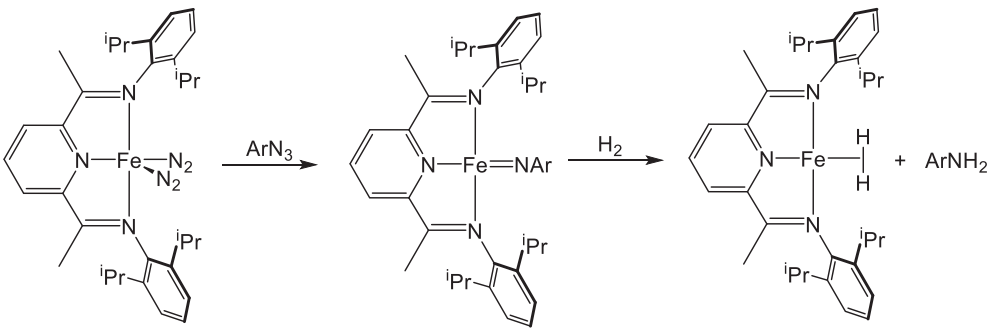

Fig. 46 Hydrogenation of aryl azides to produce anilines has been shown to be catalyzed by bis(imino)pyridine Fe–N_2 complexes. Adapted from Bart, S. C.; Lobkovsky, E.; Bill, E.; Chirik, P. J. *J. Am. Chem. Soc.* **2006**, *128*, 5302–5303.

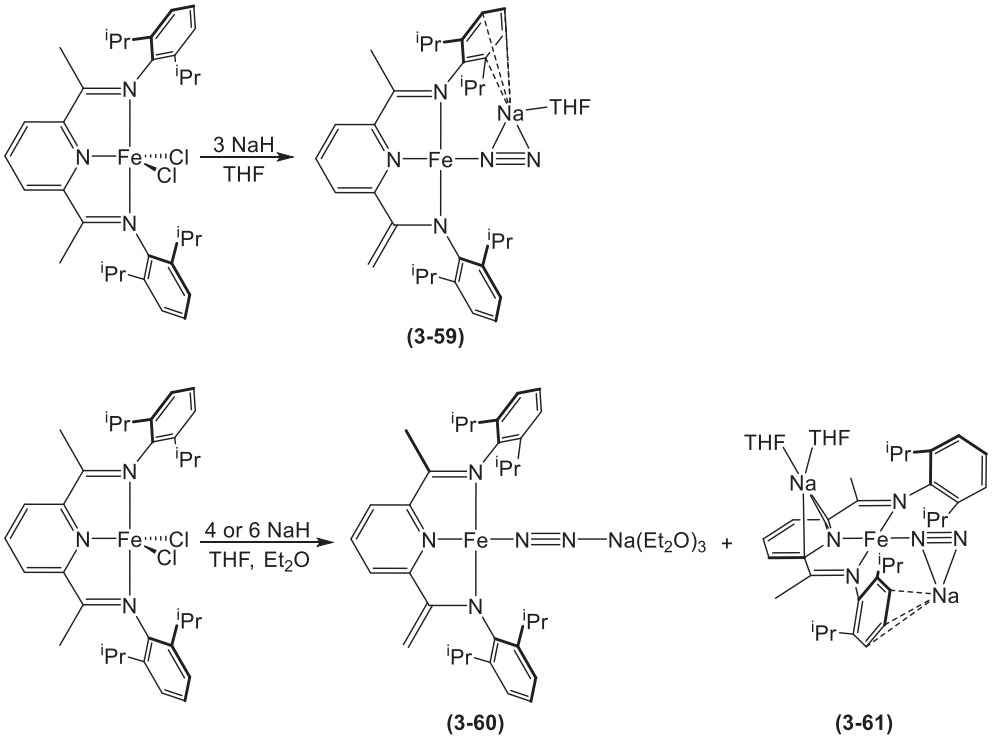

Fig. 47 The bis(imino)pyridine ligand scaffold can support Fe–N_2 complexes in a variety of oxidation states. Adapted from Scott, J.; Vidyaratne, I.; Korobkov, I.; Gambarotta, S.; Budzelaar, P. H. M. *Inorg. Chem.* **2008**, *47*, 896–911.

the metal center with a corresponding bond length of 1.113(4) Å, which is in good agreement with the observed N–N stretching frequency in the IR spectrum at 2078 cm^{-1} (Fig. 48).

Related to the CPC pincer ligand from Liu et al. in **3–62**, Wolczanski and coworkers reported the metalation of *ortho*-substituted diarylimines with *cis*-$(Me_3P)_4FeMe_2$, which generate a family of imine pincer-type complexes, **3–63** (Fig. 49).[93] The lability of the PMe_3 *trans* to the imine N atom correlates with the steric constraints imposed by the *ortho* substituents; that is, more encumbered substituents favor phosphine dissociation. Complexes **3–63** decompose if exposed to dioxygen but react with air to generate the corresponding dinitrogen complexes, **3–64**. Indeed, the seeming requirement of low-valent iron centers to bind dinitrogen predisposes such reduced compounds to adventitious side reactions with O_2 in air. This report emphasizes that judicious choice of the metal coordination sphere can mitigate side reactions and allow for selective N_2 coordination. In all cases, the N−N bond is weakly activated with ν_{NN} ranging from 2121 to 2046 cm^{-1} and the reported crystallographic N−N bond lengths are consistent with those stretching frequencies. Compounds **3–64** react with a variety of substrates, but notable mentions are the equilibrium constants of ~1 and ~0.5 determined for reaction with nitrogenase-relevant species NH_3 and H_2; the latter providing potential insight into the electronic effects that may favor the proposed H_2 loss and N_2 coordination at the E_4 state of FeMoco.

Peters and coworkers have developed a pair of tridentate ligand scaffolds reminiscent of their triphosphinoborane system to prepare a series of more reactive Fe complexes. In 2013, Suess and Peters reported the preparation of an iron-diphosphinoborane (DPB) system capable of facilitating hydrogenation of coordinated N_2. Here, the tridentate DPB ligand has sufficient flexibility to adopt a facial coordination mode rather than the meridional mode of the typical pincer ligand family. Reduction of the isopropyl-substituted DPB–$FeBr_2$ complex with 1 equiv. Na/Hg results in the production of the diiron-(μ-1,2-N_2)DPB complex (**3–65**).[94] This C_s-symmetric complex does not exhibit a N–N stretching band in the solution-phase IR spectrum, consistent with a centrosymmetric structure in solution. The solid-state structure of **3–65** displays the two Fe centers in pseudotetrahedral

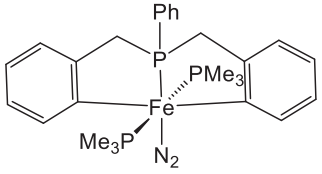

Fig. 48 *Ortho*-metalation of dibenzylphenylphosphine with an Fe(II) source yields an Fe(II)–N_2 complex. Adapted from Liu, N.; Li, X.; Sun, H. *J. Organomet. Chem.* **2011**, *696*, 2537–2542.

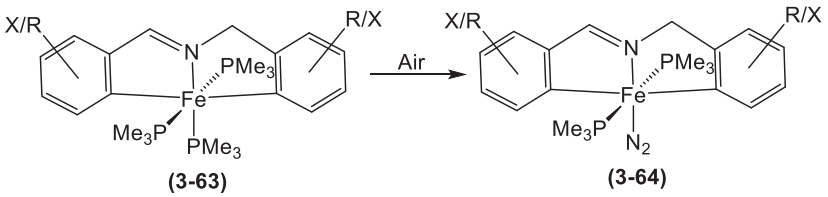

Fig. 49 Reaction of **3–51** with air produces an Fe–N_2 complex that is reactive towards nitrogenase-relevant species. R = CF_3 or MeO; X = F. Adapted from Bartholomew, E. R.; Volpe, E. C.; Wolczanski, P. T.; Lobkovsky, E. B.; Cundari, T. R. *J. Am. Chem. Soc.* **2013**, *135*, 3511–3527.

coordination geometries; however, the two iron centers show different coordination environments. One Fe center binds to the *ipso*-C of the phenyl substituent on B, whereas the other metal coordinates in an η^2-fashion to the *ortho*- and *ipso*-C of the phenyl substituent. The N–N bond length was found to be 1.17 Å, showing a mild degree of N_2 activation. When 1,2-bis(chlorodimethylsilyl) ethane is included in the Na/Hg reduction of the dibromide precursor or **3–65**, the mononuclear Fe-aminoimide complexes (**3–66**) are isolated (Fig. 50). The solid-state structure has a short Fe–N bond of ~1.66 Å, which is similar to that for the Fe–N distances in the pseudo-tetrahedral nitride **3–16** and imide complexes **3–7** and indicative of Fe≡NNR triple bond character. The doubly-silylated complex exhibits an analogous Fe-Ph η^2 interaction as observed in the dinitrogen complex **3–65**. Hydrogenation of the bound N_2 was examined using $PhSiH_3$ and H_2, with $PhSiH_3$ only reactive towards the ^{i}Pr derivative and H_2 reactive towards the Ph derivative. The resulting complex (**3–67**) from addition of $PhSiH_3$ was successfully crystallized and shows hydride insertion into the Fe–B bond—analogous to **3–48**—and N–Si bond formation between N_α and the remaining $PhSiH_2$ moiety. The N–N bond length in **3–67** is drastically elongated to 1.492 Å as compared to **3–66** and is longer than that in free N_2H_4. Reaction with H_2 results in precipitation of a $S = 2$ product in which the N–N bond is cleaved, and a hydride inserts into the Fe–B bond (**3–68**). This improved reactivity towards hydrogenation reagents was attributed to the additional flexibility that the DPB ligand platform provides to the metal center (cf. TPB).

Buscagan et al. synthesized a dinuclear complex[74] bearing a tridentate phosphine ligand similar in architecture to the complexes described in Section 8.26.3.1.2. The solid-state structure of **3–69** shows an end-on N_2 bridging two FeP_3 units with a N–N bond distance of 1.15 Å. IR spectroscopy showed no N–N stretching band, but revealed the presence of hydride ligands at each of the metal centers (ν_{FeH} = 1833 and 1734 cm^{-1}). ^{1}H NMR of **3–69** shows signals solely in the diamagnetic region, indicative of a low-spin singlet ground state which is also supported by Mößbauer spectra of the compound. Complex **3–69** was subjected to catalytic N_2 reduction conditions as described for the TPB iron complexes (see Section 8.26.3.1.2) and showed some activity (7.5 ± 0.8 equiv. NH_3 per complex). Interestingly, irradiation with a Hg lamp under these catalysis conditions greatly increased NH_3 production with turnovers of 18.1 ± 0.8 NH_3/complex. The effect of the Hg lamp was more evident at higher loadings of reductant and acid (3600 and 3000 equiv., respectively) with turnovers of 66.7 ± 4.4 equiv. (cf. 24.5 ± 1.2 equiv. sans Hg lamp). Early mechanistic studies have led to the hypothesis that photoinduced release of H_2 from a monoiron daughter complex of **3–69** is a critical step for light-assisted catalysis (Fig. 51).

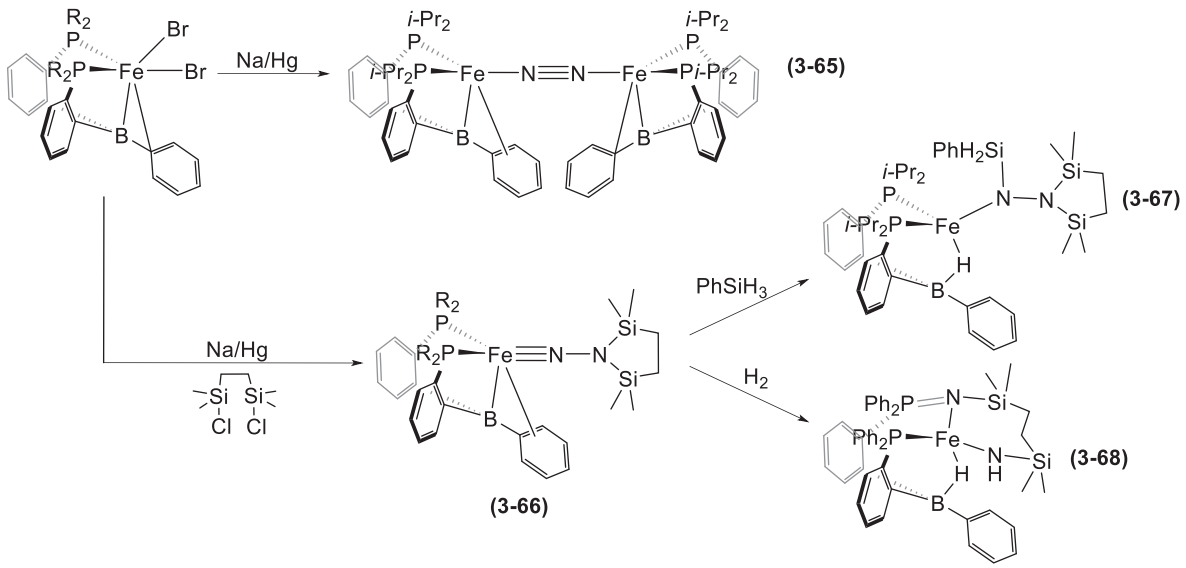

Fig. 50 The DPB ligand platform enables the Fe–N_2 complexes to react with H_2 and $PhSiH_3$. Adapted from Suess, D. L. M.; Peters, J. C. *J. Am. Chem. Soc.* **2013**, *135*, 4938–4941.

Another example of the utility of the pincer platform for Fe–N_2 chemistry was reported by Hounjet et al. in 2015 in which an iron(I)-dinitrogen complex was isolated.[95] Reaction of the iron complex of the anionic PNP pincer ligand (PNP = bis(2-(diisopropylphosphanyl)-4-methylphenyl)amido) with a slight excess of EtMgCl in Et_2O produces a mixture of two Fe-containing products—the ethyl complex, [(PNP)FeEt], and a heterobimetallic Fe/Mg complex, **3–70** (Fig. 52). The N_2 ligand is weakly activated given the observed N–N stretching frequency of 2084 cm^{-1} and bond length of 1.108 Å. The PNP ligand coordinates in a similar fashion as seen in the previously described for **3–65** and **3–69**; the *cis* di-vacant octahedral sites on the iron center facilitates coordination of the Mg and H^- groups. At the time reported, this $S = 1/2$ complex was the first isolated Fe(I)-hydride bearing a coordinated N_2 molecule. Hounjet et al. hypothesize that the FeEt co-product is a likely precursor for the N_2-containing complex as β-hydride elimination from the ethyl ligand is the most plausible source for the hydride ligand. Attempts to investigate this hypothesis yielded complicated product mixtures, complicating mechanistic studies and conclusions. Nonetheless, this complex provides a starting point to investigate the chemistry of Fe(I)–N_2-ate complexes and their potential relevance to biological N_2 reduction.

In 2018, Mézailles and coworkers reported the *Fe*-bis(N_2) complex **3–71**, prepared by KC_8 reduction of an iron dichloride precursor under N_2 atmosphere.[96] The structure of **3–71** (Fig. 53) displays a square pyramidal Fe center with the phosphine ligand occupying three sites in the basal plane, one N_2 ligand located in the fourth basal site, and the second N_2 donor coordinated in the apical position of the pyramid. Absorptions in the IR spectrum of **3–71** at 2047 and 1982 cm^{-1} are assigned as the N−N vibrations, and together with the crystallographic N−N bond lengths of 1.118 and 1.128 Å, indicate weakly-activated N_2 donors. The bis(N_2) complex was examined for catalytic ammonia production with 200 equiv. KC_8 and 200 equiv. $[H(OEt_2)_2][BAr^F{}_4]$ at −80 °C in Et_2O. Quantification of ammonia in the product mixture yielded a maximum of 3.6 equiv. per Fe complex. Additionally, no NH_3 was formed when the reaction was run in the absence of reductant.

In an attempt to isolate potential intermediates along the N_2 reduction pathway, a series of stoichiometric reactions were conducted. Addition of $HBAr^F{}_4$ to **3–71** resulted in protonation at the metal center and release of one N_2 ligand (**3–72**), similar to that seen by Mock and coworkers in a related polydentate phosphine ligand (vide infra).[97] Reduction of the protonated species produced a surprising result: an iron(II) dihydride complex is produced with intermediacy of an Fe(I)–H species. The dihydride species was also subjected to the previously described conditions for catalytic N_2 to NH_3 conversion and yielded 2.7 equiv.

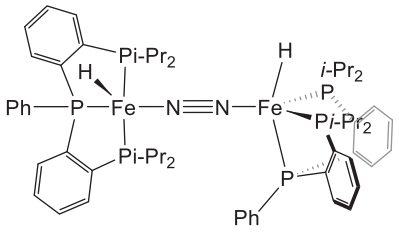

(3-69)

Fig. 51 Peters and coworkers developed a dinuclear Fe–N_2 complex that can catalytically reduce N_2. Adapted from Buscagan, T. M.; Oyala, P. H.; Peters, J. C. Angew. *Chem. Int. Ed.* **2017**, *56*, 6921–6926.

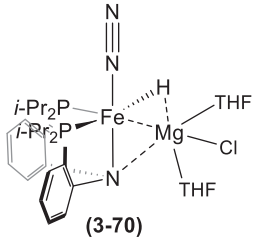

(3-70)

Fig. 52 A heterobimetallic Fe–N_2 complex that was the first isolated Fe(I)–(H)–(N_2) complex. Adapted from Hounjet, L. J.; Adhikari, D.; Pink, M.; Carroll, P. J.; Mindiola, D. J. *Z. Anorg. Allg. Chem.* **2015**, *641*, 45–48.

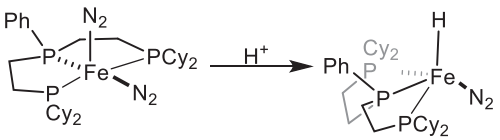

(3-71) **(3-72)**

Fig. 53 A rare example of an Fe^0-bis(N_2) complex that catalytically reduces N_2. Adapted from Cavaillé, A.; Joyeux, B.; Saffon-Merceron, N.; Nebra, N.; Fustier-Boutignon, M.; Mézailles, N. *Chem. Commun.* **2018**, *54*, 11953–11956.

NH_3/complex. From these protonation experiments and prior art, Mézailles and coworkers rationalized the high turnover numbers require addition of electrophiles to the distal N atom of the bound N_2 rather than the metal center as suggested by the work of Creutz and Peters. Metal protonation invariably results in N_2 loss and minimal N_2 reduction reactivity.

The first iron(0) dinitrogen complexes supported by *N*-heterocyclic carbenes (NHCs) were prepared by Danopoulos et al. in 2004. Utilizing the Fe(II)–Br_2 precursor complex[98] reduction of an iron(II) dibromide complex of a strongly σ-donating bis[(*N*-heterocyclic)carbene]pyridine pincer ligand, with excess Na/Hg amalgam under N_2 yielded the Fe(0)-bis(N_2) complex **3–73** (Fig. 54).[99] Structural data displayed the Fe center to be in a distorted square pyramidal geometry with one N_2 ligand coordinated in the apical position. The N−N bond lengths were found to be nearly identical at ∼1.114 Å, marginally longer than that for free N_2. The IR data agree with these bond metrics with absorptions at 2109 and 2031 cm^{-1}, which are similar to the high-spin Fe(0)-bis(N_2) complex **3–57**. DFT calculations point to a backbonding interaction from iron to the pyridyl ring competing with π-donation from the metal center to the N_2 ligands, resulting in the weaker extent of activation of the bound diatomic as compared to other iron(0) compounds.[100] Complex **3–73** readily undergoes oxidative addition with H_2 to afford in an iron-hydride complex, which facilitates C–H activation of benzene.[101]

Building from this initial tri-heterocycle pincer iron-dinitrogen system, Kiernecki et al. reported a pyridine(dipyrazole) pincer-type complex in which the pyrazole rings were substituted with tethered borane moieties (9-borabicyclo[3.3.1]nonyl, [9-BBN]).[102] Addition of 1 equiv. N_2H_4 to the Fe(II)-dihalide (Cl or Br) complex of this ligand resulted in capture of one hydrazine molecule between the two Lewis acidic B-atoms (**3–74**). Addition of a second equivalent of hydrazine generates the di-hydrazine complexes in which one N_2H_4 is coordinated to each 9-BBN motif (**3–75**). In both complexes, no interaction between the metal center and N_2H_4 was observed. The generality of these results was probed by varying the metal and removing the 9-BBN groups from the tethered units. An analogous Zn complex to **3–74** showed similar reactivity towards N_2H_4. Removal of the boranes yielded demetallation products upon addition of hydrazine, highlighting their requirement for hydrazine capture (Fig. 55).

Reduction of **3–74** with 2 equiv. KC_8 yielded a C_2-symmetric product, **3–76**, in which the N−N bond is cleaved and each of the hydrazine-derived amides bridge the Fe center and one 9-BBN moiety. In addition to N−N bond scission, the reduced complex was shown to produce ammonium in 87% yield when HCl is added to a THF solution of the dibromide derivative of complex **3–76**. Notably, the dichloride and neutral complexes yielded no ammonium when subjected to the same reaction conditions (Fig. 55).

A subsequent report on an iron complex of a borane-decorated version of the bis(NHC)pyridine complex addressed the role of sterics and Lewis acidity on hydrazine capture and reduction, and the role of the Fe center on ammonium production (Fig. 56).[103] Capture of hydrazine by the dicarbonyliron(0) complexes **3–77** and **3–78** was monitored by ^1H NMR and IR spectroscopy, which evidenced 1 equiv. of N_2H_4 per complex. X-ray diffraction of the cyclohexyl congener **3–78** revealed a polymeric structure in which one N_2H_4 bridges two Fe-pincer complexes through the tethered boranes. When the pendant borane is 9-BBN, hydrazine coordination is analogous to that for **3–74** and affords **3–79N**. In contrast to complex **3–74**, reduction of **3–79N** with 2 equiv. of KC_8 does not yield the di(μ-amide) complex and protonolysis of the product mixture yields trace ammonium (0.08 equiv.). Reduction with $KN(SiMe_3)_2$ does induce N−N bond cleavage (Fig. 57), but each produced amide group coordinates to one K^+ with the dicarbonyliron(0) acting as a spectator. The substitutionally-inert CO ligands were hypothesized to suppress the coordination of the nitrogenous donors to the metal center, suggesting that coordination to the metal center is critical for ammonia release.

8.26.3.3 Nitrogenase-Relevant Chemistry Supported by Bidentate and Related Ligand Environments

Bidentate ligands, especially those for which substituents on the ligand enforce low coordination numbers, are frequently used to access highly reactive metal centers for small molecule activation or organometallic catalysis. Expectedly then, metal complexes of such ligands are at the forefront of iron-dinitrogen chemistry. The following section is divided approximately into donor atom type, beginning with the P-based ligands, followed by the *N*,*N*-chelates, and finally, considering the *N*-heterocyclic carbene compounds.

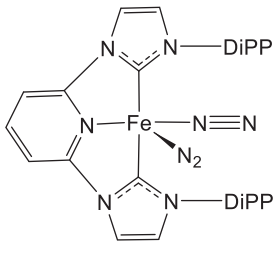

(3-73)

DiPP = $C_6H_3(^iPr)_2$

Fig. 54 The first example of a NHC-supported Fe(0)–N_2 complex. Adapted from Danopoulos, A. A.; Wright, J. A.; Motherwell, W. B. *Chem. Commun.* **2005**, 784–786.

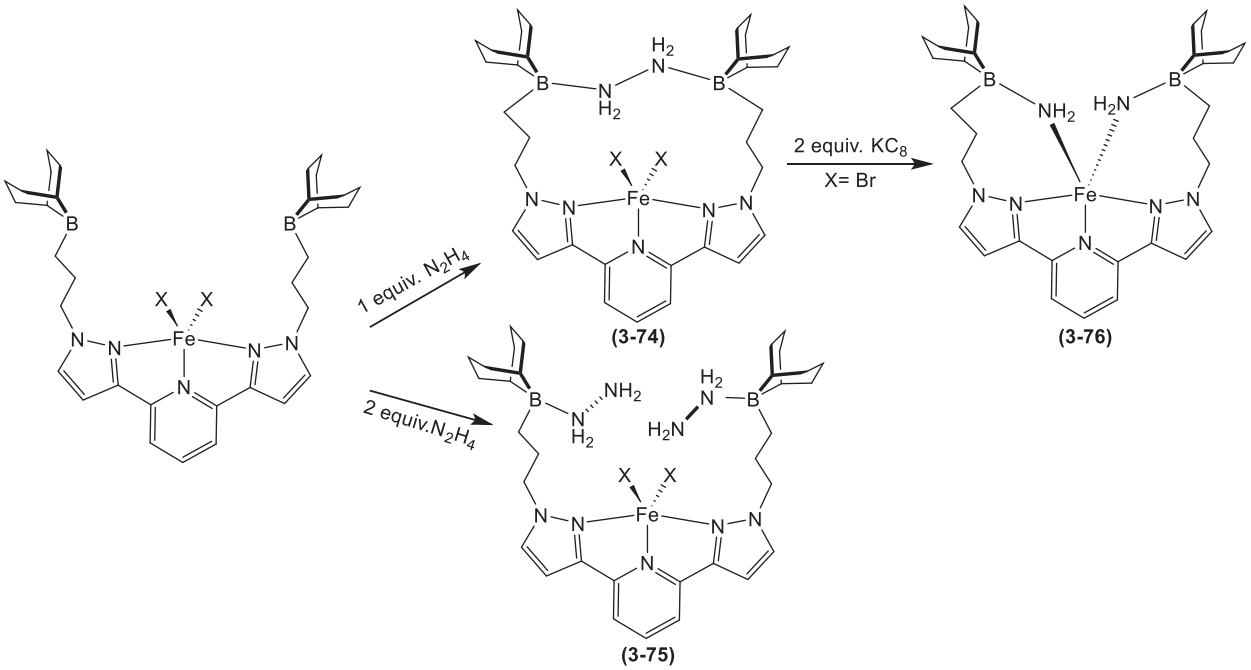

Fig. 55 Hydrazine coordinates to the tethered borane units. N—N bond cleavage occurs upon reduction. Adapted from Kiernecki, J. J.; Zeller, M.; Szymczak, N. K. *J. Am. Chem. Soc.* **2017**, *139*, 18194–18197.

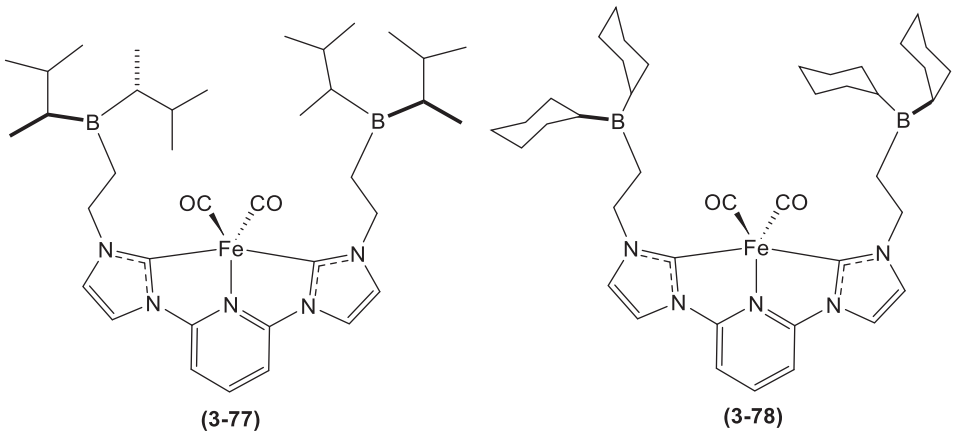

Fig. 56 Varying the borane substituents addressed steric effects on binding hydrazine. Adapted from Kiernecki, J. J.; Zeller, M.; Szymczak, N. K. *J. Am. Chem. Soc.* **2017**, *139*, 18194–18197.

For the latter category, many of the systems employ monodentate sterically-encumbered NHC ligands that lead to bis-NHC complexes, but are included here given the thematic similarity to the *cis N,N*-chelate systems.

8.26.3.3.1 Bidentate phosphine-ligated iron complexes

As noted above, the genesis of iron-dinitrogen chemistry is rooted in the phosphine-ligated iron centers reported by Sacco, Berke, Sacconi, Shilov, and Muetterties of which phosphines of varying denticities were demonstrated to support iron-dinitrogen interactions (see Section 8.26.2). Given our prior consideration of these systems, we focus here on the more recent examples.

In the mid-to-late 2000s, the Tyler group developed a series of Fe–N_2 complexes supported by bidentate bisphosphine ligands. Reaction of the *trans*-$[Fe(DMeOPrPE)_2Cl_2]^+$ complex (DMeOPrPE = 1,2-bis(bis(methoxypropyl)phosphino)ethane) complex with H_2 generates the Kubas-type complex **3–80H**, from which the H_2 ligand can be readily substituted by N_2 to afford the *trans*-hydrido(η^1-dinitrogen) complex, **3–80** (Fig. 58).[104] Given the lability of the N_2 donor of Fe-(DMeOPrPE) complexes, the structure of the complex was determined spectroscopically initially, although it was later crystallized and structurally characterized (Fig. 58).[105] The IR spectrum of **3–80** displays a sharp band at 2093 cm^{-1} corresponding to the N–N stretching vibration, which is characteristic of a terminally bound neutral N_2. The hydride was identified by ^1H and ^{31}P NMR spectroscopy; the combination of

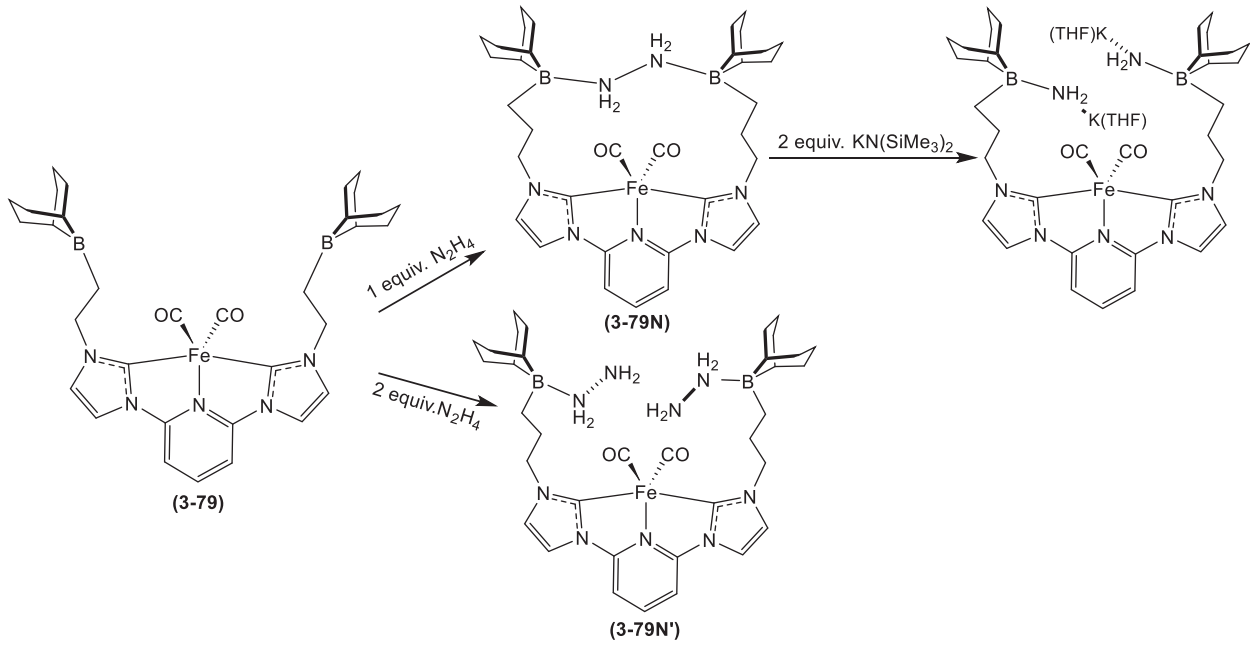

Fig. 57 Coordination of hydrazine molecules to tethered borane groups at an *Fe*-bis(NHC) complex. Adapted from Kiernecki, J. J.; Zeller, M.; Szymczak, N. K. *Inorg. Chem.* **2019**, *58*, 1147–1154.

a quintet at $\delta = -18.5$ ppm in the ^{1}H spectrum and the appearance of a doublet at $\delta = 77.3$ ppm in the ^{31}P NMR spectrum are consistent with the four P-donor atoms in the same plane and the hydride in an axial site.

Deprotonation of **3–80** by KO^{t}Bu provides access to the five-coordinate orange Fe(0) species **3–81**. The ^{1}H and ^{31}P{^{1}H} NMR spectra were particularly useful for structural information. The loss of the hydride ligand was confirmed by the ^{31}P NMR spectrum displaying only a singlet and the absence of the signal at -18.5 ppm in the ^{1}H NMR spectrum. Given that deprotonation effects metal reduction, the N–N stretching vibration shifts to lower energy and is observed at 1966 cm^{-1} in the IR spectrum in accord with the lower valence state of the iron center. Protonolysis of **3–81** by triflic acid was reported to liberate NH_4^+, $N_2H_5^+$, and the protonated phosphine ligands, which were detected by ^{1}H NMR spectroscopy. In contrast, treatment of **3–81** with HCl leads to the same nitrogen products and regenerates the starting dichloride complex. Production of ammonia by this system demonstrated the ability to reduce N_2 under mild conditions: H_2 is employed as the reductant, protonolysis occurs at room temperature, and the atmosphere is the source of N_2.

To probe the possible mechanism by which this system effects N_2 reduction, Tyler and coworkers synthesized a series of putative N_2 reduction intermediates of their iron phosphine complex. In 2007, the hydrazine complex $[Fe(DMeOPrPE)_2(N_2H_4)]^{2+}$ (**3–82**)

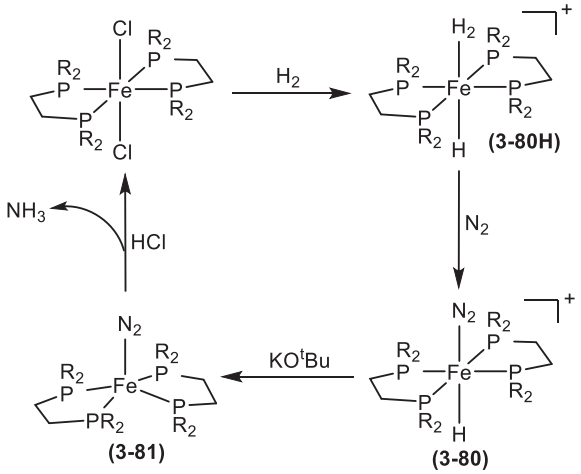

Fig. 58 Ammonia can be produced by protonation of a phosphine-based Fe–N_2 complex. All phosphines are of the PR_2 variety. Phosphine substituents have been removed for clarity. R = DMeOPrPE. Adapted from Gilbertson, J. D.; Szymczak, N. K.; Tyler, D. R. *J. Am. Chem. Soc.* **2005**, *127*, 10184–10185; Crossland, J. L.; Young, D. M.; Zakharov, L. N.; Tyler, D. R. *Dalton Trans.* **2009**, 9253–9259.

(Fig. 59) was isolated from reaction of the dichloride congener with hydrazine in the presence of $NaBPh_4$.[97] This complex was characterized spectroscopically and crystallographically and the N_2H_4 ligand was observed to be coordinated in a η^2-fashion. This complex represented the first example of this coordination mode for hydrazine. Complex **3–82** reacts with triflic acid to liberate ammonia and hydrazine, which agrees with the presumption that it is an on-pathway intermediate in the protonolysis of dinitrogen complex **3–81**.

These results, however, do not discount ammonia production by disproportionation of hydrazine liberated upon protonation of either **3–80** or **3–82**. To probe the reaction chemistry of the η^2-hydrazine complex, Crossland et al. examined deprotonation as a route to the diazene adduct. Indeed, the hydrazido-(**3–83**) and diazene complexes (**3–84**) were isolated by reaction of **3–82** with DBU (DBU = 1,8-diazabicyclo{5.4.0}undec-7-ene) and KO^tBu, respectively,[106] and the three complexes were also shown to interconvert (Fig. 60). The ability to employ sequential protonation steps to convert **3–84** to **3–83** to **3–82** provides synthetic precedent for the alternating protonation mechanism in nitrogenase N_2 reduction (Fig. 39).

The family of possible complexes along the N_2-reduction pathway starting from **3–80** was completed in 2012 with the isolation of a complete series of $FeH(N_xH_y)$ complexes (Fig. 61) in the DMeOPrPE ligand scaffold.[107] Addition of NH_3 and hydrazine to **3–80** yielded the Fe(H)–NH_3 complex (**3–85**) and the hydrazine congener (**3–86**), respectively. The diazene complex (**3–87**) was proposed to form upon chemical oxidation of **3–86** with lead(IV) acetate; a minor resonance in the $^{31}P\{^1H\}$ NMR spectrum was attributed to the diazene complex, but this species is short-lived and rapidly decomposes.

Komiya demonstrated that $Fe(N_2)(depe)_2$ could not form NH_3 when the complex was treated with HCl, as N_2 and H_2 were the only components identified in the product mixture, casting doubt on the viability of these types of complexes to reduce N_2 catalytically. Recently, Ashley and coworkers published a series of reports revisiting N_2 activation by $Fe(N_2)(dmpe)_2$ and $Fe(N_2)(depe)_2$ complexes and demonstrated that N_2 activation is indeed possible for these systems.[108] Addition of triflic acid to $Fe(N_2)L_2$ (where L = depe for **3–89** or dmpe for **3–88**) yielded both hydrazine and ammonia (Fig. 62). Their findings indicated that these complexes

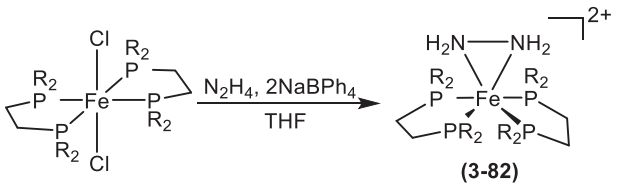

Fig. 59 Synthesis of an Fe-hydrazine complex. R = DMeOPrPE. Adapted from Crossland, J. L.; Zakharov, L. N.; Tyler, D. R. *Inorg. Chem.* **2007**, *46*, 10476–10478.

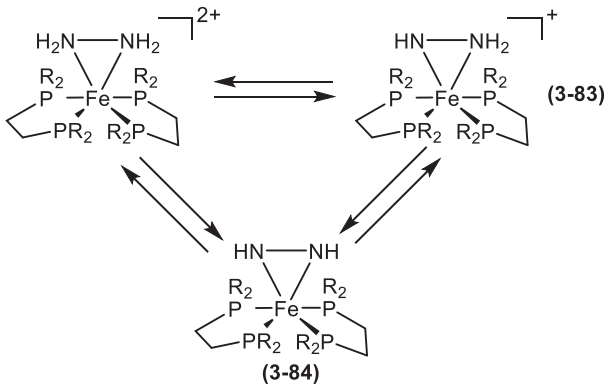

Fig. 60 A series of Fe–N_xH_y complexes shown to be interconvertible. R = DMeOPrPE. Adapted from Crossland, J. L.; Balesdent, C. G.; Tyler, D. R. *Dalton Trans.* **2009**, 4420–4422.

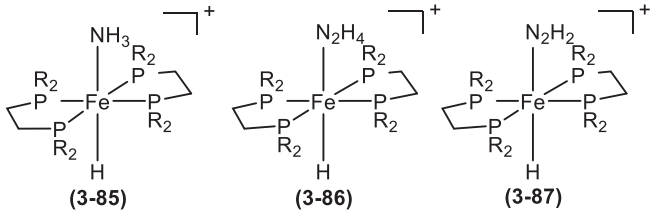

Fig. 61 A family of N_2-reduction intermediate complexes. R = DMeOPrPE. Adapted from Crossland, J. L.; Balesdent, C. G.; Tyler, D. R. *Inorg. Chem.* **2012**, *51*, 439–445.

were quite efficient towards N_2 reduction, with up to 55% conversion (per electron transferred) detected for **3–89**. In a subsequent report, the depe complex was noted to selectively yield hydrazine upon concomitant acidification and reduction using $[Ph_2NH_2][OTf]$ and Cp^*_2Co.[109] More recently, Piascik et al. synthesized the silylated diazenide derivatives, **3–90**. Although this complex did not provide direct mechanistic insight into ammonia and hydrazine, DFT calculations demonstrated that silylated derivatives could be used as surrogates to probe the N_2 activation mechanism for these bidentate phosphine complexes.[110] Indeed, a follow-up report from this group unveiled the first isolated intermediates of catalytic silylation[111] when the bis(silyl)hydrazide complexes (**3–91**) were synthesized and demonstrated to be a resting state in the catalytic process. Isolation of this product has provided a springboard for current and future mechanistic investigations into the catalytic N_2 silylation process (**Fig. 63**).

In 2013, Mock and coworkers prepared an Fe–N_2 complex using a pair of bidentate phosphine ligands decorated with a pendant amine (**3–92**) (**Fig. 64**).[112] Previously, this ligand system was exploited for proton reduction and dihydrogen oxidation under an applied potential, where the proximal amines served as proton shuttles during catalysis.[113] Complex **3–92** can be readily protonated at the pendant amine upon treatment with acid at room temperature with concomitant loss of N_2. However, reducing the temperature of this reaction prevents N_2 dissociation with the pendant amine acting as the Bronsted base. IR spectroscopy of the protonated N_2 complex shows an increase in energy for the N_2 stretching band by 25 cm^{-1}. This result raised questions regarding the electrostatic effects from nearby amino acid side chains in the active site pocket of the nitrogenase cofactors on the mechanism for N_2 activation.

Using a similar pendant-amine phosphine ligand scaffold, Mock et al. synthesized an Fe–N_2 complex (**3–93**) capable of performing catalytic silylation of N_2. Complex **3–93** (**Fig. 65**) displayed an activated N_2 moiety with a ν_{NN} at 2003 cm^{-1}, and was the first Fe(0)–N_2 complex in a P_4 ligand environment (i.e., four phosphorus donor atoms).[114] Subjecting this complex to catalytic silylation conditions of 500 equiv. KC_8 and 500 equiv. Me_3SiCl at ambient temperature affords $N(SiMe_3)_3$ in varying yields dependent on N_2 pressure: 11 ± 0.4 equiv. per complex at 1 atm. N_2 and 65 equiv. per complex at 100 atm. N_2.

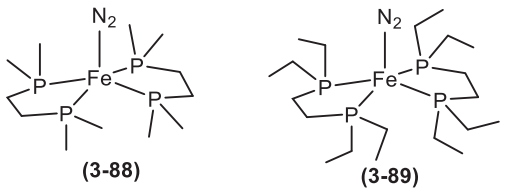

Fig. 62 **3–88** and **3–89** were both demonstrated to yield N_xH_y products upon exposure to acid. Adapted from Doyle, L. R.; Hill, P. J.; Wildgoose, G. G.; Ashley, A. E. *Dalton Trans.* **2016**, *45*, 7550–7554.

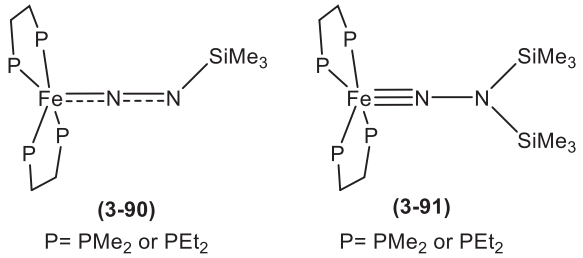

Fig. 63 Isolation of these complexes provided preliminary mechanistic insight into catalytic N_2 silylation. Adapted from Piascik, A. D.; Hill, P. J.; Crawford, A. D.; Doyle, L. R.; Green, J. C.; Ashley, A. E. *Chem. Commun.* **2017**, *53*, 7657–7660; Piascik, A. D.; Li, R.; Wilkinson, H. J.; Green, J. C.; Ashley, A. E. *J. Am. Chem. Soc.* **2018**, *140*, 10691–10694.

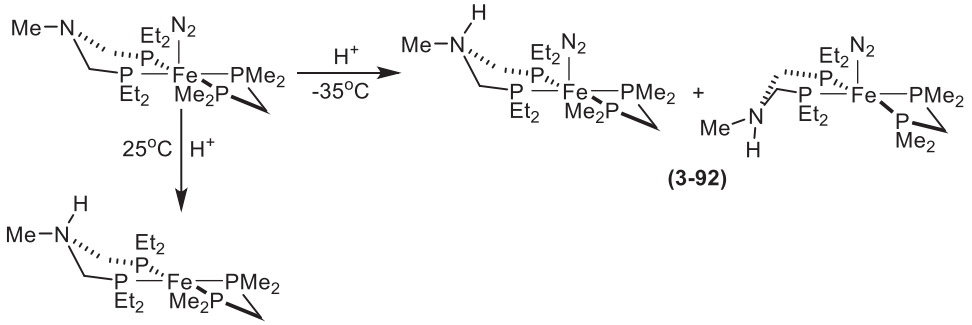

Fig. 64 Temperature affects N_2 lability upon protonation. Adapted from Heiden, Z. M.; Chen, S.; Mock, M. T.; Dougherty, W. G.; Kassel, W. S.; Rousseau, R.; Bullock, R. M. *Inorg. Chem.* **2013**, *52*, 4026–4039.

8.26.3.3.2 Iron-dinitrogen chemistry supported by N,N-chelating ligands

In 2001, Holland and coworkers successfully prepared a paramagnetic, low-coordinate μ-1,2-dinitrogen diiron(I) complex, **3–94**, supported by bulky β-diketiminate (or NAcNAc) ancillary ligands (Fig. 66). Complex **3–94** was structurally characterized by X-ray crystallography revealing a rare three-coordinate transition metal-N_2 complex as well as an elongated N−N bond distance of 1.182(5) Å (cf. 1.098 Å for free N_2).[115] As expected for the significant lengthening of this bond, the frequency for the N–N stretching mode was observed at 1778 cm^{-1} in the resonance Raman spectrum, which was confirmed by a $^{15}N_2$ labeling experiment ($\Delta\nu = 60$ cm^{-1}). Controlled stepwise reduction of the N_2 bond order was achieved by exposure of **3–94** to alkali metals (Na or K) to generate **3–95** in which the Fe–N_2–Fe core is reduced by two electrons and the alkali cations associate with the aromatic rings of the β-diketiminate substituents and the bridging N_2.

The dinitrogen-derived ligand in **3–95** is better formulated as a N_2^{2-} species; the crystallographically-determined N−N bond length of 1.23–1.24 Å and the band at 1589 cm^{-1} in resonance Raman spectra of **3–95** are consistent with double bond character. A structurally-analogous Fe–N_2–Fe complex was prepared using a less bulky, methyl-substituted β-diketiminate ligand by KC_8 reduction of the di(μ-chloride) diiron(II) complex under a N_2 atmosphere (Fig. 66). One significant difference is the two β-diketiminate chelates are coplanar in the methyl derivative, whereas these chelates are nearly orthogonal in the *t*-butyl complex. The steric demands of the large *t*-butyl groups on the ligands compress the chelate bite angle, thereby decreasing the angle between the two aryl substituents on the diketiminate and thereby disfavor the coplanar arrangement in **3–95**.[108] Computational studies on these dinitrogen complexes revealed a strong backbonding interaction from the Fe centers to the N_2 π^* orbital, which is enhanced upon incorporation of the alkali metal cations (see Fig. 66).[116]

Substitution reactions of **3–94** and **3–94Me** with various ligands provided additional context for the extent of N_2 activation in this system (Fig. 67). First, the ease of scrambling of the coordinated N_2 was evaluated for **3–94** and **3–94Me** by resonance Raman spectroscopy. For the $^{t\text{-Bu}}$NAcNAc Fe–N_2 complex (**3–94**), minimal $^{15}N_2$ incorporation was observed after several days at room temperature, which evidences the absence of N_2 cleavage, recombination, or facile N_2 loss. In contrast, the less sterically-encumbered ^{Me}NAcNAc Fe–N_2 complex (**3–94Me**) displays significant incorporation of $^{15}N_2$ after 2 days at −78 °C, showing the sterics of the ligand backbone contribute significantly to the lability of the N_2 ligand. The iron centers in **3–94** and **3–94Me** were shown to be Lewis acidic as addition of pyridine to either Fe–N_2 complex (**3–94** or **3–94Me**) yields the corresponding

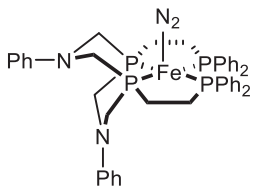

(3-93)

Fig. 65 An Fe–N_2 complex in a P_4 ligand environment, catalyzes silylation of N_2. Adapted from Prokopchuk, D. E.; Wiedner, E. S.; Walter, E. D.; Popescu, C. V.; Piro, N. A.; Kassell, W. S.; Bullock, R. M.; Mock, M. T. *J. Am. Chem. Soc.* **2017**, *139*, 9291–9301.

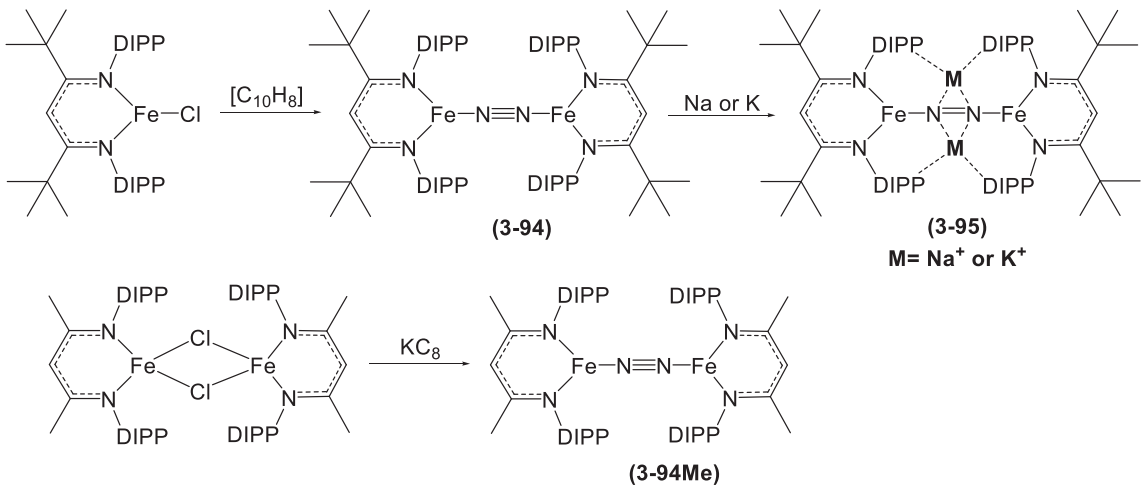

(3-94) **(3-95)**

(3-94Me)

Fig. 66 Several bridging Fe–N_2 complexes have been prepared by Holland's group using β-diketiminate ligands. DIPP = 2,6-diisopropylphenyl. Adapted from Smith, J. M.; Lachicotte, R. J.; Pittard, K. A.; Cundari, T. R.; Lukat-Rodgers, G.; Rodgers, K. R.; Holland, P. L. *J. Am. Chem. Soc.* **2001**, *123*, 9222–9223.

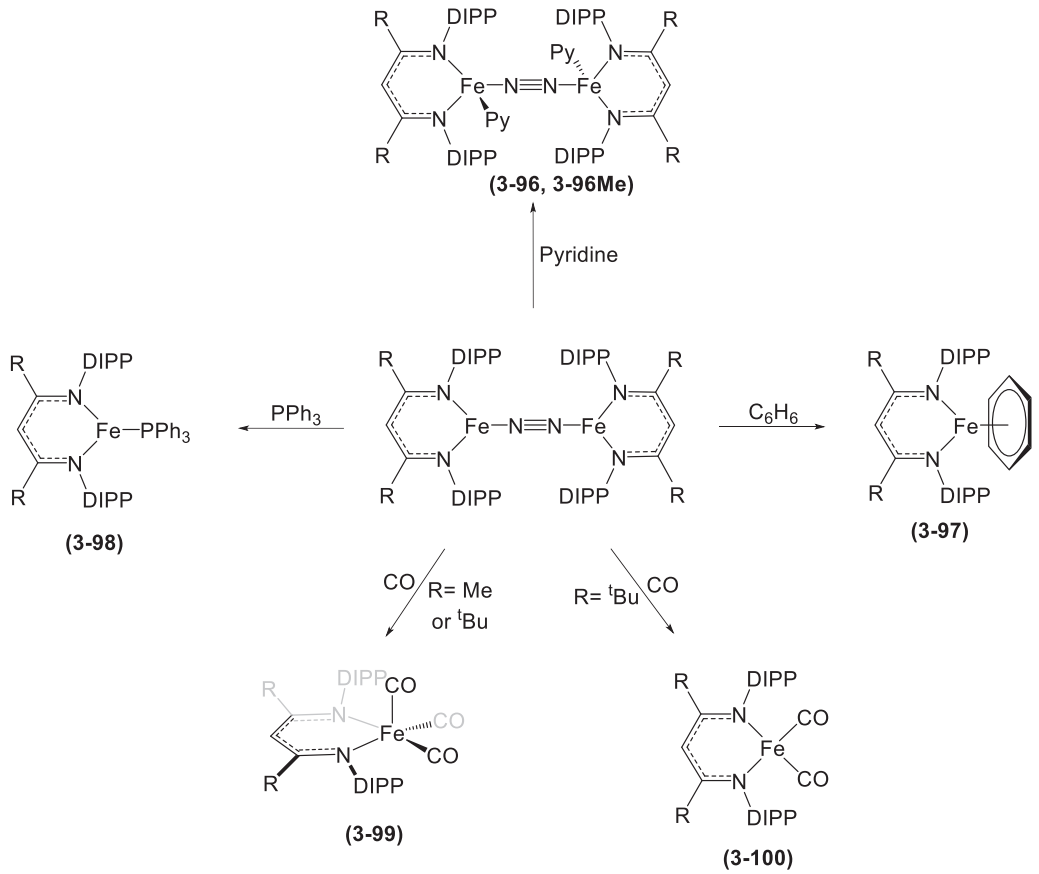

Fig. 67 The bridging N_2 unit is readily displaced when **3–35** or **3–35Me** are exposed to a variety of substrates. Adapted from Smith, J.M.; Sadique, A.R.; Cundari, T.R.; Rodgers, K.R.; Lukat-Rodgers, G.; Lachicotte, R.J.; Flaschenriem, C.J.; Vela, J.; Holland, P.L. *J. Am. Chem. Soc.* **2006**, *128*, 756–769.

four-coordinate compound in which pyridine occupies one coordination site (**3–96** or **3–96Me**). Finally, the N_2 ligand in **3–94Me** was readily displaced by several stronger ligands, including benzene, CO, and PPh_3, leading a series of monoiron complexes.

In addition to the substitution reactions described above, complexes **3–94** and **3–94Me** were shown to be 1-electron reducing agents through reductive coupling of ketones and aldehydes. A surprising reaction, however, was that with 1-adamantyl azide; one expected outcome would be formation of the azide complex and subsequent N_2 loss to afford the terminal iron imide. However, reaction of **3–94Me** at −78 °C or **3–94** at room temperature with 2 equiv. 1-adamantyl azide affords the hexazene-bridged diiron complexes **3–101** and **3–101Me** (Fig. 68).[117] The bond distances measured for the hexazene support a dianionic formulation, suggesting the iron centers are in the 2+ oxidation state. The Mößbauer data additionally supported a formal 2+ oxidation state assignment to each iron, but could not unequivocally rule out the possibility of a diiron(I) complex. Combining the structural and spectroscopic data, as well as results from a magnetic susceptibility study, the complex was formulated as having two high-spin Fe(II) centers.

Reaction of **3–95** with chelating agents such as crown ethers (e.g., 18-crown-6 and 12-crown-4) demonstrated the significant stabilizing effect the alkali cations have on the structure of the compound.[118] Addition of 2 equiv. 18-crown-6 to a diethyl ether solution of the methyl-substituted analog of **3–95** under a N_2 atmosphere (Fig. 69) led to the formation of a cation-sequestered analog of **3–95**. When the solution was cooled to −35 °C, the complex decomposed to the mononuclear iron-bis(N_2) complex **3–102**. Structural characterization of the mononuclear complex reveals that both dinitrogen donors are coordinated η^1 to the Fe center, but one N_2 bridges to an 18-crown-6-encapsulated K^+ cation. As one might anticipate, the N—N bond length for the μ-1,2-dinitrogen is longer than for the terminal N_2, suggesting the coordinated cation promotes backbonding from the iron center into the N_2 π* orbital. The results of these experiments reinforce the beneficial effects of cation-dinitrogen interactions in the second coordination sphere of the iron complex (Fig. 69).

Recently, the mixed-valent (μ-1,2-dinitrogen)diiron(I/0) complex **3–103** was synthesized by careful one-electron reduction of complex **3–94Me** using KC_8 and 18-crown-6.[119] Crystallographic data revealed a N—N bond length of 1.186(6) Å, which is significantly longer than the bond in free N_2 but strikingly similar to that reported for the (μ-1,2-dinitrogen)diiron(I) compound **3–94** and the monoiron bis(dinitrogen) species **3–102**. Interestingly, the N–N stretching mode in **3–103** is IR-active whereas this mode is IR-silent for the other analogous homo-valent diiron compounds. This observation indicates that **3–103** is non-centrosymmetric

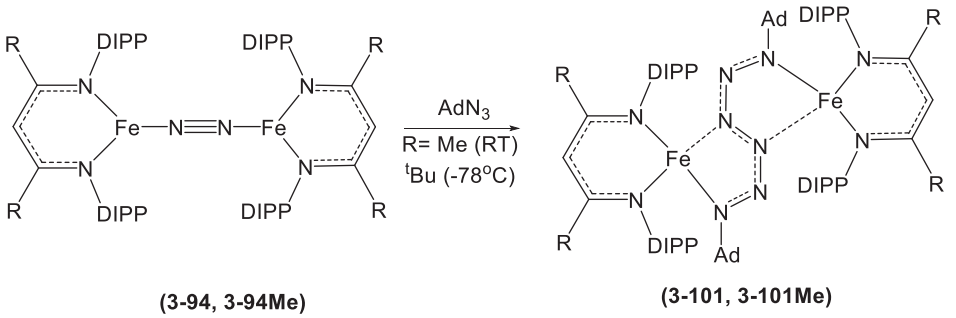

Fig. 68 The bridging N_2 complexes can also act as 1-electron reductants and have been used to reductively couple 2 equiv. of adamantyl azide to generate a hexazenide complex. Adapted from Cowley, R. E.; Elhaïk, J.; Eckert, N. A.; Brennessel, W. W.; Bill, E.; Holland, P. L. *J. Am. Chem. Soc.* **2008**, *130*, 6074–6075.

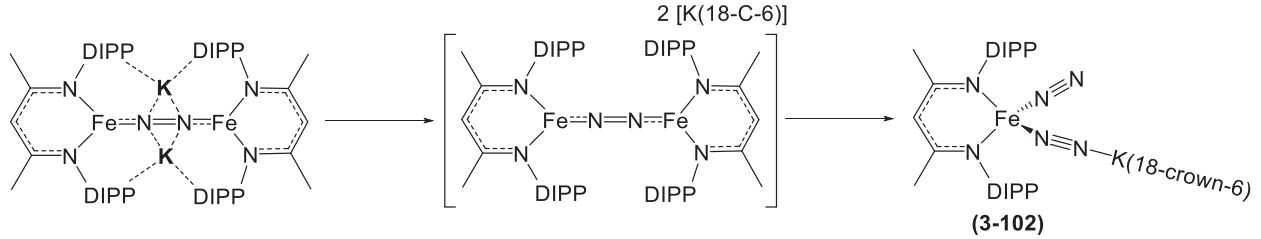

Fig. 69 Encapsulation of the potassium cations yields the mononuclear *Fe*-bis(N_2) complex. Adapted from McWilliams, S. F.; Bill, E.; Lukat-Rodgers, G.; Rodgers, K. R.; Mercado, B. Q.; Holland, P. L. *J. Am. Chem. Soc.* **2018**, *140*, 8586–8598.

and likely valence-localized on the method timescale. Whereas the two quadrupole doublets observed in the Mößbauer spectra of **3–103** agree with this oxidation state formalism, ^{1}H NMR spectra support a D_{2d} or D_{2h} symmetric complex as expected for a delocalized system (Fig. 70).

In 2011, Rodriguez et al. reported the first iron system to cleave the N_2 triple bond to afford nitrides.[120] Using a sterically less-demanding β-diketiminate ligand than their DIPP analog (cf. **3–94**), reduction of the di(μ-chlorido)diiron(II) complex **3–104** with KC_8 in THF under a dinitrogen atmosphere yielded the tetrairon di(μ-nitride) species **3–105** (Fig. 71). Activation of atmospheric N_2 was confirmed by performing the reduction under either $^{15}N_2$, resulting in the ^{15}N isotopologue, or under an Ar atmosphere, which does not generate **3–105**.

Complex **3–105** was characterized using various spectroscopic techniques and by X-ray crystallography and displays several unique features. Most notably, complex **3–105** has a triiron core that encapsulates the nitride groups and a dangling fourth iron center associated with the two K^+ centers through two μ-chlorides. Three quadrupole doublets are observed in Mößbauer spectra of **3–105**, which implies that two of the four Fe centers are equivalent and the remaining two metal centers are unique. The equivalent Fe sites were determined to be high-spin tetrahedral Fe(III) sites and assigned as the two Fe centers coordinated to both nitride donors. The dangling iron site was assigned as a high-spin pseudo-tetrahedral Fe(II) center, and the third Fe center bound to the Fe_2N_2 rhomboid as a high-spin trigonal planar Fe(II). The reader is directed to a recent publication for a detailed treatment of the proposed mechanism for N_2 cleavage and formation of **3–105**.[121] Structurally analogous compounds with respect to the Fe_3N_2 core of the cluster can be prepared using Na- or Rb-based reductants in lieu of KC_8.[122b] The Na^+ analog, synthesized by reduction of **3–104** by Na, lacks the dangling Fe center, whereas the Rb congener, formed by RbC_8 reduction of **3–104**, retains this fourth Fe center.

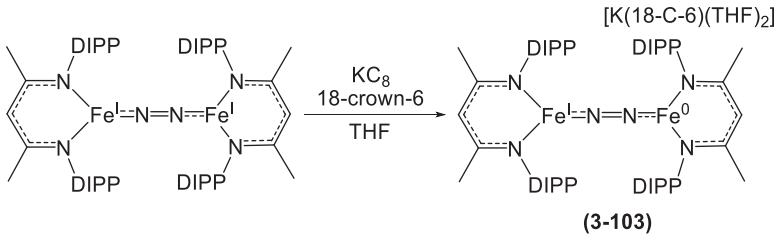

Fig. 70 A mixed-valent Fe–N_2 complex was recently isolated by the Holland group. Adapted from McWilliams, S. F.; Bunting, P. C.; Kathiresan, V.; Mercado, B. Q.; Hoffman, B. M.; Long, J. R.; Holland, P. L. *Chem. Commun.* **2018**, *54*, 13339–13342.

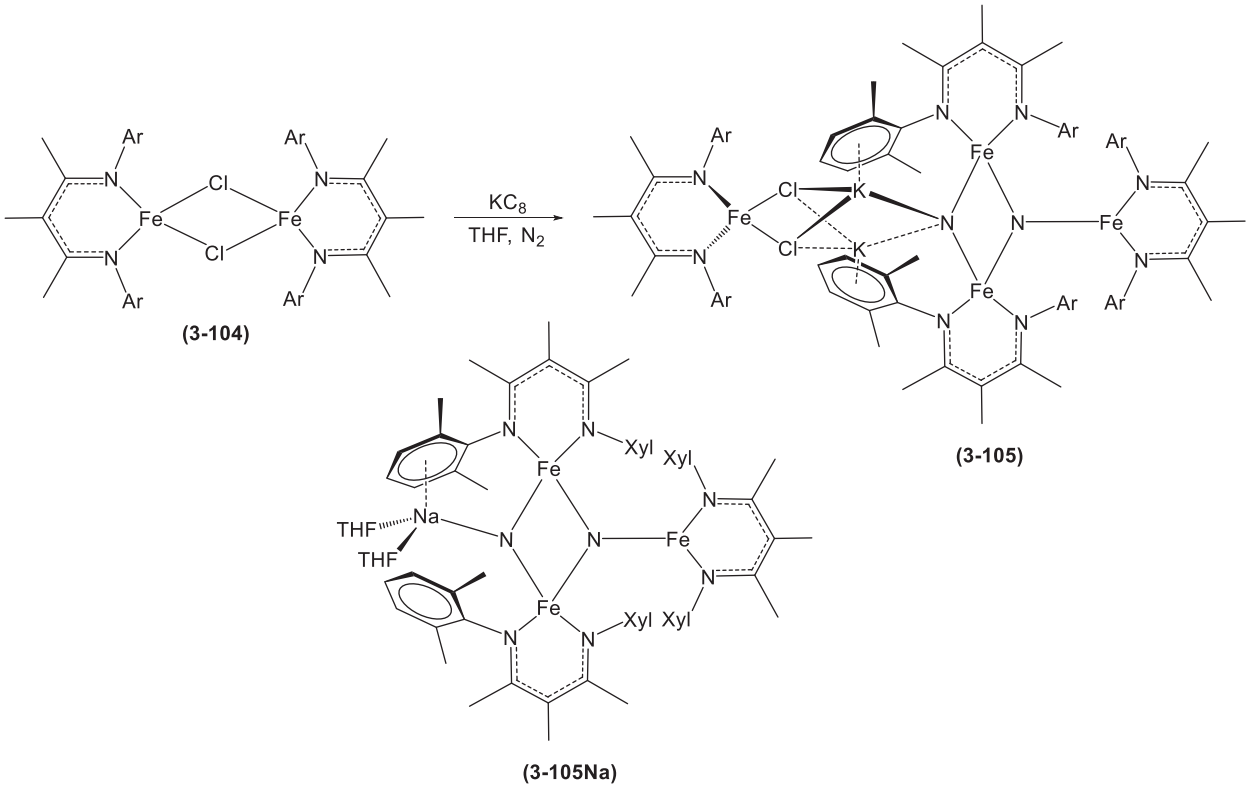

Fig. 71 Using a less bulky ligand, a novel bis(nitride) species was generated upon KC_8 reduction under an atmosphere of N_2. Adapted from Rodriguez, M. M.; Bill, E.; Brennessel, W. W.; Holland, P. L. *Science* **2011**, *334*, 780–783.

In addition to its unique structure, complex **3–105** displays an array of reactivity and highlights the surprising ease with N−N bond formation can be facilitated on iron centers. Similar to the substitution reactions reported for complexes **3–94** and **3–94Me**, the di(μ-nitride) complex **3–105** readily reacts with various σ-only and π-acid ligands. When dissolved in benzene, **3–105** surprisingly undergoes an intramolecular nitride coupling to expel N_2 and generates 4 equiv. of the mononuclear Fe^{I}-(η^6-C_6H_6) compound (**3–106**). Reaction of CO and CNXyl (or 2,6-dimethylphenyl isocyanide) with **3–105** affords an analogous outcome to benzene: the nitride complex reductively eliminates dinitrogen and affords the mononuclear iron complexes of the added Lewis bases (**3–107**, **3–108**) (Fig. 72).[122a]

The di(nitride) complex was also examined for its capability of producing NH_3 upon reaction with proton or H-atom sources. Addition of ethereal HCl to a solution of **3–105** generated NH_4^+ in yields as high as 86% whereas hydrogenation by H_2 in benzene affords no detectable ammonia.[115] The hydrogenation reaction results in a di(μ-hydrido)diiron(II) compound (**3–109**) and the Fe^{I}-benzene complex (**3–106**). One drawback from the need for protonation to release ammonia is the concomitant degradation of the (β-diketiminato)iron species, rendering this process non-catalytic. Alternative sources of protons were analyzed, and tri-tertbutylphenol was found to be a sufficient H^+ donor and, importantly, did not decompose the Fe-NAcNAc core; suggesting the possibility for electrocatalytic NH_3 production.

Use of tri-tertbutylphenol as the acid also allowed for increased mechanistic insight into the NH_3 production process (Fig. 73).[123] A triiron imide-nitride, a triiron amide-nitride, and a diiron di(amide) complexes were individually isolated and provided a more specific outline of the protonation pathway. Synthesis of the imide-nitride complex was affected by using a terminal alkyne as the acid source, which resulted in a triiron(II, III, III) species and an iron(II)-acetylide product. A proton-coupled electron transfer by exposing the imide-nitride complex to the aforementioned phenol results in the amide-nitride congener. Lastly, the di(amide) complex is produced by two proton transfers and a single electron transfer when the amide-nitride species is exposed to $(^tBu)_3PhOH$.

A series of triangular triiron-$(\mu\text{-}1,2\text{-}N_2)_n(\mu\text{-}Cl)_m$ ($n = 2$ or 3; $m = 0$ or 1) were developed concurrently with the synthesis of **3–105** (Fig. 74).[122b] Reduction of **3–104** by 2 equiv. of CsC_8 did not show the same N−N bond scission as evident in **3–105**, but rather binding of two N_2 moieties in bridging end-on modes. The third "edge" of the triangular unit is formed by a bridging chloride ligand, suggestive of incomplete reduction of the starting Fe_2Cl_2 complex. Attempts for further reduction by an additional equivalent of CsC_8 showed no change in the spectroscopic data. Addition of a fourth equivalent, however, results in the formation of the $Fe_3(\mu\text{-}N_2)_3$ analog. Crystallographic data of both complexes shows elongation of the N_2 units to 1.234 Å and 1.191 Å for the bis(μ-N_2) and the tris(μ-N_2) complexes, respectively. Analogous reduction by 4 equiv. KC_8 and RbC_8 results in isostructural triiron complexes with the Rb-analog exhibiting similar structural parameters (K-analog was not structurally characterized due to

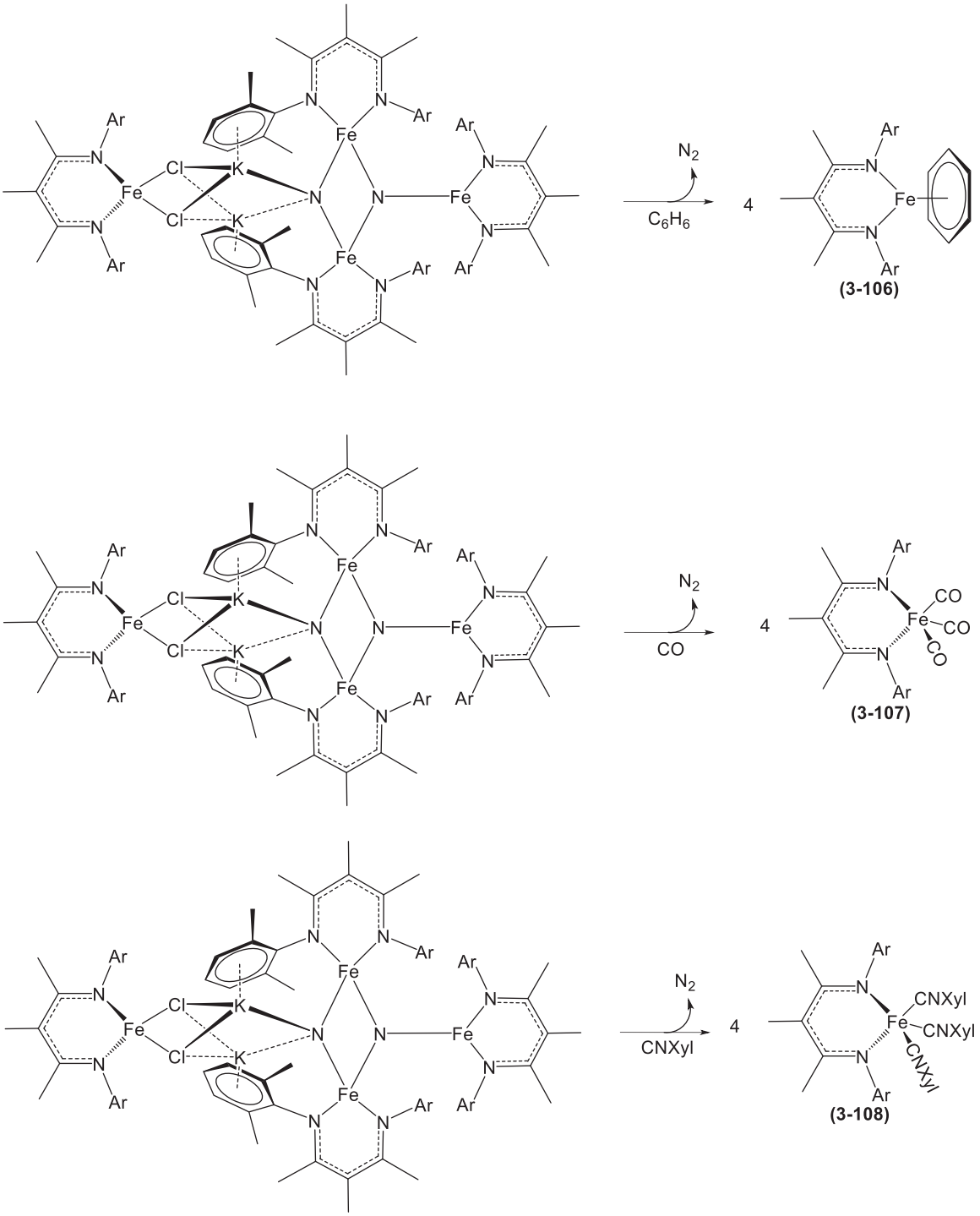

Fig. 72 In the presence of Lewis basic substrates, the bis(nitride) complex decomposes into 4 equiv. of the corresponding mononuclear iron(I)-LB complex. Adapted from Macleod, K.C.; Vinyard, D.J.; Holland, P.L. *J. Am. Chem. Soc.* **2014**, *136*, 10226–10229.

significant decomposition, but identified by ^{1}H NMR spectroscopy). The structural data clearly illustrate that additional reducing equivalents decreases the extent of N_2 activation (cf. **3–105**, which uses 1e$^-$ per Fe center). The authors proposed that the large difference arises from a cooperative interaction between multiple Fe centers that is only accessible when the metal centers are less reduced, as in complex **3–105**. Over-reduction of the Fe sites induces increased M^+-π interactions, forcing the core to expand.

Somewhat related to the β-diketiminate system are the phosphazene-ligated iron-dinitrogen species **3–111** reported by reported by Masuda and coworkers (Fig. 75) and the silylene iron-dinitrogen complex from the Cui group (Fig. 76).[117] For the former, the crystal structure of **3–111** revealed a dimetallic Fe(I) complex containing a single bridging N_2 unit. The N—N bond length of 1.184 Å

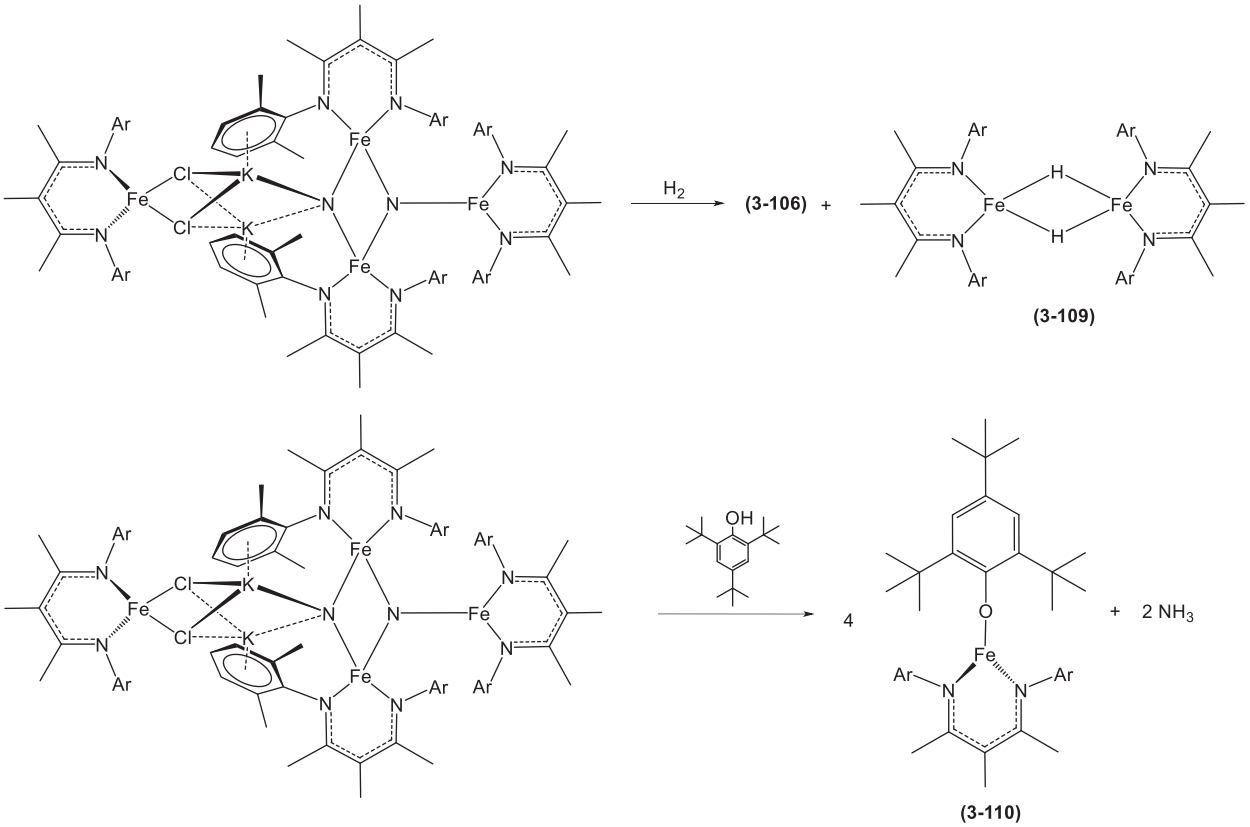

Fig. 73 NH_3 can be produced from the bis(nitride) complex when exposed to H^+ sources. Tri-tertbutylphenol was found to be a particularly useful H^+ donor. Adapted from Macleod, K. C.; McWilliams, S. F.; Mercado, B. Q.; Holland, P. L. *Chem. Sci.* **2016**, *7*, 5736–5746.

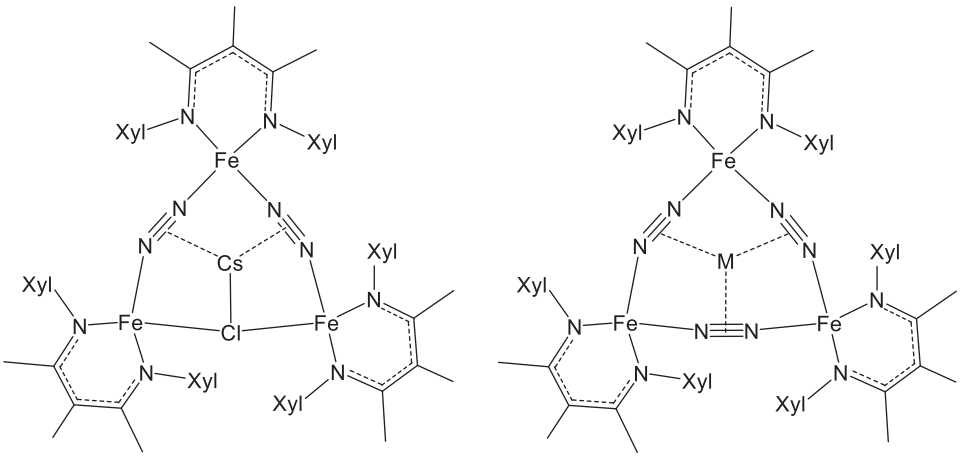

Fig. 74 A series of triangular triiron complexes were synthesized by varying the equivalents of MC_8 reductant (M = K, Rb, Cs). Adapted from Grubel, K.; Brennessel, W.W.; Mercado, B.Q.; Holland, P.L. *J. Am. Chem. Soc.* **2014**, *136*, 16807–16816.

is very similar to Holland's dimetallic NAcNAc-coordinated system (**3–94**), which is shorter than one would predict based on the 1755 cm^{-1} IR absorption—the lowest energy reported for Fe(I)–N_2 complexes (cf. **3–94** and related derivatives). The DFT calculations suggest that the highly σ-donating ligand scaffold enhances the π-backbonding into the bridging N_2, consequently lowering the energy of the N–N stretching vibration and implying that the dinitrogen donor is best described as a formally reduced N_2 moiety.

Use of an arene-tethered silylene ligand by Bai et al. was shown to yield an Fe(0)–N_2 complex in a low-coordination environment.[124] Arguably, the imine nitrogen was the likely intended donor, although the low-valent iron center demonstrates a preference for the arene as had been demonstrated for low-valent late 3d centers in related NAcNAc ligated compounds.[125] The N_2 complex

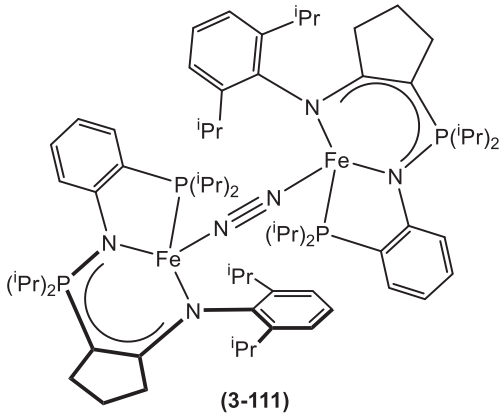

(3-111)

Fig. 75 A phosphazene-ligated Fe–N_2 complex with the lowest reported ν_{NN} for an Fe(I)–N_2 complex. Adapted from Suzuki, T.; Wasada-Tsutsui, Y.; Ogawa, T.; Inomata, T.; Ozawa, T.; Sakai, Y.; Fryzuk, M. D.; Masuda, H. *Inorg. Chem.* **2015**, *54*, 9271–9281.

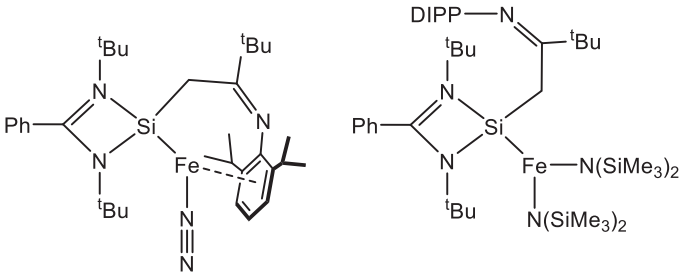

(3-112) (3-113)

Fig. 76 Addition of amide cleaved the Fe—N_2 bond in **3–112** yielding the bis(amide) analog. Adapted from Bai, Y.; Zhang, J.; Cui, C. *Chem. Commun.* **2018**, *54*, 8124–8127.

(**3 − 112**) was synthesized by reduction of a dimeric Fe–Br_2 complex with KC_8. The solid-state structure shows the Fe–N_2 moiety coordinated to silylene and in an η^6 fashion between Fe and the tethered arene. The N—N bond length was found to be 1.133 Å, but the absence of a N—N stretching vibration in the IR spectrum of vacuum-dried solid suggested a labile N_2 unit. Reaction of the precursor iron bromide dimer with $LiN(SiMe_3)_2$ produced the bis(amide) derivative (**3 − 113**), for which the X-ray crystal structure evidences a three-coordinate Fe center and no observed η^6-arene interaction. Complexes **3–112** and **3–113** were demonstrated similar efficacies for catalytic silylation of N_2 with yields of ~47 equiv. per Fe atom, which is the highest efficiency reported for Fe-based catalysts normalized to metal ion content (cf. Mock and Nishibayashi catalysts).

Multimetallic cooperation is a common theme across a variety of N_2-activating species; biological N_2 activation occurs at a polyiron site and aggregates of transition metal complexes effect N_2 cleavage (vide supra). In 2013, Guillet et al. synthesized a triiron-tribromide complex templated by a tris(β-diketiminate) cyclophanate, in which the arrangement of the donor arms orients the frontier orbitals of the metal centers towards the internal cavity of the complex.[126] Shortly thereafter, Lee et al. communicated that reduction of this complex by KC_8 under a N_2 atmosphere (Fig. 77) produced $Fe_3(NH_x)_3\mathbf{L}^{Et/Me}$ (**3–114**).[127] Crystallography data of **3–114** illustrated the complex comprises a Fe_3N_3 planar hexagonal core with each iron in a distorted tetrahedral environment. The IR spectrum of **3–114** displays a weak absorption at 3397 cm^{-1} consistent with the presence of bridging N–H_x donors. The difference map enabled the location of the H-atom bonded to each bridging N-atom and was freely refined, implying that NH_x groups in the structure were imide ligands with three formally iron(III) centers for charge balance. Mößbauer spectra on this product, however, implicate a mixed-valent cluster and, therefore, a distribution of imide and amide donors that are unresolved in the X-ray diffraction data. Reduction of $Fe_3Br_3\mathbf{L}^{Et/Me}$ under a $^{15}N_2$ atmosphere was performed as well and expected energy shifts in the IR spectrum were observed. ^1H NMR spectra on the acid treated complex derived from $^{14}N_2$ or $^{15}N_2$ revealed the expected triplet and doublet consistent with the isotopically labeled ammonium. Indophenol assay of the product mixture revealed a relatively low NH_3 yield of 30.2%.

The structural and spectroscopic data provided insight into the possible N_2 reduction pathway by $Fe_3Br_3\mathbf{L}^{Et/Me}$. Intramolecular N_2 bond scission would afford a $\{Fe_3N_2\}$ core; thus, observation of a third N-atom suggested an intermolecular cooperative process where N_2 is cleaved at the interface between two complexes. Indeed, evidence supporting this mechanism was obtained through a dimeric species that co-crystallized with **3–114**, indicating that the steric constraints of the cyclophanate

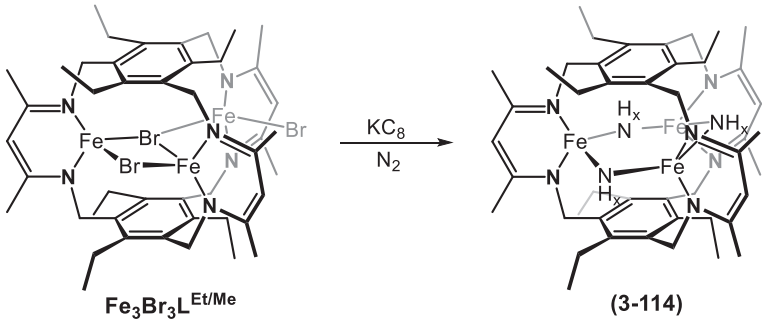

Fig. 77 Synthesis of a triiron complex bearing NH_x ligands derived from reduced N_2. Adapted from Lee, Y.; Sloane, F. T.; Blondin, G.; Abboud, K. A.; García-Serres, R.; Murray, L. J. *Angew. Chem. Int. Ed.* **2015**, *54*, 1499–1503.

ligand did not preclude intercluster approach. The structure of this dimeric species was highly disordered, making its identity elusive, but two K^+ were found bridging the two complexes. The latter structure bears strong resemblance to alkali cations in **3–105**. Mechanistic questions for dinitrogen activation by this system remain to be elucidated, of which one is whether only an intercluster pathway is operating.

In 2018, Ferreira et al. reported that a family of triiron complexes supported by the tris(β-diketiminate) cyclophanate ligand are competent for the catalytic silylation of dinitrogen. This series of compounds varies by metal oxidation states and ancillary bridging ligands, and was the first systematic demonstration of nitrogenase-like chemistry in multimetallic systems.[128] Using the same catalytic silylation protocols across the series of complexes (viz. 500 equiv. KC_8 and 500 equiv. Me_3SiCl), generation of $N(SiMe_3)_3$ was detected by GC and quantified indirectly by ^1H NMR spectra recorded on acid-digested product mixtures. The triiron tri-bromide, tri-fluoride, and tri-sulfide complexes demonstrated the highest catalytic activity at room temperature with yields of 57(7), 64(6), and 58(1) $N(SiMe_3)_3$/catalyst after 24 h. Contrastingly, the tri(μ-hydrido)triiron(II) and the (μ_3-hydrido)dicarbonyltriiron(I/I/II) complexes were the worst under the same conditions with yields of 34(5) and 35(3) $N(SiMe_3)_3$/catalyst, respectively. Temperature also influences catalytic performance in this system; reactions performed using the tri-bromide complex at −35 °C for 96 h afforded 83 ± 7 $N(SiMe_3)_3$/catalyst in contrast to a comparable yield after 96 h and 24 h at room temperature. Unfortunately, a well-defined trend is not readily apparent across the series of complexes; however, it is notable that catalysts with ancillary π-donor ligands generally perform better. This correlation may arise from the ease of dissociation of these ligands upon reduction with KC_8 as compared to the π acidic ligands.

8.26.3.3.3 Iron-dinitrogen species ligated by two N-heterocyclic carbenes

In 2015, Ung and Peters synthesized a two-coordinate Fe(0) complex using a cyclic(alkyl)(amino)carbene (CAAC) ligand (Fig. 78).[129] Cooling a solution of **3–115** to temperatures below −80 °C resulted in coordination of N_2 to the Fe(0) center, and this binding was reversible upon warming/cooling cycles. The thermal instability of this bis(CAAC)Fe^0–N_2 complex rendered crystallization difficult. However, reduction of **3–115** by KC_8 and addition of 18-crown-6 successfully trapped the formally Fe(–I)–N_2 complex (**3–116**) for which single crystals were isolated. The solid-state structure of **3–116** displays the Fe center in a distorted trigonal planar geometry with a terminally coordinated N_2 ligand with a N—N bond length of 1.035 Å. The solid-state bond metrics are at odds with the N–N stretching frequency at 1850 cm^{-1} and may suggest vibration effects in the structure determination. These

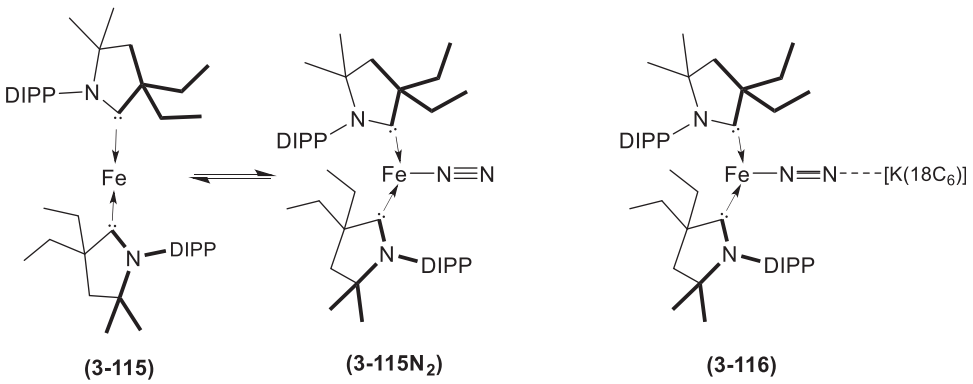

Fig. 78 A two-coordinate Fe–N_2 complex was isolated at low temperatures. Adapted from Ung, G.; Peters, J. C. *Angew. Chem. Int. Ed.* **2015**, *54*, 532–535.

CAAC complexes were subjected to catalytic N_2 reduction conditions; 50 equiv. KC_8 and $[H(OEt_2)_2][BAr^F{}_4]$ were added to an ethereal solution of **3–115** and **3–116** with both having minimal catalytic activity with yields of 3.3 ± 1.1 equiv. NH_3 and 2.6 ± 0.6 equiv. NH_3 per catalyst, respectively. Despite the poor catalytic performance for N_2 reduction to ammonia, **3–115** showed significantly more activity for catalytic silylation of N_2, yielding 24.4 ± 2.7 equiv. of $N(SiMe_3)_3$ when large quantities of reductant and silyl were used (600 equiv. each) were employed.

8.26.3.4 Iron-Dinitrogen Complexes With Sulfur-Based Ligands

As described in the preceding sections spectroscopically and/or structurally characterized Fe–N_2 complexes have been synthesized using ligands rich in pnictogen donors (P and N) in the primary coordination sphere of the Fe center. These complexes have helped develop many new insights into the activity of the nitrogenase enzymes but deviate from the donor atom types for the biological system (i.e., predominantly inorganic sulfides and carbide). Iron-dinitrogen complexes employing thiolate donors were a significant contribution of Sellmann and coworkers; recent work by others have expanded on that prior work and extended the field towards inorganic sulfide-containing complexes.

In 2004, Vela et al. developed a (μ-sulfido)diiron complex in which each Fe center was ligated by a β-diketiminate ligand. Several nitrogenase-relevant substrates—acetonitrile, ammonia, methylhydrazine, 1,1-dimethylhydrazine, and phenylhydrazine—were shown to react with this diiron complex to afford the corresponding adduct in all cases.[130] One equivalent of acetonitrile binds per complex in an η^1-mode, whereas 1 equiv. of methylhydrazine, 1,1-dimethylhydrazine, and ammonia coordinate in a terminal mode to each metal center within complex. Reaction with phenylhydrazine produced a unique mixed-valent $Fe^{II}Fe^{III}$ complex **3–117** (Fig. 79) for which the structural data evidence an anionic bridging phenylhydrazide ligand and Mößbauer data confirming the valence-localized formalism.

In an effort to move towards a more biomimetic coordination sphere, an Fe–N_2 complex supported by two thiolates and one C-donor was prepared by Čorić et al. by a two-step KC_8 reduction of an $Fe(THF)_2$ complex under a N_2 atmosphere (Fig. 80).[131] The first reduction step yielded complex **3–118** in which the Fe center is bound to the central arene in an η^6-fashion. The second reduction step, accompanied by K^+ sequestration with added 18-crown-6, produced the desired Fe–N_2 complex. The crystal structure of **3–118** shows N_2 (d(N–N) = 1.132(7) Å) is bound at a pseudotetrahedral Fe(0) center, which has slipped to an η^2-coordination mode with the central arene. The Fe—S bond lengths are slightly longer (2.32–2.35 Å) than those observed in FeMoco E_0 state (2.25–2.27 Å), but the Fe—C bond is of similar length (2.04 Å) to the Fe_6—C bond in the E_0 state (2.01 Å). An analogous tris(thiolato) Fe(THF) complex was synthesized to investigate a three-coordinate and unsaturated complex, to provide a more mimetic system to FeMoco. Indeed, KC_8 reduction of the tri-thiolate complex yielded complex **3–118**, illustrating that Fe—S bond scission likely facilitates N_2 binding. The N_2 ligand is substantially activated with an IR band appearing at 1880 cm^{-1}, corroborating the elongated N—N bond observed in the crystal structure (see bond length above). The observed frequency is among the lowest observed for a terminally bound Fe–N_2 complex.

The Peters group has also synthesized Fe–N_2 complexes bearing thiolate and thioether ligands. Their first report came in 2011 with the preparation of a thioether-containing derivative of their $[SiP^R{}_3]^-$ ligand[132] (see Section 8.26.3.1.2). Protonation of the mono(thioether) Me-coordinated Fe(II) complex with $HBAr^F{}_4$ in Et_2O afforded methane and the cationic Fe(II)–N_2 complex **3–119** (Fig. 81). The same reaction conditions with the bis(thioether) complex yielded only the solvent adduct and methane. In the structure of the N_2-containing complex, the Fe center is in a distorted trigonal bipyramidal geometry, which is a significant deviation from that observed in the analogous $[SiP^R{}_3]^-$ complex. This difference in geometry was attributed to the smaller steric pressure imposed by the thioether arms as compared to the PR_2 arms in $[SiP^R{}_3]^-$ compounds. The N_2 ligand was found to be weakly activated with a stretching frequency of 2156 cm^{-1}, consistent with the π acidic character of the thioether donors. Addition of $NaBEt_3H$ to **3–119** or the Et_2O solvated complex yielded the corresponding neutral hydride-N_2 complexes. In contrast to the $[SiP^R{}_3]^-$ system, reduction of the thioether complexes by KC_8 or Na/Hg leads to a mixture of decomposition products. Yet, reduction of the solvent adduct with milder reductants, such as Cp_2Co or $Cr(C_6H_6)_2$, afforded a mixed-valent diiron-(μ-N_2) complex (**3 − 120**). The structure of this dimetallic complex was probed using spectroscopic methods. A ν_{NN} of 1881 cm^{-1} suggested a dimetallic system, as it is considerably lower than the mononuclear analogs and similar to complex (**3–30**) in which the dinitrogen is capped by a Na^+ ion. The appearance of the N–N stretching band in

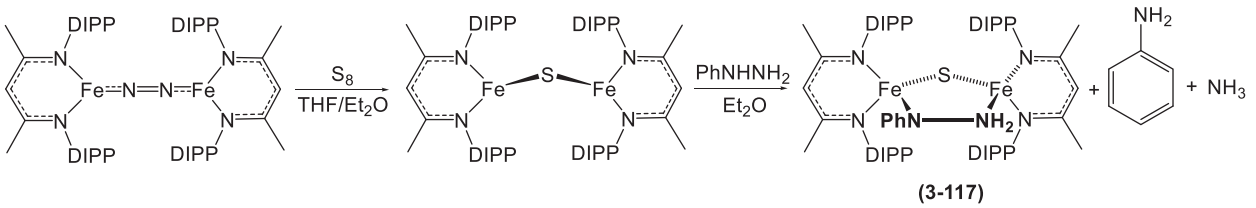

Fig. 79 Nitrogenase-relevant substrates were observed to react with a diiron-μ-sulfide complex. Adapted from Vela, J.; Stoian, S.; Flaschenriem, C. J.; Münck, E.; Holland, P. L. *J. Am. Chem. Soc.* **2004**, *126*, 4522–4523.

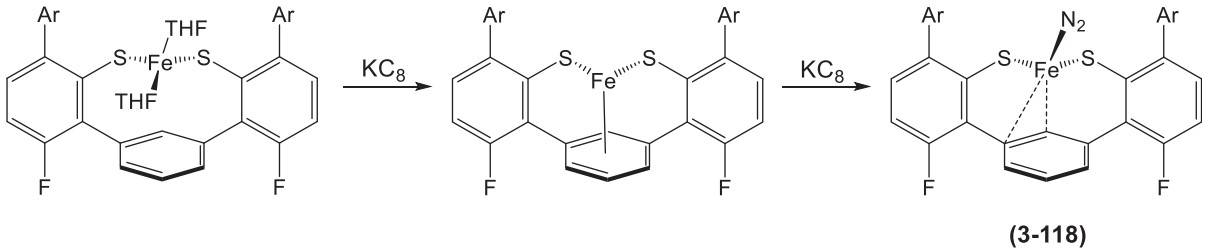

Fig. 80 Hemilabile interactions between the Fe center and the central arene ring facilitate N_2 binding. Adapted from Čorić, I.; Mercado, B. Q.; Bill, E.; Vinyard, D. J.; Holland, P. L. *Nature* **2015**, *526*, 96–99.

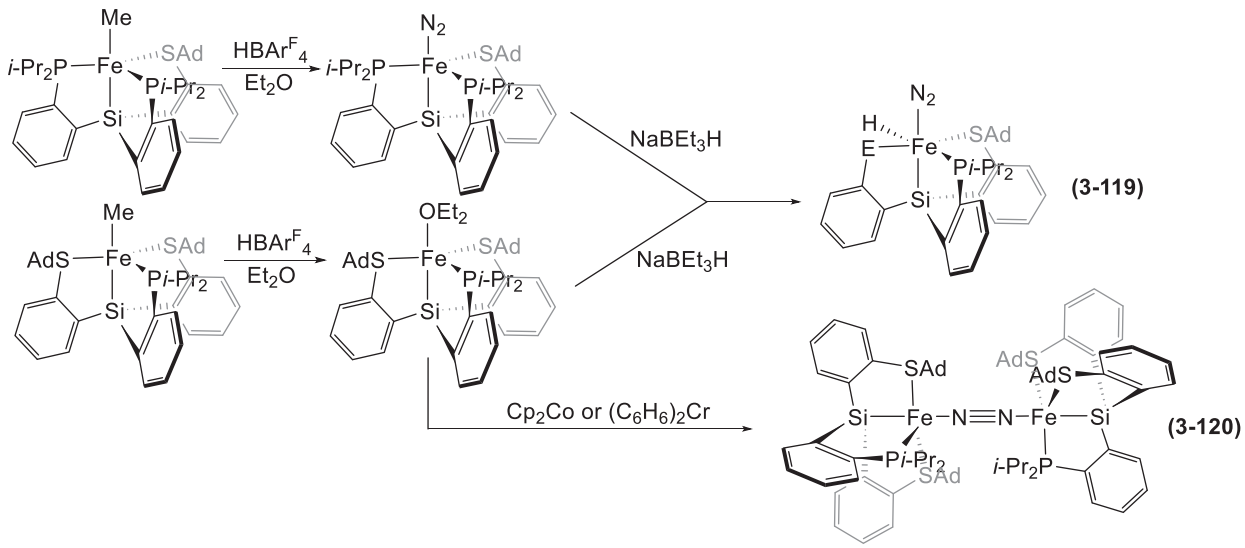

Fig. 81 N_2 can bind to an Fe complex bearing thioether coordinating arm(s). (E = $P^{(iPr)2}$ or S^{Ad}). Adapted from Takaoka, A.; Mankad, N. P.; Peters, J. C. *J. Am. Chem. Soc.* **2011**, *133*, 8440–8443.

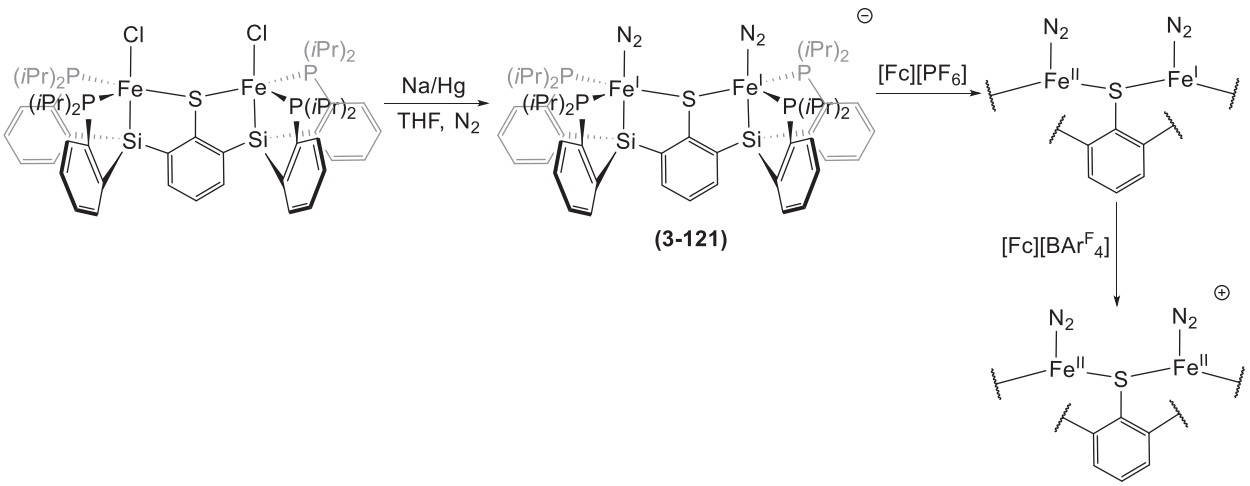

Fig. 82 A diiron-bis(N_2) complex was isolated bearing a thiophenolate ligand scaffold. Adapted from Creutz, S. E.; Peters, J. C. *J. Am. Chem. Soc.* **2015**, *137*, 7310–7313.

the IR spectrum also suggested an asymmetric complex. Further confirmation of the mixed-valence nature of **3–120** arises from near-IR spectra in which an absorption consistent with an intervalence charge transfer band is observed. A 20 K EPR spectrum supported a Kramer's doublet ground state indicative of $S > 1/2$, and variable temperature magnetic susceptibility measurements were best modeled as arising from a $S = 3/2$ system.

A diiron-bis(N_2) complex (**3−121**) was prepared (Fig. 82) using a disilyl-thiophenolate ligand by deprotonation of the diiron-dichloride precursor followed by reduction of the putative diiron-chloride intermediate with excess Na/Hg.[133] Sequestration of the Na cation with 12-crown-4 allowed for isolation of a crystalline product **3–121**. Structural data shows a N_2 molecule coordinated at each Fe center, *trans* to the silyl anchor. IR data shows the complex to have a weakly activated N_2 ligand with $\nu_{NN} = 2017$ and 1979 cm^{-1} (symmetric and asymmetric stretches, respectively). As similarly observed for the monoiron complexes, a series of dinitrogen adducts in which the metal oxidation states were readily accessible: sequential oxidation of **3–121** with [Fc][PF_6] (Fc = ferrocenium) to remove one and then two electrons affords the Fe^{II}/Fe^{I} mixed-valent congener and the all ferrous complex, respectively. As before, the N−N bond distances and stretching frequencies correlate inversely with formal oxidation state.

Of particular interest is access to a multiiron complex with hydride and dinitrogen donor(s); spectroscopic data for such a species would complement data on the proposed hydride-containing intermediates of FeMoco. Thus, reduction of the dichloride precursor with excess Na/Hg in benzene affords the hydride-dinitrogen complex **3–122** (Fig. 83).

Complex **3–121** is, however, a poor catalyst for catalytic N_2 reduction with reported yields of 1.8 ± 0.3 equiv. NH_3 per complex under the conditions typically employed by this group, suggesting that a possible interplay between iron-hydride reductive elimination and dinitrogen activation. The complex was shown to be an effective precatalyst for hydrazine disproportionation to NH_3 and N_2, converting 50 equiv. of N_2H_4 to 29 equiv. of NH_3. Retention of both N_2 ligands across multiple redox states provides evidence supporting the purported low-valent intermediates proposed in the FeMoco catalytic cycle.

Preceding this complex was an analogous diiron complex bearing a [Si_2P_4O] ligand scaffold showing similarity to the disilyl-thiophenolate scaffold. Addition of 2 equiv. $FeBr_2$ in the presence of 4 equiv. Na/Hg under N_2 resulted in the isolation of a $Fe_2(\mu\text{-}H)_2(N_2)$ complex (Fig. 84).[25] The bridging hydrides presumably originate from in situ activation of the Si–H upon addition of $FeBr_2$ and reductant. One Fe center coordinates one N_2 molecule in an end-on mode and the structural data show a weakly activated dinitrogen ligand (1.114 Å). Reducing the temperature under an N_2 atmosphere results in coordination of a second molecule of N_2 to the second Fe atom based on variable temperature IR experiments on **3–123** and affords a neutral diiron-bis(N_2) complex (**3–124**). Exposure of **3–123** to excess Na/Hg in the presence of 12-crown-4 under N_2 yields the mixed-valent diiron-bis(N_2) congener (**3–125**). Electrochemical experiments of both complexes revealed that a 10^6-fold increase in N_2 binding is observed upon reduction of the neutral diiron complex. This result highlights the impact a single electron transfer step can have on substrate binding.

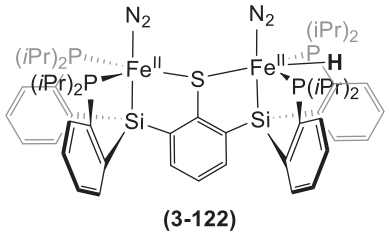

(3-122)

Fig. 83 Excess Na/Hg reduction of the dichloride derivative yields the diiron(II)-hydride congener. Adapted from Creutz, S. E.; Peters, J. C. *J. Am. Chem. Soc.* **2015**, *137*, 7310–7313.

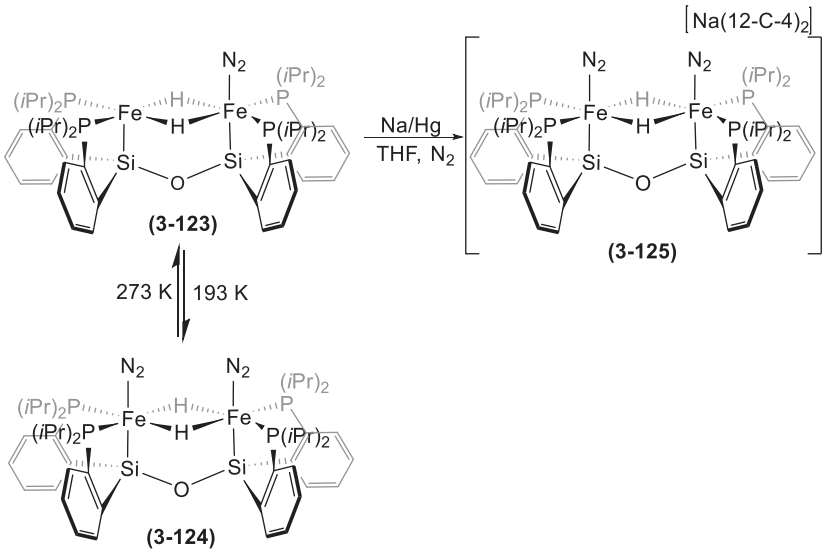

Fig. 84 Electrochemical experiments conducted on these analogous diiron complexes showed how important a single-electron transfer step is on N_2 coordination. Adapted from Rittle, J.; McCrory, C.C.L.; Peters, J.C. *J. Am. Chem. Soc.* **2014**, *136*, 13853–13862.

8.26.4 Concluding Remarks and Outlook

As highlighted in this chapter, numerous synthetic Fe–N_2 complexes have been developed and have begun to illuminate many mysteries about biological N_2 reduction. Iron-dinitrogen chemistry has seen remarkable advances over the last several decades, beginning with the first observations of molecular Fe–N_2 complexes to more recent demonstrations of prowess as catalysts for N_2 fixation. The development of this body of work has highlighted the competence for iron as the reaction center for N_2 binding and activation in the enzymatic systems. Notable advances include the following:

- Successful synthesis of numerous N_2 to N_2H_x or $N_2(SiR_3)_x$ species, clearly defining the bounds of a Chatt cycle wherein the distal protonation drives N−N bond scission, on different ligand platforms, but featured prominently in the complexes from Peters' and coworkers,
- The interplay between iron-hydride and iron-dinitrogen chemistry with respect to priming the metal centers for dinitrogen binding and as part of preferential N_2 activation vs. N_2 dissociation, which preceded the proposed structure of the N_2 reactive state (E_4) of the iron-molybdenum cofactor, and
- Demonstration that numerous iron complexes are competent for N_2 reduction to either ammonia or tris(trimethylsilyl) amine, employing either separate electron and proton sources or a proton-coupled electron transfer reagent.

With these advances, future and ongoing directions aim to answer recent questions derived from the study of the enzyme system. For example, many of the reported complexes utilize phosphine ancillary ligands and incorporated fragments of the sulfide and C-donor environment of the enzyme cofactor or employed nitrogen-donor ligands (e.g., NAcNAc); no ligand system has as yet set itself apart as reproducing the likely electronic structure afforded by the μ_6-carbide and the sulfide rich coordination environment observed in the enzyme. In addition, questions abound on the site and mode of binding and pathway of N_2 activation; recent assignment of the Mo^{III} center and of sulfide lability in the cofactor will likely influence the design and development of model compounds. In addition, probing the role of secondary coordination sphere effects in the facilitating N_2 bond scission are in their infancy, but are likely key to future understanding of how directed proton transfer to the N_2 fragment shifts catalysis towards N_2 and away from unproductively regenerating iron-hydride species. Finally, the importance of the carbide center on cofactor function remains an open question; hypotheses such as imparting structural integrity to the cluster, storing H-atoms, or allowing for tunable metal-ligand interactions during N_2 activation remain incompletely answered and require future attention.

References

1. UNEP; WHRC. *Reactive Nitrogen in the Environment: Too Much or Too Little of a Good Thing*, United Nations Environment Programme, 2007.
2. (a) Vitousek, P. M.; Howarth, R. W. *Biogeochemistry* **1991,** *13,* 87; (b) Falkowski, P. G. *Nature* **1997,** *387,* 272–275.
3. Canfield, D. E.; Glazer, A. N.; Falkowski, P. G. *Science* **2010,** *330,* 192–196.
4. Pople, J. A.; Curtiss, L. A. *J. Chem. Phys.* **1991,** *95,* 4385–4388.
5. Jia, H.-P.; Quadrelli, E. A. *Chem. Soc. Rev.* **2014,** *43,* 547–564.
6. Frost, D. C.; McDowell, C. A. *Roy. Soc. London. Math. Phys. Sci.* **1956,** *236,* 278–284.
7. Nørskov, J.; Contacts, B.; Miranda, R.; et al. *Sustainable Ammonia Synthesis Exploring the Scientific Challenges Associated With Discovering Alternative, Sustainable Processes for Ammonia Production DOE Roundtable Report,* 2016.
8. Bazhenova, T. A.; Shilov, A. E. *Coord. Chem. Rev.* **1995,** *144,* 69–145.
9. Holland, P. L. *Dalton Trans.* **2010,** *39,* 5415–5425.
10. Smil, V. *Nature* **1999,** *400,* 415.
11. Ertl, G. *Angew. Chem. Int. Ed.* **2008,** *47,* 3524–3535.
12. Schlögl, R. *Angew. Chem. Int. Ed.* **2003,** *42,* 2004–2008.
13. Metz, B.; Davidson, O. R.; Bosch, P. R.; Dave, R.; Meyer, L. A. *Contribution of Working Group III to the Fourth Assessment Report of the Intergovernmental Panel on Climate Change*, Cambridge University Press: Cambridge, United Kingdom and New York, NY, USA, 2007.
14. (a) Falicov, L. M.; Somorjai, G. A. *Proc. Natl. Acad. Sci. U. S. A.* **1985,** *82,* 2207–2211; (b) Strongin, D. R.; Carrazza, J.; Bare, S. R.; Somorjai, G. A. *J. Catal.* **1987,** *103,* 213–215.
15. (a) Freund, H.-J.; Bartos, B.; Messmer, R. P.; Grunze, H.; Kuhlenbeck, H.; Neumann, M. *Surf. Sci.* **1987,** *185,* 187–202; (b) Grunze, M.; Golze, M.; Hirschwald, W.; Freund, H.-J.; Pulm, H.; Seip, U.; Tsai, M. C.; Ertl, G.; Küppers, J. *Phys. Rev. Lett.* **1984,** *53,* 850–853.
16. (a) Einsle, O.; Tezcan, F. A.; Andrade, S. L. A.; Schmid, B.; Yoshida, M.; Howard, J. B.; Rees, D. C. *Science* **2002,** *297,* 1696–1700; (b) Tezcan, F. A.; Kaiser, J. T.; Mustafi, D.; Walton, M. Y.; Howard, J. B.; Rees, D. C. *Science* **2005,** *309,* 1377–1380; (c) Spatzal, T.; Aksoyoglu, M.; Zhang, L.; Andrade, S. L. A.; Schleicher, E.; Weber, S.; Rees, D. C.; Einsle, O. *Science* **2011,** *334,* 940.
17. (a) Spatzal, T.; Schleiser, J.; Burger, E.-M.; Sippel, D.; Zhang, L.; Andrade, S. L. A.; Rees, D. C.; Einsle, O. *Nat. Commun.* **2016,** *7,* 10902; (b) Bjornsson, R.; Neese, F.; DeBeer, S. *Inorg. Chem.* **2017,** *56,* 1470–1477; (c) Lancaster, K. M.; Roemelt, M.; Ettenhuber, P.; Hu, Y.; Ribbe, M. W.; Neese, F.; Bergmann, U.; DeBeer, S. *Science* **2011,** *334,* 974–977.
18. (a) Holland, P. L. In *Comprehensive Coordination Chemistry II;* McCleverty, J. A., Meyer, T. J., Eds.; Pergamon: Oxford, 2003; pp 569–599; (b) Burgess, B. K.; Lowe, D. J. *Chem. Rev.* **1996,** *96,* 2983–3011.
19. (a) Dos Santos, P. C.; Igarashi, R. Y.; Lee, H.-I.; Hoffman, B. M.; Seefeldt, L. C.; Dean, D. R. *Acc. Chem. Res.* **2005,** *38,* 208–214; (b) Barney, B. M.; Igarashi, R. Y.; Dos Santos, P. C.; Dean, D. R.; Seefeldt, L. C. *J. Biol. Chem.* **2004,** *279,* 53621–53624; (c) Sarma, R.; Barney, B. M.; Keable, S.; Dean, D. R.; Seefeldt, L. C.; Peters, J. W. *J. Inorg. Biochem.* **2010,** *104,* 385–389.
20. (a) Dance, I. *Chem. Asian J.* **2007,** *2,* 936–946; (b) Dance, I. *Dalton Trans.* **2008,** 5977–5991; (c) Dance, I. *Dalton Trans.* **2012,** *41,* 7647–7659; (d) Dance, I. *Chem. Commun.* **2013,** *49,* 10893–10907; (e) Dance, I. *Dalton Trans.* **2015,** *44,* 18167–18186; (f) Dance, I. *Sci. Rep.* **2013,** *3,* 3237; (g) Dance, I. *Inorganics* **2019,** *7,* 8.
21. (a) Spatzal, T.; Perez, K. A.; Einsle, O.; Howard, J. B.; Rees, D. C. *Science* **2014,** *345,* 1620–1623; (b) Sippel, D.; Rohde, M.; Netzer, J.; Trncik, C.; Gies, J.; Grunau, K.; Djurdjevic, I.; Decamps, L.; Andrade, S. L. A.; Einsle, O. *Science* **2018,** *359,* 1484–1489; (c) Siegbahn, P. E. M. *J. Am. Chem. Soc.* **2016,** *138,* 10485–10495.
22. McKee, M. L. *J. Phys. Chem. A* **2016,** *120,* 754–764.

23. Thorneley, R. N. F.; Lowe, D. J. *Molybdenum Enzymes*; ; Wiley-Interscience Publications: New York, 1985; pp 221–284.
24. (a) Simpson, F. B.; Burris, R. H. *Science* **1984,** *224,* 1095–1097; (b) Guth, J. H.; Burris, R. H. *Biochemistry* **1983,** *22,* 5111–5122.
25. Rittle, J.; McCrory, C. C. L.; Peters, J. C. *J. Am. Chem. Soc.* **2014,** *136,* 13853–13862.
26. (a) Igarashi, R. Y.; Dos Santos, P. C.; Niehaus, W. G.; Dance, I. G.; Dean, D. R.; Seefeldt, L. C. *J. Biol. Chem.* **2004,** *279,* 34770–34775; (b) Dos Santos, P. C.; Mayer, S. M.; Barney, B. M.; Seefeldt, L. C.; Dean, D. R. *J. Inorg. Biochem.* **2007,** *101,* 1642–1648; (c) Barney, B. M.; Lukoyanov, D.; Igarashi, R. Y.; Laryukhin, M.; Yang, T.-C.; Dean, D. R.; Hoffman, B. M.; Seefeldt, L. C. *Biochemistry (Mosc.)* **2009,** *48,* 9094–9102; (d) Hoffman, B. M.; Lukoyanov, D.; Yang, Z.-Y.; Dean, D. R.; Seefeldt, L. C. *Chem. Rev.* **2014,** *114,* 4041–4062; (e) Harris, D. F.; Yang, Z.-Y.; Dean, D. R.; Seefeldt, L. C.; Hoffman, B. M. *Biochemistry* **2018,** *57,* 5706–5714; (f) Lukoyanov, D.; Khadka, N.; Dean, D. R.; Raugei, S.; Seefeldt, L. C.; Hoffman, B. M. *Inorg. Chem.* **2017,** *56,* 2233–2240; (g) Khadka, N.; Milton, R. D.; Shaw, S.; Lukoyanov, D.; Dean, D. R.; Minteer, S. D.; Raugei, S.; Hoffman, B. M.; Seefeldt, L. C. *J. Am. Chem. Soc.* **2017,** *139,* 13518–13524; (h) Lukoyanov, D.; Yang, Z.-Y.; Khadka, N.; Dean, D. R.; Seefeldt, L. C.; Hoffman, B. M. *J. Am. Chem. Soc.* **2015,** *137,* 3610–3615.
27. (a) Münck, E.; Rhodes, H.; Orme-Johnson, W.; Davis, L.; Brill, W.; Shah, V. *Biochim. Biophys. Acta, Protein Struct.* **1975,** *400,* 32–53; (b) Huynh, B.; Henzl, M.; Christner, J.; Zimmermann, R.; OrmeJohnson, W.; Münck, E. *Biochim. Biophys. Acta* **1980,** *623,* 124–138; (c) Huynh, B.; Münck, E.; Orme-Johnson, W. *Biochim. Biophys. Acta, Protein Struct.* **1979,** *576,* 192–203; (d) Yoo, S. J.; Angove, H. C.; Papaefthymiou, V.; Burgess, B. K.; Münck, E. *J. Am. Chem. Soc.* **2000,** *122,* 4926–4936.
28. Sacco, A.; Aresta, M. *Chem. Commun.* **1968,** *4,* 1223–1224.
29. Aresta, M.; Giannoccaro, P.; Rossi, M.; Sacco, A. *Inorg. Chim. Acta* **1971,** *5,* 115–118.
30. (a) Bianco, V. D.; Doronzo, S.; Aresta, M. *J. Organomet. Chem.* **1972,** *42,* C63–C64; (b) Bianco, V. D.; Doronzo, S.; Rossi, M. *J. Organomet. Chem.* **1972,** *35,* 337–339.
31. Schrauzer, G. N.; Schlesinger, G. *J. Am. Chem. Soc.* **1970,** *92,* 1808–1809.
32. Newton, W. E.; Corbin, J. L.; Schneider, P. W.; Bulen, W. A. *J. Am. Chem. Soc.* **1971,** *93,* 268–269.
33. Birk, R.; Berke, H.; Huttner, G.; Zsolnai, L. *Chem. Ber.* **1988,** *121,* 471–476.
34. (a) Stoppioni, P.; Mani, F.; Sacconi, L. *Inorg. Chim. Acta* **1974,** *11,* 227–230; (b) Ghilardi, C. A.; Midollini, S.; Sacconi, L.; Stoppioni, P. *J. Organomet. Chem.* **1981,** *205,* 193–202.
35. Bazhenova, T. A.; Ivleva, I. N.; Kachapina, L. M.; Shilova, A. K.; Shilov, A. E.; Tchoubar, B. *J. Organomet. Chem.* **1985,** *296,* 95–101.
36. Gerlach, D. H.; Peet, W. G.; Muetterties, E. L. *J. Am. Chem. Soc.* **1972,** *94,* 4545–4549.
37. Hills, A.; Hughes, D. L.; Jimenez-Tenorio, M.; Leigh, G. J. *J. Organomet. Chem.* **1990,** *391,* C41–C44.
38. Leigh, G. J.; Jimenez-Tenorio, M. *J. Am. Chem. Soc.* **1991,** *113,* 5862–5863.
39. Hirano, M.; Akita, M.; Morikita, T.; Kubo, H.; Fukuoka, A.; Komiya, S. *J. Chem. Soc. Dalton Trans.* **1997,** *26,* 3453–3458.
40. Field, L. D.; Hazari, N.; Li, H. L. *Inorg. Chem.* **2015,** *54,* 4768–4776.
41. George, T. A.; Rose, D. J.; Chang, Y.; Chen, Q.; Zubieta, J. *Inorg. Chem.* **1995,** *34,* 1295–1298.
42. Sellmann, D.; Kunstmann, H.; Knoch, F.; Moll, M. *Inorg. Chem.* **1988,** *27,* 4183–4190.
43. Sellmann, D.; Soglowek, W.; Knoch, F.; Moll, M. *Angew. Chem. Int. Ed.* **1989,** *28,* 1271–1272.
44. Betley, T. A.; Peters, J. C. *J. Am. Chem. Soc.* **2003,** *125,* 10782–10783.
45. (a) Chatt, J.; Dilworth, J. R.; Richards, R. L. *Chem. Rev.* **1978,** *78,* 589–625; (b) Leigh, G. J. *Acc. Chem. Res.* **1992,** *25,* 177–181; (c) Yandulov, D. V.; Schrock, R. R.; Rheingold, A. L.; Ceccarelli, C.; Davis, W. M. *Inorg. Chem.* **2003,** *42,* 796–813.
46. Yandulov, D. V.; Schrock, R. R. *Science* **2003,** *301,* 76–78.
47. Betley, T. A.; Peters, J. C. *J. Am. Chem. Soc.* **2004,** *126,* 6252–6254.
48. Rohde, J.-U.; Betley, T. A.; Jackson, T. A.; Saouma, C. T.; Peters, J. C.; Que, L., Jr. *Inorg. Chem.* **2007,** *46,* 5720–5726.
49. Hendrich, M. P.; Gunderson, W.; Behan, R. K.; Green, M. T.; Mehn, M. P.; Betley, T. A.; Lu, C. C.; Peters, J. C. *Proc. Natl. Acad. Sci. U. S. A.* **2006,** *103,* 17107–17112.
50. (a) Buhr, J. D.; Taube, H. *Inorg. Chem.* **1979,** *18,* 2208–2212; (b) Man, W.-L.; Tang, T.-M.; Wong, T.-W.; Lau, T.-C.; Peng, S.-M.; Wong, W.-T. *J. Am. Chem. Soc.* **2004,** *126,* 478–479; (c) Seymore, S. B.; Brown, S. N. *Inorg. Chem.* **2002,** *41,* 462–469.
51. Saouma, C. T.; Moore, C. E.; Rheingold, A. L.; Peters, J. C. *Inorg. Chem.* **2011,** *50,* 11285–11287.
52. Chomitz, W. A.; Arnold, J. *Dalton Trans.* **2009,** 1714–1720.
53. McSkimming, A.; Harman, W. H. *J. Am. Chem. Soc.* **2015,** *137,* 8940–8943.
54. Cummins, D. C.; Yap, G. P. A.; Theopold, K. H. *Eur. J. Inorg. Chem.* **2016,** 2349–2356.
55. (a) Scepaniak, J. J.; Fulton, M. D.; Bontchev, R. P.; Duesler, E. N.; Kirk, M. L.; Smith, J. M. *J. Am. Chem. Soc.* **2008,** *130,* 10515–10517; (b) Martinez, J. L.; Lin, H.-J.; Lee, W.-T.; Pink, M.; Chen, C.-H.; Gao, X.; Dickie, D. A.; Smith, J. M. *J. Am. Chem. Soc.* **2017,** *139,* 14037–14040.
56. Hickey, A. K.; Muñoz, S. B., III; Lutz, S. A.; Pink, M.; Chen, C.-H.; Smith, J. M. *Chem. Commun.* **2017,** *53,* 412–415.
57. Ouyang, Z.; Cheng, J.; Li, L.; Bao, X.; Deng, L. *Chem. A Eur. J.* **2016,** *22,* 14162–14165.
58. (a) MacBeth, C. E.; Harkins, S. B.; Peters, J. C. *Can. J. Chem.* **2005,** *83,* 332–340; (b) Mankad, N. P.; Whited, M. T.; Peters, J. C. *Angew. Chem., Int. Ed.* **2007,** *46,* 5768–5771.
59. Lee, Y.; Mankad, N. P.; Peters, J. C. *Nat. Chem.* **2010,** *2,* 558–565.
60. (a) Sellmann, D.; Shaban, S. Y.; Heinemann, F. W. *Eur. J. Inorg. Chem.* **2004,** 4591–4601; (b) Yu, Y.; Brennessel, W. W.; Holland, P. L. *Organometallics* **2007,** *26,* 3217–3226; (c) Albertin, G.; Antoniutti, S.; Bordignon, E.; Chimisso, F. *Inorg. Chem. Commun.* **2001,** *4,* 402–404; (d) Sellmann, D.; Soglowek, W.; Knoch, F.; Ritter, G.; Dengler, J. *Inorg. Chem.* **1992,** *31,* 3711–3717.
61. Mankad, N. P.; Müller, P.; Peters, J. C. *J. Am. Chem. Soc.* **2010,** *132,* 4083–4085.
62. Bontemps, S.; Bouhadir, G.; Dyer, P. W.; Miqueu, K.; Bourissou, D. *Inorg. Chem.* **2007,** *46,* 5149–5151.
63. Moret, M.-E.; Peters, J. C. *Angew. Chem. Int. Ed.* **2011,** *50,* 2063–2067.
64. Moret, M.-E.; Peters, J. C. *J. Am. Chem. Soc.* **2011,** *133,* 18118–18121.
65. Creutz, S. E.; Peters, J. C. *Chem. Sci.* **2017,** *8,* 2321–2328.
66. Rudd, P. A.; Liu, S.; Gagliardi, L.; Young, V. G., Jr.; Lu, C. C. *J. Am. Chem. Soc.* **2011,** *133,* 20724–20727.
67. Rudd, P. A.; Planas, N.; Bill, E.; Gagliardi, L.; Lu, C. C. *Eur. J. Inorg. Chem.* **2013,** 3898–3906.
68. Field, L. D.; Guest, R. W.; Vuong, K. Q.; Dalgarno, S. J.; Jensen, P. *Inorg. Chem.* **2009,** *48,* 2246–2253.
69. Field, L. D.; Guest, R. W.; Turner, P. *Inorg. Chem.* **2010,** *49,* 9086–9093.
70. Field, L. D.; Li, H. L.; Dalgarno, S. J.; McIntosh, R. D. *Eur. J. Inorg. Chem.* **2019,** 2006–2011.
71. Anderson, J. S.; Rittle, J.; Peters, J. C. *Nature* **2013,** *501,* 84–87.
72. (a) Anderson, J. S.; Cutsail, G. E.; Rittle, J.; Connor, B. A.; Gunderson, W. A.; Zhang, L.; Hoffman, B. M.; Peters, J. C. *J. Am. Chem. Soc.* **2015,** *137,* 7803–7809; (b) Del Castillo, T. J.; Thompson, N. B.; Peters, J. C. *J. Am. Chem. Soc.* **2016,** *138,* 5341–5350.
73. Chalkley, M. J.; Del Castillo, T. J.; Matson, B. D.; Roddy, J. P.; Peters, J. C. *ACS Cent. Sci.* **2017,** *3,* 217–223.
74. Buscagan, T. M.; Oyala, P. H.; Peters, J. C. *Angew. Chem. Int. Ed.* **2017,** *56,* 6921–6926.
75. (a) Rittle, J.; Peters, J. C. *Proc. Natl. Acad. Sci. U. S. A.* **2013,** *110,* 15898–15903; (b) Creutz, S. E.; Peters, J. C. *J. Am. Chem. Soc.* **2014,** *136,* 1105–1115.
76. Chalkley, M. J.; Del Castillo, T. J.; Matson, B. D.; Peters, J. C. *J. Am. Chem. Soc.* **2018,** *140,* 6122–6129.
77. (a) Arashiba, K.; Miyake, Y.; Nishibayashi, Y. *Nat. Chem.* **2011,** *3,* 120–125; (b) Kuriyama, S.; Arashiba, K.; Nakajima, K.; Tanaka, H.; Kamaru, N.; Yoshizawa, K.; Nishibayashi, Y. *J. Am. Chem. Soc.* **2014,** *136,* 9719–9731; (c) Kuriyama, S.; Arashiba, K.; Nakajima, K.; Tanaka, H.; Yoshizawa, K.; Nishibayashi, Y. *Chem. Sci.* **2015,** *6,* 3940–3951.

78. Yuki, M.; Tanaka, H.; Sasaki, K.; Miyake, Y.; Yoshizawa, K.; Nishibayashi, Y. *Nat. Commun.* **2012,** *3,* 2264/1–2264/6.
79. Kuriyama, S.; Arashiba, K.; Nakajima, K.; Matsuo, Y.; Tanaka, H.; Ishii, K.; Yoshizawa, K.; Nishibayashi, Y. *Nat. Commun.* **2016,** *7,* 12181.
80. Rittle, J.; Peters, J. C. *J. Am. Chem. Soc.* **2016,** *138,* 4243–4248.
81. Sekiguchi, Y.; Kuriyama, S.; Eizawa, A.; Arashiba, K.; Nakajima, K.; Nishibayashi, Y. *Chem. Commun.* **2017,** *53,* 12040–12043.
82. Higuchi, J.; Kuriyama, S.; Eizawa, A.; Arashiba, K.; Nakajima, K.; Nishibayashi, Y. *Dalton Trans.* **2018,** *47,* 1117–1121.
83. Imayoshi, R.; Nakajima, K.; Takaya, J.; Iwasawa, N.; Nishibayashi, Y. *Eur. J. Inorg. Chem.* **2017**, (32), 3769–3778.
84. Bart, S. C.; Lobkovsky, E.; Chirik, P. J. *J. Am. Chem. Soc.* **2004,** *126,* 13794–13807.
85. (a) Kandler, H.; Gauss, C.; Bidell, W.; Rosenberger, S.; Burgi, T.; Eremenko, I. L.; Veghini, D.; Orama, O.; Burger, P.; Berke, H. *Chem. A Eur. J.* **1995,** *1,* 541–548; (b) Perthuisot, P.; Jones, W. D. *New J. Chem.* **1994,** *18,* 621–628; (c) Komiya, S.; Akita, M.; Yoza, A.; Kasuga, N.; Fukuoka, A.; Kai, Y. *Chem. Commun.* **1993,** 787–788; (d) Berke, H.; Bankhardt, W.; Huttner, G.; Von Seyrel, J.; Zsolnai, L. *Chem. Ber.* **1981,** *114,* 2754–2768.
86. (a) Cable, R. A.; Green, M.; Mackenzie, R. E.; Timms, P. L.; Turney, T. W. *Chem. Commun.* **1976,** 270–271; (b) Hills, A.; Hughes, D. L.; Jimenez-Tenorio, M.; Leigh, G. J.; Rowley, A. T. *J. Chem. Soc. Dalton Trans.* **1993,** 3041–3049.
87. (a) De Bruin, B.; Bill, E.; Both, E.; Weyhermueller, T.; Wieghardt, K. *Inorg. Chem.* **2000,** *39,* 2936–2947; (b) Budzelaar, P. H. M.; De Bruin, B.; Gal, A. W.; Wieghardt, K.; Van Lenthe, J. H. *Inorg. Chem.* **2001,** *40,* 4649–4655.
88. (a) Russell, S. K.; Darmon, J. M.; Lobkovsky, E.; Chirik, P. J. *Inorg. Chem.* **2010,** *49,* 2782–2792; (b) Archer, A. M.; Bouwkamp, M. W.; Cortez, M.-P.; Lobkovsky, E.; Chirik, P. J. *Organometallics* **2006,** *25,* 4269–4278; (c) Trovitch, R. J.; Lobkovsky, E.; Bill, E.; Chirik, P. J. *Organometallics* **2008,** *27,* 1470–1478; (d) Stieber, S. C. E.; Milsmann, C.; Hoyt, J. M.; Turner, Z. R.; Finkelstein, K. D.; Wieghardt, K.; Debeer, S.; Chirik, P. J. *Inorg. Chem.* **2012,** *51,* 3770–3785.
89. Tondreau, A. M.; Atienza, C. C. H.; Weller, K. J.; Nye, S. A.; Lewis, K. M.; Delis, J. G. P.; Chirik, P. J. *Science* **2012,** *335,* 567–570.
90. Bart, S. C.; Lobkovsky, E.; Bill, E.; Chirik, P. J. *J. Am. Chem. Soc.* **2006,** *128,* 5302–5303.
91. Scott, J.; Vidyaratne, I.; Korobkov, I.; Gambarotta, S.; Budzelaar, P. H. M. *Inorg. Chem.* **2008,** *47,* 896–911.
92. Liu, N.; Li, X.; Sun, H. *J. Organomet. Chem.* **2011,** *696,* 2537–2542.
93. Bartholomew, E. R.; Volpe, E. C.; Wolczanski, P. T.; Lobkovsky, E. B.; Cundari, T. R. *J. Am. Chem. Soc.* **2013,** *135,* 3511–3527.
94. Suess, D. L. M.; Peters, J. C. *J. Am. Chem. Soc.* **2013,** *135,* 4938–4941.
95. Hounjet, L. J.; Adhikari, D.; Pink, M.; Carroll, P. J.; Mindiola, D. J. *Z. Anorg. Allg. Chem.* **2015,** *641,* 45–48.
96. Cavaillé, A.; Joyeux, B.; Saffon-Merceron, N.; Nebra, N.; Fustier-Boutignon, M.; Mézailles, N. *Chem. Commun.* **2018,** *54,* 11953–11956.
97. Crossland, J. L.; Zakharov, L. N.; Tyler, D. R. *Inorg. Chem.* **2007,** *46,* 10476–10478.
98. Danopoulos, A. A.; Tsoureas, N.; Wright, J.; Light, M. *Organometallics* **2004,** *23,* 166–168.
99. Danopoulos, A. A.; Wright, J. A.; Motherwell, W. B. *Chem. Commun.* **2005,** 784–786.
100. Danopoulos, A. A.; Pugh, D.; Smith, H.; Saßmannshausen, J. *Chem. A Eur. J.* **2009,** *15,* 5491–5502.
101. Yu, R. P.; Darmon, J. M.; Semproni, S. P.; Turner, Z. R.; Chirik, P. J. *Organometallics* **2017,** *36,* 4341–4343.
102. Kiernecki, J. J.; Zeller, M.; Szymczak, N. K. *J. Am. Chem. Soc.* **2017,** *139,* 18194–18197.
103. Kiernecki, J. J.; Zeller, M.; Szymczak, N. K. *Inorg. Chem.* **2019,** *58,* 1147–1154.
104. Gilbertson, J. D.; Szymczak, N. K.; Tyler, D. R. *J. Am. Chem. Soc.* **2005,** *127,* 10184–10185.
105. Crossland, J. L.; Young, D. M.; Zakharov, L. N.; Tyler, D. R. *Dalton Trans.* **2009,** 9253–9259.
106. Crossland, J. L.; Balesdent, C. G.; Tyler, D. R. *Dalton Trans.* **2009,** 4420–4422.
107. Crossland, J. L.; Balesdent, C. G.; Tyler, D. R. *Inorg. Chem.* **2012,** *51,* 439–445.
108. Doyle, L. R.; Hill, P. J.; Wildgoose, G. G.; Ashley, A. E. *Dalton Trans.* **2016,** *45,* 7550–7554.
109. Hill, P. J.; Doyle, L. R.; Crawford, A. D.; Myers, W. K.; Ashley, A. E. *J. Am. Chem. Soc.* **2016,** *138,* 13521–13524.
110. Piascik, A. D.; Hill, P. J.; Crawford, A. D.; Doyle, L. R.; Green, J. C.; Ashley, A. E. *Chem. Commun.* **2017,** *53,* 7657–7660.
111. Piascik, A. D.; Li, R.; Wilkinson, H. J.; Green, J. C.; Ashley, A. E. *J. Am. Chem. Soc.* **2018,** *140,* 10691–10694.
112. Heiden, Z. M.; Chen, S.; Mock, M. T.; Dougherty, W. G.; Kassel, W. S.; Rousseau, R.; Bullock, R. M. *Inorg. Chem.* **2013,** *52,* 4026–4039.
113. (a) Henry, R. M.; Shoemaker, R. K.; Newell, R. H.; Jacobsen, G. M.; DuBois, D. L.; DuBois, M. R. *Organometallics* **2005,** *24,* 2481–2491; (b) Henry, R. M.; Shoemaker, R. K.; DuBois, D. L.; DuBois, M. R. *J. Am. Chem. Soc.* **2006,** *128,* 3002–3010.
114. Prokopchuk, D. E.; Wiedner, E. S.; Walter, E. D.; Popescu, C. V.; Piro, N. A.; Kassell, W. S.; Bullock, R. M.; Mock, M. T. *J. Am. Chem. Soc.* **2017,** *139,* 9291–9301.
115. Smith, J. M.; Lachicotte, R. J.; Pittard, K. A.; Cundari, T. R.; Lukat-Rodgers, G.; Rodgers, K. R.; Holland, P. L. *J. Am. Chem. Soc.* **2001,** *123,* 9222–9223.
116. Smith, J. M.; Sadique, A. R.; Cundari, T. R.; Rodgers, K. R.; Lukat-Rodgers, G.; Lachicotte, R. J.; Flaschenriem, C. J.; Vela, J.; Holland, P. L. *J. Am. Chem. Soc.* **2006,** *128,* 756–769.
117. Cowley, R. E.; Elhaïk, J.; Eckert, N. A.; Brennessel, W. W.; Bill, E.; Holland, P. L. *J. Am. Chem. Soc.* **2008,** *130,* 6074–6075.
118. McWilliams, S. F.; Bill, E.; Lukat-Rodgers, G.; Rodgers, K. R.; Mercado, B. Q.; Holland, P. L. *J. Am. Chem. Soc.* **2018,** *140,* 8586–8598.
119. McWilliams, S. F.; Bunting, P. C.; Kathiresan, V.; Mercado, B. Q.; Hoffman, B. M.; Long, J. R.; Holland, P. L. *Chem. Commun.* **2018,** *54,* 13339–13342.
120. Rodriguez, M. M.; Bill, E.; Brennessel, W. W.; Holland, P. L. *Science* **2011,** *334,* 780–783.
121. Bhutto, S. M.; Holland, P. L. *Eur. J. Inorg. Chem.* **2019,** 1861–1869.
122. (a) Macleod, K. C.; Vinyard, D. J.; Holland, P. L. *J. Am. Chem. Soc.* **2014,** *136,* 10226–10229; (b) Grubel, K.; Brennessel, W. W.; Mercado, B. Q.; Holland, P. L. *J. Am. Chem. Soc.* **2014,** *136,* 16807–16816.
123. Macleod, K. C.; McWilliams, S. F.; Mercado, B. Q.; Holland, P. L. *Chem. Sci.* **2016,** *7,* 5736–5746.
124. (a) Suzuki, T.; Wasada-Tsutsui, Y.; Ogawa, T.; Inomata, T.; Ozawa, T.; Sakai, Y.; Fryzuk, M. D.; Masuda, H. *Inorg. Chem.* **2015,** *54,* 9271–9281; (b) Bai, Y.; Zhang, J.; Cui, C. *Chem. Commun.* **2018,** *54,* 8124–8127.
125. Cowley, R. E.; Holland, P. L. *Inorg. Chem.* **2012,** *51,* 8352–8361.
126. Guillet, G. L.; Sloane, F. T.; Ermert, D. M.; Calkins, M. W.; Peprah, M. K.; Knowles, E. S.; Čizmár, E.; Abboud, K. A.; Meisel, M. W.; Murray, L. J. *Chem. Commun.* **2013,** *49,* 6635–6637.
127. Lee, Y.; Sloane, F. T.; Blondin, G.; Abboud, K. A.; García-Serres, R.; Murray, L. J. *Angew. Chem. Int. Ed.* **2015,** *54,* 1499–1503.
128. Ferreira, R. B.; Cook, B. J.; Knight, B. J.; Catalano, V. J.; García-Serres, R.; Murray, L. J. *ACS Catal.* **2018,** *8,* 7208–7212.
129. Ung, G.; Peters, J. C. *Angew. Chem. Int. Ed.* **2015,** *54,* 532–535.
130. Vela, J.; Stoian, S.; Flaschenriem, C. J.; Münck, E.; Holland, P. L. *J. Am. Chem. Soc.* **2004,** *126,* 4522–4523.
131. Čorić, I.; Mercado, B. Q.; Bill, E.; Vinyard, D. J.; Holland, P. L. *Nature* **2015,** *526,* 96–99.
132. Takaoka, A.; Mankad, N. P.; Peters, J. C. *J. Am. Chem. Soc.* **2011,** *133,* 8440–8443.
133. Creutz, S. E.; Peters, J. C. *J. Am. Chem. Soc.* **2015,** *137,* 7310–7313.